DEVELOPMENT AND APPLICATION OF A CONGRUENCE-BASED KNEE MODEL

IN ANTERIOR CRUCIATE LIGAMENT INJURED ADOLESCENTS

Claire Emily Warren, B.A.Sc.

Thesis submitted to the University of Ottawa in partial fulfillment of the requirements for the M.Sc. Degree in Human Kinetics

School of Human Kinetics

Faculty of Health Sciences

University of Ottawa

Committee Members:

Allison L. Clouthier, PhD

Thomas K. Uchida, PhD

Supervisor:

Daniel L. Benoit, PhD

TABLE OF CONTENTS

ACKNOWLEDGEMENTS

I am so grateful to the wonderful people that made my Master's experience as incredible as it was. Someone told me at the beginning of my Master's that your acknowledgements section is the most fun part of your thesis to write, and as I think of all the people who helped me get to where I am now, that sentiment couldn't be more true.

First and foremost, thank you to my incredible supervisor Dr. Daniel Benoit, for your guidance and mentorship in my research journey, your unparalleled enthusiasm for learning and for giving me the freedom to explore my own ideas and opportunities as they came. Because of you, I could confidently say I had fun at my job for over two years. I hate that I had to edit this to read that you scored a goal on me twice, but other than that, I am so grateful for the time I spent as your student.

Grazie mille to my wonderful supervisors at the University of Bologna, Drs. Michele Conconi and Nicola Sancisi, for hosting me during my time in Italy. I learned so much in such a short time about modelling, morphology and about myself in four months, and I will be forever grateful to you both for how much time you put into teaching me. Thank to my UNIBO colleagues, Giulia, Andrea, João and Matthias, for all the aperitivos, nights spent watching football and Italian lessons. I miss you all every day.

Thank you to my committee members, Drs. Allison Clouthier and Tom Uchida. It has been a pleasure to be able to learn from you both, as two leaders in musculoskeletal biomechanics research. Whether through your courses, individual meetings, or your thoughtful and insightful feedback, you made me a more thorough researcher. I am so fortunate to have worked with you.

To all the people I've met through CBRU: Teresa, Mike, Nick, Céline, J-F, Maude, Lisa, Chrissy, Blake, Farid, Joana, Laryssa, Aidan and Elodie, what a pleasure it's been working with you all. Thank you in particular to my desk-mate and confidante, Joanna Geck. I will remember our squash rivalry, our UNO games, our carpool karaoke, our dumpling parties and so much more forever. You made this experience so memorable, and I am so lucky to call you my best friend.

To my wonderful roommate Cat, for her friendship and killer recipe for Italian wedding soup. To my former teammates, Mary and Dodger, for making Ottawa feel like home for the last two years. To STOH hockey, for the stress relief and laughs every Friday afternoon. To Amanda, because a FaceTime call with you can fix anything. Thank you all so much, I am so lucky to have you in my life.

To my incredible parents and sister, I love you beyond what I could ever put into words. Thank you for all your support, patience and love no matter where in the world I was. I miss you all every single day and think of you anytime I feel compelled to do a Jacques Clouseau impression (which is always). You are three of the most important people in my life, and I hope you know that I would never have completed this without you.

And finally, thank you so much to Ellen, my partner and best friend. You are the kindest, funniest, warmest and most creative person I have ever met. Whether we were 5000, 1400 or half a kilometer away, you always put in so much effort to make me feel loved, supported and appreciated. Thank you for every date night, for your encouragement as I tried to finish my thesis, and for making me far too emotionally attached to a rabbit. There are not enough words to tell you just how much you mean to me, but I will do my best with seven: I love you, thank you for everything.

CONTRIBUTIONS

Manuscript 1: **Development of a congruence-based model of natural knee motion from magnetic resonance images in anterior cruciate ligament injured adolescents.** *(Results accepted as a poster presentation at the North American Conference of Biomechanics (NACOB) in 2022)*

The first manuscript of this thesis focused on using patient-specific images to identify natural tibiofemoral joint motion from articulating surface geometry. The theoretical development of this experiment was a joint effort between C. E. Warren, M. Conconi, N. Sancisi and D.L. Benoit. The model is based on the previous Ph.D. thesis of K.B Smale. Participant recruitment for this study was collected as part of a larger study designed by M.J. Del Bel, D.L Benoit and S. Carsen. Magnetic resonance images for 12 participants were selected by C. E Warren and acquired as DICOM images by H. Livock. First, second and third segmentations were performed by C. E Warren and reviewed by M. Conconi. Additional joint processing, such as smoothing of segmentations, conversion of ligament insertions to point clouds, reference frame alignment and extraction of articular contacts was performed by C.E Warren and reviewed by M. Conconi. Design and execution of the tibiofemoral joint congruence optimizer was performed by M. Conconi. The construction of all scripts for generating joint coordinate systems, analyzing knee joint angles and ligament lengths and statistical analyses were written by C.E Warren, while scripts for data storage were written by B.S Miller. C.E Warren was responsible for all statistical analyses performed regarding this manuscript. The manuscript was written by C.E. Warren and edited by M. Conconi, N. Sancisi and D.L. Benoit.

Manuscript 2: **Prediction of simplified articular contacts for natural knee motion from external anthropometric measurements and marker trajectories.** *(Results accepted as a podium presentation at the North American Conference of Biomechanics (NACOB) in 2022)*

The second manuscript of this thesis used the previously collected data to predict the coordinates and radii of the simplified articular contact spheres using principal component analysis (PCA). The theoretical conceptualization for using PCA to predict articular spheres was led by C.E Warren, with input from A.L. Clouthier and D.L. Benoit. Selection of appropriate tests and mathematical principles to follow was decided by C.E. Warren, N. Sancisi and M. Conconi. C.E. Warren was also responsible for writing for writing necessary scripts to execute all tests, which were then reviewed by N. Sancisi and M. Conconi. C.E. Warren and N. Romanchuk selected the appropriate machine-learning based validation, which was then converted into scripts by C.E Warren and B.S. Miller. The manuscript was written by C.E. Warren and edited by M. Conconi, N. Sancisi, and D.L. Benoit.

LIST OF ACRONYMS

AA	Abduction/Adduction
AAA	Abduction/Adduction angle
ACL	Anterior Cruciate Ligament
ACLi	Anterior Cruciate Ligament Injured
ACS	Anatomical Coordinate System
EMG	Electromyography
FL	Femoral Lateral (sphere)
FM	Femoral Medial (sphere)
IE	Internal/External
IEA	Internal/External angle
LCL	Lateral Collateral Ligament
LOOCV	Leave-One-Out Cross Validation
MCL	Medial Collateral Ligament
MRI	Magnetic Resonance Image/Imaging
OA	Osteoarthritis
OS	*OpenSim*
PC	Principal Components
PCA	Principal Component Analysis
PCL	Posterior Cruciate Ligament
SSM	Statistical Shape Model
TFJ	Tibiofemoral joint
TL	Tibial Lateral (sphere)
TM	Tibial Medial (sphere)

LIST OF TABLES

LIST OF FIGURES

GENERAL ABSTRACT

Objective: Patient-specific musculoskeletal models have emerged as a reliable method to study how tibiofemoral joint (TFJ) morphology influences anterior cruciate ligament (ACL) injuries. However, there are no such models for adolescent populations that can be scaled to accommodate growth. To serve as the foundation for such models, the objective of this thesis was therefore to i) build a patient-specific model of natural knee motion in an ACL-injured (ACLi) adolescent sample using joint congruency and ii) to attempt to reconstruct patient-specific simplified articular contacts using principal component analysis (PCA).

Design: Twelve magnetic resonance images (MRI) of ACLi adolescents were segmented and used to generate spheres of simplified TFJ articulations. A congruence-based optimization algorithm was used to determine the envelope of tibiofemoral configurations that optimize joint congruency. Descriptive statistics were used to compare model outputs to existing literature. Combinations of marker trajectories and anthropometrics were used to determine the feasibility of reconstructing articular sphere simplifications using PCA. Root-mean squared error (RMSE) was used to compare predicted sphere contacts to MRI-extracted contacts.

Results: Average knee joint angles of the femur with respect to the tibia was slightly abducted and externally rotated, with a range of motion (ROM) of 1.60º ± 0.66 and 7.64 º ± 2.34 across 102° of flexion respectively. The percent elongation of the posterior cruciate ligament (PCL) varied the most across participants (8.65± 6.2%) compared to the ACL (2.34± 2.1%), MCL (1.41± 0.5%) and LCL (1.75 ± 1.6%) respectively. The combination of femur markers and anthropometrics was able to reconstruct simplified tibiofemoral articulations the best, but not within 5 mm of RMSE.

Conclusion: Inter-subject variability in passive kinematic motion derived from patient-specific morphology highlights the need for personalized and accessible musculoskeletal models in growing populations. Furthermore, simplified distal femur morphology can be reconstructed from anthropometrics and marker positions, but proximal tibia morphology requires more information.

Key Words: Adolescents, Anterior Cruciate Ligament (ACL), Knee Motion,

Joint Congruence, Patient-Specific Modelling, Principal Component Analysis (PCA), Predictive Modelling

CHAPTER 1: INTRODUCTION

The anterior cruciate ligament (ACL) is the most commonly injured ligament in the knee, and its injury incidence is rising in adolescent populations (Dekker et al., 2017; L. Shaw & Finch, 2017a; Werner et al., 2016). During puberty, the knee undergoes anatomical changes in bone geometry and skeletal alignment (Dekker et al., 2018; Edmonds et al., 2014) which can decrease congruency of the tibiofemoral joint (Marra et al., 2018). When joint congruency is decreased, it can lead to more pathologic anterior tibial translation, thus increasing the risk of obtaining an ACL injury (Cahuzac Ph. et al., 1995; Schneider et al., 2018). These injuries often lead to long term secondary sequelae such as inactivity, obesity and knee osteoarthritis (Englund et al., 2004; G. Myer et al., 2014). Understanding how bone geometry affects knee joint biomechanics could lead to age-specific interventions that may improve treatments and reduce these sequelae.

One approach to evaluating joint congruency is by using musculoskeletal modelling to investigate internal factors of ACL injury mechanisms that are otherwise difficult to measure *in vivo* (Delp et al., 2007; Rajagopal et al., 2016; Seth et al., 2018). In order to accommodate variations in knee joint biomechanics within and between populations, musculoskeletal models need to be tailored to patient specific parameters. This can be achieved through linear scaling algorithms with anthropometrics and motion capture data (Schellenberg et al., 2017), or by building patient-specific models with magnetic resonance imaging (MRI) (Brito da Luz et al., 2017; Smale et al., 2019). However, currently available linearly scaled knee musculoskeletal models are not a biofidelic representation of the joint, whereas MRI-based models are both labor and time intensive, limiting their accessibility (Ding et al., 2019; Smale et al., 2019). Furthermore, neither technique can accommodate changes in bone geometry and congruence that occur during puberty, as they can not be readily scaled as surface morphology is finalized (Carsen et al., 2021).

To address this research gap, a new musculoskeletal knee model must be developed that can be adjusted based on external anatomical measurements, such that joint congruency can be modelled through adolescence. This way, individual morphological changes that occur through pubertal development can be accommodated. Therefore, the purpose of this thesis is to build this new model using existing MRIs from ACL injured (ACLi) adolescents such that an atlas of shapes representative of an adolescent ACLi population at all stages of puberty can be created. The model will be built by generating three-dimensional (3D) models from medical images and by representing the patient-specific femoral and tibial condyles as spherical approximations (Conconi et al., 2021). These spherical approximations will be used to identify the orientations of the tibiofemoral joint (TFJ) that minimize joint pressure during knee flexion, also known as the envelope of natural knee motion. Using a congruency optimization algorithm (Conconi et al., 2018, 2021), the feasibility of scaling the aforementioned spheres with external measurements, such as marker trajectories and/or anthropometrics, will be tested via principal component analysis (PCA). This process would allow researchers to acquire partially patient-specific models for adolescent knees, regardless of their access to medical images or labor-intensive processing techniques.

The construction of an adolescent knee model would allow for patient-specific kinematics and kinetics to be tracked through the entire rehabilitation period, and subsequently through each patient's remaining pubertal development. It is also possible that the contribution of muscles could be added in the future, such that internal knee loading can be studied through puberty. Idenfying these changes will help researchers understand when and why adolescent populations are most at risk for suffering an ACL injury, which can be used to design specific rehabilitation guidelines and predict long-term changes in knee function and health.

CHAPTER 2: LITERATURE REVIEW

2.1 ACL Injury Incidence

The ACL is the most commonly injured ligament in the knee (Sanders et al., 2016a) and its rate of injury is rising in paediatric and adolescent populations (Beck et al., 2017; Herzog et al., 2017, 2018a; L. Shaw & Finch, 2017a). According to a study conducted by Herzog et al. (2018), adolescents between 13-17 saw a 37% increase in isolated ACL tears between 2002 and 2014. When comparing these rates to an adult population over 18 years of age, the same study found not only lower incidence rates in adults, but consistent rates of isolated ACL injury with increasing age post-puberty (Herzog et al., 2018b). Understanding mechanisms and risk factors associated with ACL injury are of great interest, as ACL injuries have been associated with long term sequelae such as knee osteoarthritis, and increased rates of obesity, inactivity and dysfunction of adjacent limbs (Englund et al., 2004; G. Myer et al., 2014).

Numerous risk factors associated with increases in ACL injury incidence have been examined. Increases in the number of athletes, early single-sport specialization and year-round sport participation have all been hypothesized as reasons behind this increasing trend (Andrews et al., 1994; Arbes et al., 2007; Kocher et al., 2002). Although ACL injuries have been studied in paediatric and adolescent populations for years, the effects of developmental, physiological and morphological changes associated with the onset of puberty on the risk of ACL injury is poorly described (Edmonds et al., 2014).

Significant sex differences also exist regarding ACL injury incidence, with females being up to four times more likely to tear their ACLs than males following pubertal development (Flanigan et al., 2014; Joseph et al., 2013). Furthermore, females and males undergo varying morphological changes during growth as the female skeleton shifts to a more valgus knee alignment (Fayad et al., 2003; Prince et al., 2005). These risk factors are considered "non-modifiable" in nature, meaning that they are definite in nature and cannot be easily altered in any way to reduce risk (Price et al., 2017a). The aforementioned valgus skeletal alignment has been attributed to differences in neuromuscular activations in the lower limb (Buchanan & Lloyd, 1997; Flaxman et al., 2014) and increased valgus loading during high-risk noncontact movement patterns (Krosshaug et al., 2007; G. D. Myer et al., 2005; Olsen et al., 2004). Additionally, tibiofemoral joint (TFJ) morphological differences were also discovered between uninjured and ACLi knees, including decreased intercondylar notch width(Liu et al., 2008; Zeng et al., 2013) and increased tibial slope (Dare et al., 2015; O'Malley et al., 2015). However, there is limited knowledge regarding how these changes in morphology affect biomechanical factors, namely knee joint kinematics, during puberty. As such, an investigation regarding the impact of differences in bone morphology associated with both pubertal change and sex on variables associated with ACL injury is warranted.

2.2 Effects of Puberty and Sex on Knee Joint Anatomy

During puberty, the body undergoes a significant transition both anatomically and physiologically, which can influence ACL injury risk. This is also not consistent between sexes, with females being twice as likely to incur an ACL injury compared to their male counterparts (Herzog et al., 2017; Landry et al., 2007; Sanders et al., 2016b; L. Shaw & Finch, 2017b) . Figure 1 in Appendix A shows results from a study by Prince et al. (2005) which used magnetic resonance images (MRIs) to evaluate characteristics of ACL injury and its relation to skeletal maturity. The ACL injuries of the skeletally immature cohort were more likely to be sustained by males but transitioned to female injury dominance when patients were skeletally mature (Prince et al., 2005). Furthermore, partial tears were more prevalent amongst the skeletally immature group, whereas complete tears were more common as skeletal maturity progressed (Prince et al., 2005). A possible explanation for this discrepancy is the large inundation of sex-steroid hormones, estrogen and testosterone, that occurs during the onset of puberty (Malina et al., 2004; Wild et al., 2012). Increased estrogen levels in females have been linked to weaker ACL structural and mechanical integrity, such as the deformation and energy absorbed prior to failure, and increased knee joint laxity (Woodhouse et al., 2007). From a loading perspective, anthropometric changes that occur during the onset of puberty may also increase ACL injury risk. The adolescent growth spurt causes increases to both the mass and length of the lower limbs, contributing to increased variation in the moment of inertia of the segments, and changing the alignment of the skeleton and joint load distributions (Jensen & Nassas, 1988; Prince et al., 2005; Stein & Micheli, 2010).

Differences in anatomical structures of the knee joint specifically have been associated with increased ACL injuries among skeletally immature adolescents (Wild et al., 2012). Dare et al. (2015) found that ACLi children had a steeper posterior lateral tibial slope of 5.7° ± 2.4° compared to a healthy control group of 3.4° ± 1.7° ($p < 0.001$). O'Malley et al. (2015) found similar differences when examining skeletally immature adolescents, with ACLi posterior tibial slope measuring 10.6° ± 3.1° compared to slopes of 8.5° ± 3.7° in an uninjured cohort ($p = 0.0128$). Increasing posterior tibial slope has been associated with increases in anterior tibial translation (Giffin et al., 2004), tibial shear force (Shelburne et al., 2011), and ACL force during functional tasks in adult populations (Todd et al., 2010). Furthermore, a controlled laboratory study conducted by Lipps et al (2012) found that the increased lateral tibial slope of female cadaveric knees increased peak ACL strain under dynamic loading conditions (Lipps et al., 2012). Another anatomical structure of the knee joint that has been associated ACL injury is a small intercondylar notch width, which is more prevalent in females (Shaw et al., 2015). Despite the fact that both pubertal and sex-based differences influence anatomy of the knee and ACL injury rates, the effects of these differences on knee joint biomechanics continues to be investigated, and an insight into how inter-patient morphological variability affects knee kinetics and kinematics is necessary.

2.3 Anatomy and Joint Congruency on Knee Kinematics

While we are aware that anatomical differences at the knee exist between adults and children, and that these changes occur over the course of pubertal development, the effects of growth on knee joint biomechanics continues to be investigated. As addressed in the rationale, researchers have successfully shown how differences in morphology can influence knee joint biomechanics in adult populations. Due to the unique curvatures of the femoral and tibial condyles, the contact area between the joint changes during motion, subjecting the joint to different magnitudes of pressure. This measure of how much contact there is between two articulating surfaces is defined as *joint congruence* (Conconi & Castelli, 2014). Researchers have studied the relationship between joint congruence and pathologies such as osteoarthritis risk in adult populations (Conconi et al., 2014; Schneider et al., 2018). Schneider et al examined postoperative computed tomography to evaluate the tibial slopes, concavity, convexity and joint congruency of the medial and lateral components of the tibiofemoral joint in 276 ACLi participants. They demonstrated that in an ACLi population, medial ($p < 0.01$) and lateral ($p < 0.001$) tibiofemoral compartments were more incongruent in females than in males, while noting that anatomical factors like steeper tibial slopes may also contribute negatively to outcomes of ACL reconstruction surgery. Marouane et al. (2015) used finite element modelling techniques to simulate how increasing posterior tibial slope (PTS) during gait affects knee kinematics and ACL force. Simulated anterior tibial translation and ACL force both increased with increasing tibial slope, with simulated ACL force increasing from 181 N to 317N and 460 N following a 5º and 10º increase respectively (Marouane et al., 2015). Lansdown et al. (2017) built a kinematic statistical shape (SSM) model of the knee using MRIs to simulate standing and the initiation of a bodyweight squat to identify bone shapes associated with abnormal knee kinematics. Increases in tibial slope, decreased medial femoral condyle sphericity, and decreased length of the anterior aspect of the tibial plateau showed anterior side to side differences in tibial position for pre-operative ACLi patients (D. A. Lansdown et al., 2017). In addition, Shelburne et al. (2011) used musculoskeletal modelling techniques and reported that increased posterior tibial slope is associated with higher shear forces on the ACL during standing, squatting and walking. Simulated changes in tibial slope were determined by rotating the tibial plateau about an axis 2 cm below the distal tibial plateau for a range of values obtained through cadaveric studies (Shelburne et al., 2011).

In Section 2.2, numerous studies were referenced that highlighted the relationship between specific knee joint anatomy and ACL injury incidence (Dare et al., 2015; O'Malley et al., 2015; Shaw et al., 2015; Wild et al., 2012). These studies showed morphological differences between ACLi and uninjured knees, but not between sexes. Additionally, studies that showed sex-specific morphological variation between ACLi and uninjured patients were conducted on older, post-pubescent subjects (Murshed et al., 2005; Siegel et al., 2012; van Diek et al., 2014). Identifying how morphology influences knee joint biomechanics in a developing period regardless of sex may help to improve non-modifiable ACL injury risk factor identification by investigating how anatomical differences influence knee joint biomechanics. Therefore, there exists a need to develop a method to visualize, interpret and measure the changes in knee biomechanics during puberty in a way that encompasses patient sex, anatomical differences and various levels of skeletal maturity.

2.4 Musculoskeletal Modelling

Due to the invasiveness of certain experimental procedures (Fregly et al., 2012), identifying how differences in anatomy can affect biomechanical factors of movement can be challenging. Musculoskeletal modelling techniques have emerged as a method of investigating the complexities of the skeletal system through computer simulation, and there are multiple musculoskeletal modelling software packages that can be applied to biomechanics research. The ergonomic optimization software *AnyBody* is known for it's robust linear scaling methods and computational prowess (Damsgaard et al., 2006; Rasmussen, 2003). Additionally, AnyBody models can have an environmental input, which allows biomechanical simulations in environments with specific mechanical properties, such as movement underwater (Langholz et al., 2016). However, in order to ensure full accessibility, the modelling software must be purchased. This limits the ability of other researchers to collaborate and even validate AnyBody models, which is not useful for widespread academic and clinical use.

In contrast, the software *OpenSim* is the most commonly used musculoskeletal modelling software, having accrued over 35000 and counting unique user downloads. (Reinbolt et al., 2011; Seth et al., 2018). The framework of *OpenSim* is open sourced, providing a larger and more collaborative environment for sharing models, techniques and code among researchers in comparison to *AnyBody*'s commercial modelling platform (Damsgaard et al., 2006; Seth et al., 2018). In both *OpenSim* and *AnyBody*, generic musculoskeletal models were built from the combination of MRI and cadaveric data from a single subject (Arnold et al., 2010; Carbone et al., 2015). New developments in generic *OpenSim* models have included muscle architecture derived from 21 cadavers and the medical images of 24 adult subjects, improving the model's generalization (Killen, 2019). *OpenSim* also has advanced movement simulation capabilities; its unique interfaces allow users to perform both forward simulation to investigate neuromuscular control and reflex pathways or inverse simulation to solve for kinetic contributions that generate a given movement. These processes are defined by Seth et al (2018) and outlined in Figure 16-2 of Appendix A.

In order to perform kinematic and kinetic analysis in *OpenSim*, patient specific anthropometrics and movement patterns must be applied to the generic model without introducing physiologically impossible configurations of the joints, such as bone overlap (Lund et al., 2015). Typically, this is a two-pronged process known as "scaling", where body mass, height and retroreflective surface markers are used to identify segment lengths (Ali et al., 2014; Chen et al., 2014; Rasmussen et al., 2005; Schellenberg et al., 2017), then surface marker trajectories from motion capture trials are used to identify local coordinate systems for each body segment to compute joint angles (Schellenberg et al., 2017). The process of using body segment parameters as inputs for equations of motion to estimate joint angles is known as inverse kinematics, while the subsequent measurement of accompanying joint forces and moments is known as inverse dynamics (Winter, 2009). This process can either be performed manually for each subject by applying the same marker set used during motion capture trials to a generic model, or by combining segment length optimization algorithms and manual scaling to automate landmark identification for inverse dynamics (Damsgaard et al., 2006; Lund et al., 2015; Rasmussen et al., 2005).

2.4.1 Limitations in Musculoskeletal Modelling

Despite the benefits of musculoskeletal modelling for biomechanical analysis, there are still limitations that must be considered when using these techniques. The first limitation is the errors due to soft tissue artifact (STA) caused by recording markers placed on the skin rather than registering the motion of the underlying bone itself (Benoit et al., 2006; Lund et al., 2015; Reinbolt et al., 2005; Reinschmidt et al., 1997). Soft tissue artifact affects the inputs of kinematic analyses during dynamic tasks resulting form skin deformation and muscle contractions which can cause the markers to shift on a body segment relative to the underlying bone (Leardini et al., 2005). Ensuring accurate initial parameters for kinematic analysis is critical, as inaccurate inputs can produce compounding errors and generate unfeasible results.

Other limitations in musculoskeletal modelling include the methods by which patient-specific anatomy are applied to generalized musculoskeletal models. To reduce potential errors, generic musculoskeletal models are often adjusted to match specific participants through a technique known as “linear scaling”. Linear scaling alters up to three dimensions of each bone (anterior/posterior, medial/lateral and/or superior/inferior), which are adjusted to match the anthropometrics of a given patient. It is an effective technique for scaling when time and cost of modelling are a factor, as linear scaling techniques are algorithmic and not computationally heavy. Improving the sensitivity of linear scaling processes continue to be investigated. Some approaches that have been used to improve the fidelity of these scaling methods, as to reduce negative effects from assumed marker positions, (Ding et al., 2019; Lund et al., 2015; Schellenberg et al., 2017). Lund et al. (2015) incorporated both static and dynamic reference trials to successfully reduce variation in knee joint contact forces during heel strike from 1.44 bodyweight (BW) to 1.0 BW when scaling from static reference trials and even further to 0.44

BW when scaling using dynamic walking trials. Ding et al (2019) developed an anatomical atlas from models generated based on medical imaging for scaling purposes that considers gender and anthropometric similarity of the hip, knee and ankle joints of the lower limb. Using this technique, joint contact forces at the ankle, knee and hip were reduced between 50 and 67% when compared to a generic model (Ding et al., 2019). Lastly, Schellenburg et al. (2017) determined that the use of functional centre of rotations of lower limb segments while scaling reduced the root mean squared error between 3-8 mm from patient reference movement data and various musculoskeletal modelling inputs.

While these processes allow patient-specific dimensions to be applied to generic musculoskeletal models, linear scaling does not alter the morphology of the generic bones. Unfortunately, this negates the impacts of the interpatient variability in bone geometry and resulting effects on joint contact forces (Lerner et al., 2015), moments (Tsai et al., 2012), and angles (Scheys et al., 2011). Therefore, a new model must be developed that both can account for interpatient variability without compromising the open-sourced framework of musculoskeletal modelling.

2.5 MRI Based Modelling

Musculoskeletal models built from medical images have emerged as a method to generate reliable simulations of joint contacts (Davico et al., 2019). Imaging techniques such as magnetic resonance images (MRI) (Clouthier et al., 2019; Smale et al., 2019; Valente et al., 2017), computed tomography (CT) (Barzan et al., 2019), and biplanar radiography (BVR) (Fernandez et al., 2008; Zheng et al., 2014) have been used to extract patient specific anatomy to build more biofidelic knee musculoskeletal models in adult and paediatric populations. Despite this, CT and BVR generated images require doses of radiation and, in addition to high costs and/or lengthy processing times, may not be the most effective method for generating patient specific images. In contrast, MRI images do not rely on ionizing radiation, and are more suitable for capturing high-resolution images of softer tissues, such as muscles, tendons and ligaments (Lin, 2010).

While patient-specific imaging may improve the accuracy of biomechanical models when compared to models that have been just been linearly scaled (Nardini et al., 2020; Smale et al., 2019), there are limitations that affect their repeatability. Manual and semi-automatic segmenting require access to imaging equipment, computationally and economically expensive processing software and labour trained in image processing. All of these limit the amount of collaboration between researchers and the reproducibility of research. (Fripp et al., 2010; Jaremko et al., 2006; Liukkonen et al., 2017; Yu et al., 2016). Jaremko et al. (2006) reported that technicians responsible for semi-automatic segmentation of cartilage often requires three months training, and that the process of generating 3D models can take several hours per knee. There are also additional limitations accessibility and repeatability. Although no exposure to radiation is required to collect an MRI, those who have metal implants like bone screws or pacemakers must be cautious of potential movement generated by the heavy magnetic field. Furthermore, MRI images provide an instance of the knee at the time of imaging alone, and are not able to accommodate changes in growth that occur over time. The feasibility of manually scaling generalized bones and applying patient-specific morphology to perform unique kinematic analysis for each participant has not been investigated in paediatric populations, where bone morphology is highly variable during adolescent development. As such, a new universal paediatric knee joint model that can account for variations in bone geometry through puberty without requiring the use of specialized technicians or equipment is needed.

2.6 *Statistical Shape Modelling*

Statistical shape modelling (SSM) techniques are used in computational biomechanics to simplify differences in morphology by identifying a range of shapes that can best describe variations of a population (Heitz et al., 2005; D. A. Lansdown et al., 2017). These variations can be identified using Principal Component Analysis (PCA), with the goal of reducing the dimensionality of the population while maintaining as much of the original variation as possible (Jollife & Cadima, 2016). The resulting modes represent the minimum number of shapes that can successfully describe the variation within the sample, such as comparing different cervical vertebrae (Figure 16-3 in Appendix A illustrates what these modes may look like). This technique has become extremely popular in medical imaging analysis as a method of quantifying anatomical bone shape differences in both healthy (Clouthier et al., 2019) and pathological cohorts (D. A. Lansdown et al., 2017). More specifically to the knee, SSM has been used to identify how articular geometry affects knee kinematics during simulation (Clouthier et al., 2019; Lansdown et al., 2017), incorporated into computer-assisted ACL reconstruction surgery techniques (Fleute et al., 1999), and identify bone geometry differences between healthy and osteoarthritic patients with as much as 95% accuracy (Lynch et al., 2019).

Since SSMs are able to generate an atlas of shapes to classify a given population, they have been used in combination with linear scaling techniques to improve the biofidelity of musculoskeletal modelling (Bahl et al., 2019; Lynch et al., 2019; Suwarganda et al., 2019). Most notably, the development of the Musculoskeletal Atlas Project (MAP) has successfully allowed researchers to match MRI images of the hip joint to the appropriate 3D model derived from SSM (Zhang et al., 2014). The development of the MAP has allowed for open-sourced distribution of patient-specific models, as researchers are not required to have access to expensive modelling software or technicians to have access to a biofidelic model (Bahl et al., 2019; Suwarganda et al., 2019; Zhang et al., 2014). In addition, researchers have created similar models at the knee for shape modelling in adult populations (Clouthier et al., 2019; Lynch et al., 2019). However, there are no shape models specifically designed for paediatric knee anatomy, and all existing models require access to some sort of medical images. Therefore, the development of a paediatric knee joint model that accounts for patient-specific anatomical variability without requiring the use of external imaging software and processing is warranted.

2.7 Validation and Verification

When developing a new musculoskeletal model, it is imperative that the outputs of the simulation are accurate when validated against existing "gold-standard" methods of analysis (Lund et al., 2012). The two-pronged analysis of the accuracy of model outputs in addition to its applicability in experimental settings is known as verification and validation (V & V) (Lund et al., 2012). V & V techniques are common in engineering practices, especially in computer aided design (CAD), where an abundance of real-world data was available to complement predictions from CAD models (Babuska & Oden, 2004). However, in biomechanics, namely musculoskeletal modelling, it is strenuous to truly validate a model due to the difficulty of acquiring experimental data, such as internal parameters of movement, non-invasively (Lund et al., 2012). As a result, there have been limited studies on validation processes within the biomechanics field.

Henninger et al. (2010) and Anderson et al (2012) have explored how the individual components of V & V analyses are instrumental in the development of a successful musculoskeletal model (Anderson et al., 2012; Henninger et al., 2010; Hicks et al., 2015). With the verification stages, evidence is provided that shows how a proposed model is sufficient in generating an accurate result (Anderson et al., 2012; Henninger et al., 2010; Lund et al., 2012). This can either be by examining the code used to calculate a solution or the mathematical concept behind a model. With model validation, the focus of the analysis shifts to the predictive power of a model and the assurance that any errors between experimental and simulated outputs produce little to no consequences (Anderson et al., 2012; Henninger et al., 2010). When considering the development of musculoskeletal models of the knee joint, experimental data for V&V processes is scarce. As mentioned in Section 8.4, existing models have been validated using limited cadaveric data as reference, for parameters such as ligament and tendon properties, that are otherwise difficult to obtain non-invasively (Delp et al., 1990; Hamner et al., 2010; Rajagopal et al., 2016). However, this does not necessarily indicate that musculoskeletal modelling techniques cannot be validated for specific applications by applying V & V techniques similarly to other researchers, such as validating a musculoskeletal model for human gait based on knee forces collected via prosthetic implants (Fregly et al., 2012; Manal & Buchanan, 2013; Moissenet et al., 2014, 2017). Therefore, in order to truly develop a model than can be applied to any person undergoing pubertal development, it must be accessible and validated for its intended application prior to distribution.

CHAPTER 3: OBJECTIVES AND HYPOTHESES

There are two primary research objectives relating to this thesis: I) To determine if magnetic resonance image-based modelling is suitable for an ACLi adolescent population and II) Use principal component analysis to determine if patient-specific articulations can be predicted from anthropometric measurements and positions of anatomical landmarks. To achieve this, two specific research questions will be tested.

Q1) Can a magnetic resonance imaging-based model be developed to describe natural knee motion kinematics in an adolescent population?

A musculoskeletal model developed and validated by Michele Conconi (2018, 2021), used patient-specific tibiofemoral articulations and joint congruence to determine a person's natural knee motion while considering the viscoelastic properties of cartilage through elastic conforming contact. (Johnson, 1985). The model was built from segmenting patient-specific MRIs to form 3D bone models with surrounding soft tissue, and optimizing congruence such that joint pressure is minimized during passive flexion/extension, reproducing the natural knee motion of the adult knee. We will apply similar techniques to the adolescent male and female knee and hypothesize that flexion/extension, abduction/adduction and internal/external rotation angles will be within two standard deviations of literature reported passive knee joint angles across all degrees of freedom, while maintaining ligament isometry.

Q2) Can we predict congruency measures from anthropometric and marker position data using Principal Component Analysis for the adolescent knee?

Using positional data from six retroreflective markers attached to anatomical landmarks of the injured lower limb in addition to anthropometric measurements of leg length and width, principal component analysis will be used to predict the 3D positional coordinates and the radius of the spherical approximations of articulation extracted during Study 1. The root-mean squared error (RMSE) of the predicted outputs will then be compared to the extracted values of condyle spheres and radii to determine if patient-specific approximations of joint articulation can be predicted from in-vivo landmarks. It is hypothesized that the RMSE between the predicted patient-specific spheres and the original spheres will fall within two standard deviations of MRI-measured data (Hicks et al., 2015).

CHAPTER 4: METHODS

4.1 General Methodology

This thesis is divided into two studies. The first study aimed to build a simplified model of the adolescent knee by using spheres to represent articular contact surfaces that optimize joint congruency, thus reducing joint contact pressure. This would produce an envelope of tibiofemoral configurations that would serve as the "path of least resistance" across all degrees of freedom. This model was originally developed by Conconi et al. (2018, 2021), then successfully implemented by Smale et al. (2019) in an ACLi adult population. The second study objective was to determine if partially patient-specific approximations of articular contacts could be predicted from *in-vivo* markers, and anthropometric data, eliminating the need for MRIs when building future patient-specific models. Descriptive statistics from the optimized DOF in Study 1 were compared ranges of motion ROM reported in existing literature. For study two, the 3D position data of the sphere centroids and radii were compared to the original sphere centroid locations and radii of each of the knee to determine the efficacy of reconstructing patient-specific knee from anthropometric data and anatomical landmarks. A summarized workflow is identified in Figure 4-1, while a full comprehensive workflow can be found in Appendix A.

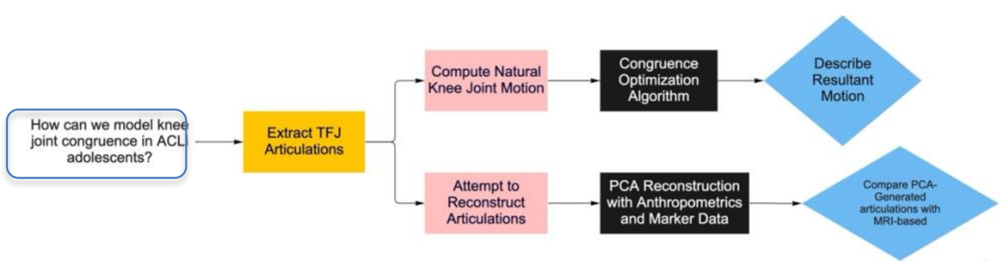

Figure 4-1 General methodology flowchart for Study 1 (Top) and Study 2 (Bottom). Articulations refer to the interaction of the medial and lateral surfaces of the femur and tibia

The MRI and functional movement data in these studies were adapted from previously collected data, as part of a larger collaborative project between the University of Ottawa Clinical Biomechanics Research Unit and the Children's Hospital of Eastern Ontario (CHEO). The adapted project followed a test-retest design, whereby ACLi patients completed a series of isometric strength, functional movement tasks and endurance-based tests, defined in Appendix B. Patients were tested prior to their surgery, approximately six months following ACL reconstruction (ACL-R) surgery and two years following ACL-R surgery, after each participant has been cleared for return-to-play by their attending orthopaedic surgeon

Upon arriving at the lab for testing, participants were asked to sign a consent form that had been approved by the University of Ottawa Research Ethics Board, and given a range of questionnaires to complete regarding their overall knee function (Pedi-IKDC) (Kocher et al., 2011), assessment of sport exposure (Pedi-FABS) (Fabricant et al., 2013), classification of current puberty stage (Tanner stage) (Marshall & Tanner, 1969, 1970) and activity level (Tegner activity scale). Participants were then outfitted with retro-reflective markers and electromyography (EMG) electrodes outfitted on major muscle groups of the lower limb. They were then asked to complete a series of single limb isometric strength tasks, single-leg hopping and dynamic movement tasks and an endurance-based strength test that can be found in Appendix B. Each of these tasks are used to evaluate functional capacity in a clinical setting. Two successful hopping and five successful dynamic movement trials must be collected before a participant can complete the next task to preserve data quality. For the sake of this thesis, only pre-operative ACLi participant Tanner stages, anthropometrics, and static position marker trajectories were used in both studies.

4.2 Study Design

Both studies in this thesis follow an observational study design, as no changes were made to the current testing or rehabilitation protocols being implemented as a part of the larger study outlined in Section 10.1. Due to the novelty of this proposed model, this thesis focuses on the "proof of concept" work, therefore the highest priority of participant recruitment was chosen to represent as many of the five Tanner stages as possible, encompassing the widest range of pubertal development. Eight of the 12 participants were unique Tanner stage/sex combinations, and all remaining participants were selected at random from those who had their MRIs collected at CHEO.

4.3 Participants

Twelve patients (five males, seven females) who were between the ages of 10 and 18 years old at the time of data collection, had a confirmed full or partial ACL rupture via MRI, and no prior history of ACL injury were included in this study. For study one, all twelve were used in the construction of the congruence-based musculoskeletal model. For study two, the data was split into a group of 11 participants to build the model and one to validate prediction efficacy. This process was repeated 12 times to ensure each participant was equally considered as either a model development knee or a validation knee, and is explained further in Section 3.2.8. Participant general anthropometrics are defined in Table 3.1.

Table 4-1 Averages of patient demographics used in this study

Participant Information			
Age (yrs)	**Height (cm)**	**Weight (kg)**	**Tanner Stage**
15.42 ± 1.4	165.8 ± 6.5	67.35 ± 15.6	3.92 ± 1.2

4.4 Kinematic & Kinetic Data

Each participant was fitted with a marker set of 82 retroreflective markers (Mantovani & Lamontagne, 2017). Kinematic data were collected using a 10-camera motion capture system (6 MX and 4 T series, Vicon Oxford Metrics, UK) and Nexus software (v 1.8.5, Vicon Oxford Metrics, UK) and sampled at a rate of 1000 Hz. Ground reaction forces (GRF) were collected using two piezoelectric force plates at 1000 Hz (AMTI-OR6, AMTI, USA). All marker trajectories were labelled in Nexus using a market set adapted from Mantovani and Lamontagne (2017) and .c3d files were exported to MATLAB (2020a, Mathworks, USA) for processing. The 3D marker positions and GRF for the standing static pose (Figure 10-2) for each participant were the only trajectories used for this thesis.

Figure 4-2 Marker configuration and execution of the static pose used in data collections

4.5 MRI Acquisition & Segmentation

Magnetic resonance images were collected at 1.5 Tesla, with a repetition time/echo time of 1400/17 ms, field of view of 160 mm and slice thickness of 0.8mm (Siemens Magnetom Skyra, Siemens Healthineers AG, Germany) at CHEO in accordance with their standard of care for ACL-R surgery. The Proton-Density Cube sequence was chosen for segmenting because it produced clear images in all three planes (sagittal, frontal and axial), while allowing for easier identification and segmentation of soft tissues like articular cartilage. The femur, tibia and fibula were segmented into 3D models using an open-sourced software Workbench (Workbench 2018.10, MITK, Germany), with the knee joint centre defined as the midway point between the medial and lateral femoral epicondyles. All long bones were segmented with the inclusion of their respective articular cartilage, such that both the bone and cartilage could be modelled as a single solid. Medial and lateral menisci were segmented as individual soft tissue structures. Lastly, the femoral and tibial insertion points of the anterior and posterior cruciate ligaments, and the medial and lateral collateral ligaments were segmented for the ligament optimization process for identifying patient-specific knee motion described in Section 10.2.6. The lengths of these ligaments were interpolated from the origins, which were discernable in all MRIs.

Long bones and menisci were refined by smoothing .stl files using Geomagic Studio (Geomagic Studio 2012, 3D Systems, USA). Articular surfaces were then isolated using *Rhinoceros 3D* (Version 5.0, McNeel & Associates, Seattle, USA) then decimated to ~6000 triangles for computational efficiency. Additionally, all femoral and tibial origin and insertion sites of the anterior and posterior cruciate ligaments, and the medial and lateral collateral ligaments were converted into point clouds on their corresponding surfaces (Figure 10-3), such that the fibre corresponding to the most isometric ligament during passive knee flexion could be identified. Best-fitting spherical approximations for the femoral and tibial condyles were also isolated in Geomagics, from the posterior femoral condyle surface and the surface of the tibial plateau (Figure 10-4). For each participant, four smoothed models were created for the congruence optimization: the femur, the tibia, the fibula and the tibia with both menisci.

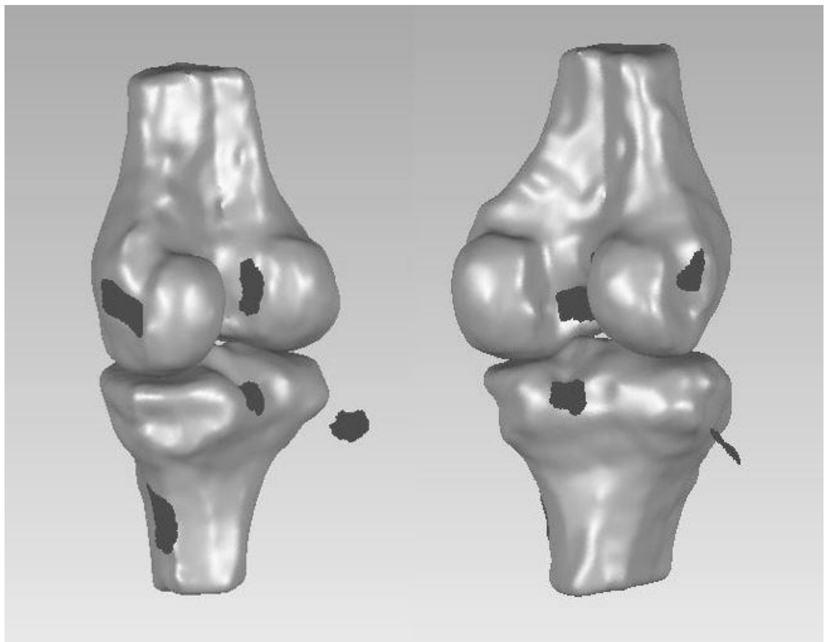

Figure 4-3 Point clouds of ligament origins and insertions

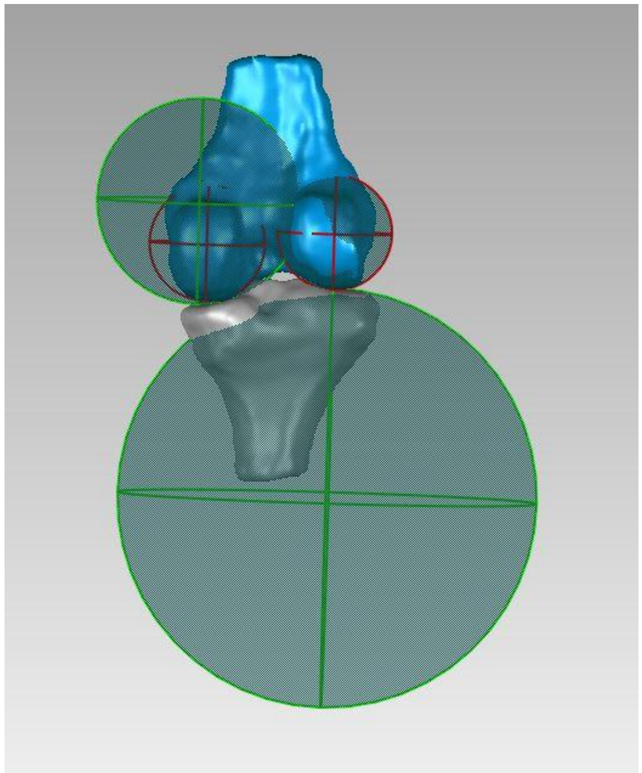

Figure 4-4 Four spherical approximations of the femoral articulations (red) and tibial articulations (green) extracted from MRI

After segmentation and smoothing, anatomical coordinate systems (ACS) were defined for both the femur and the tibia in a custom MATLAB script. Coordinate systems were derived from anatomical landmarks of the long bones, and based on previous coordinate systems defined by Benoit et al. (2007) and Gray et al (2019). The purpose of these systems was to define femoral and tibial ligament orientations, spherical approximations and natural knee motion with respect to each bone. The definition of these coordinate systems is indicated in Figure 10-5, Table 10-2 and Table 10-3 respectively.

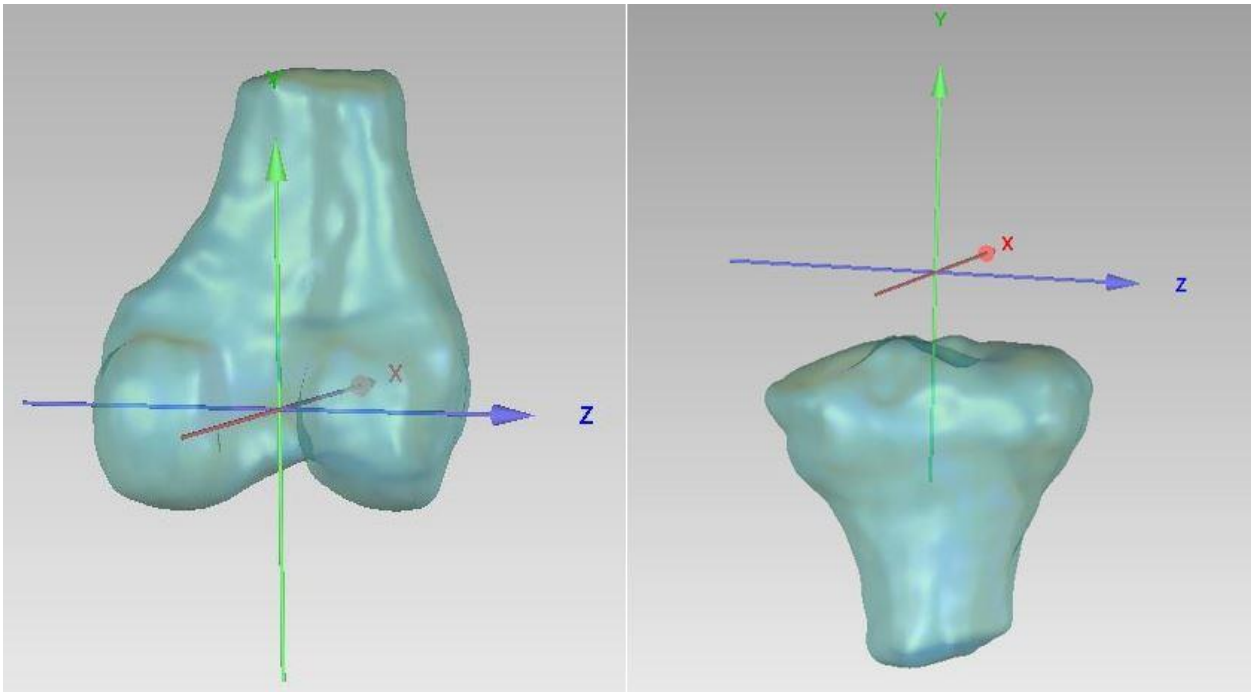

Figure 4-5 Anatomical coordinate system (ACS) definition of the femur (left) and tibia (right) in accordance with Gray et al. (2019)

Table 4-2 Femur anatomical coordinate (ACS) system axes definition

Femur	
$\mathbf{X_f}$	Cross product between long axis (line of best fit through the diaphysis) axis and the Z_f
$\mathbf{Y_f}$	Cross product between Z_f and X_f
$\mathbf{Z_f}$	Vector directed to the right, passing through the centroid of the medial and lateral femoral epicondyles

O_f	Midpoint between the medial and lateral femoral condyles

Table 4-3 Tibia anatomical coordinate (ACS) system axes definition

Tibia & Fibula	
X_t	Cross product between Y_t and a vector passing between tibial eminence centroids
Y_t	Long axis vector starting from the midpoint of the tibial eminence
Z_t	Cross product between X_t and Y_t
O_t	Projection of O_f onto Y_t

4.6 Alignment

Once the 3-D models have been constructed for each participant, they must be aligned with generic models of the femur and tibia in order to obtain patient specific joint centres for the hip and ankle. Scaling and aligning the patient-specific coordinates of segmented bones to a generic model allows for the model to be transferred to *OpenSim* without compromising the patient-specific anatomical differences of the cohort. This process was performed in *Rhinoceros* (4.0, McNeel & Associates, USA) and *OpenSim* (4.0, SimTK, Stanford, USA), following the protocol defined by Smale et al (2018, 2019). The femur and tibia obtained from the Rajagopal lower limb model (Rajagopal et al., 2016) were used as generic bones for alignment, and scale factors were applied directly to the generic bones in *Rhinoceros*, using scale factors derived from six retroreflective markers and previously collected anthropometric measurements (Table 10-4). Once the *OpenSim* generic bones were scaled, they were aligned to the MRI-frame fully segmented femur and tibia using the built-in function *Orient3pt* (Figure 10-6). The knee joint centre was approximated as the midpoint between the medial and lateral epicondyles, and the hip joint centre was approximated by defining a vertical plane in *Rhinoceros.* Vertical plane definition was done by creating an arbitrary point in *z* (0,0, 250 mm), then using that point to conduct preliminary alignment to the hip joint center. The scaled *OpenSim* knee joint centre, hip joint centre and medial epicondyle markers were aligned to the MRI virtually palpated markers using the built-in function *Orient3pt*. After preliminary alignment, the generic *OpenSim* bones were manually adjusted to best-fit the volume of the generic bones inside the MRI bone volume in order to obtain coordinates for the six markers in Table 3-5 in the MRI frame. These new coordinate positions were used as features for the active shape model development in study two.

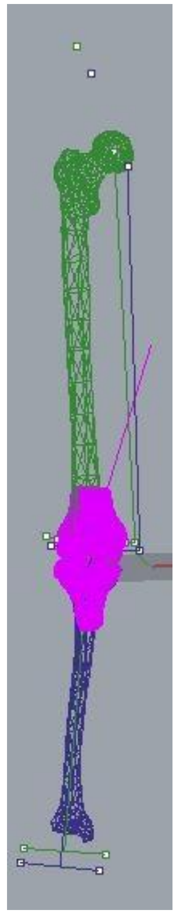

Figure 4-6 Alignment of the OpenSim femur (green) and tibia (purple) to the patient specific MRI (pink). White squares represent marker positions used for Orient3pt function

Table 4-4 Marker trajectories extracted from the Rajagopal OpenSim model (2016) and used in PCA

Lower Leg Body	**Anatomical Landmark**
Hip Markers	Hip Joint Centre (HJC), Anterior Superior Iliac Spine (ASIS)
Knee Markers	Medial Epicondyle (MKNL), Lateral Epicondyle (LKNL)

Ankle Markers	Medial Malleolus (MANL), Lateral Malleolus (LANL)

Table 4-5 Scale factors applied to generic bone along given axis using corresponding marker pairs

Scaled Component (direction)	**Marker Pairs**
Total Leg Length (y)	ASIS to MANL
Leg Width (z)	MKNL to LKNL
Tibia Length (y)	LKNL to LANL

4.7 Patient-Specific Natural Motion

A measure of joint congruency for highly conforming surfaces (i.e.: articular cartilage) was defined by Conconi and Parenti-Castelli (2014) based on Winkler's elastic foundation contact model (Johnson, 1985). The ratio between peak pressure and resultant contact force can be estimated based on the ability of a set of given articulating surfaces in any orientation to distribute applied load (Conconi and Castelli, 2014; Johnson, 1985). As a result, joint congruence is maximized when peak pressure is minimized (Conconi and Castelli, 2014). This approach has been validated using in-vitro testing (Forlani et al., 2016), sensitivity analysis (Conconi et al., 2015a) and has been successfully implemented for musculoskeletal modelling in an adult ACL injured population (Smale et al., 2019). The simplified mathematical expression of joint congruency is summarized using Equation 1.

$$\frac{F}{p_0} = \frac{V}{\Delta} = CM \qquad (1)$$

Where the congruence measure (CM) between two conforming shapes is defined as the relationship between force (F) over peak pressure (p_0), or the Boolean intersection volume (V) over the maximum indentation (Δ) .

Building on the work of Smale et al. (2019), natural motion of each patient was computed in controlled increments of knee flexion. Simulated passive knee flexion was applied to the segmented tibiofemoral joint from 10° extension to 120° flexion at 2° increments, while the remaining five DOFs were optimized to the envelope of tibiofemoral joint configurations that maximize joint congruency. The spheres representing the articulating surfaces were also optimized to each participant (maximum variation: plus/minus 2mm), such that they remained in contact with the medial and lateral condyles (Conconi et al., 2018).

Natural knee motion requires that ligament isometry be maintained (Wu et al., 2010). Therefore, the origin and insertion of the ACL, PCL, MCL and LCL was identified in each of their respective point clouds as the most isometric fibre during the entire flexion/extension range of motion. Percent elongation was calculated from each's participants initial knee position to evaluate ligament strain during movement (Smale, 2018).

4.8 Principal Component Analysis

Once the simplified patient-specific articular contact spheres were created, the next step was to determine if their centroid locations and radii could be predicted from external parameters, such that MRIs would not be required to establish natural knee motion. Principal component analysis (PCA) is a technique to reduce the dimensionality of large data sets while still preserving as much variation within the original data as possible (Jollife & Cadima, 2016).

Four datasets were conducted to determine the feasibility of reconstructing the articulating contact spheres: (1) using the *OpenSim* coordinates of six lower-limb markers on both the femur and tibia aligned in the MRI reference frame (Table 10-4); (2) using the *OpenSim* coordinates of six *OpenSim* lower-limb markers on both the femur and tibia, with the inclusion of subject anthropometrics (Table 10-6); (3) using the *OpenSim* coordinates of four femoral markers aligned in the reference frame; (4) using the *OpenSim* coordinates of four femoral markers aligned in the reference frame, with the inclusion of anthropometrics. For sets (3) and (4), only the feasibility of recreating the femoral articulating contact spheres was examined.

Table 4-6 Anthropometric measurements used as features

Anthropometric Measurement	Definition
Height	Against wall, standing straight, measure from top of head to ground
Knee Width	Caliper measure between medial and lateral epicondyles
Thigh Circumference	Tape measure around largest portion of the thigh
Shank Circumference	Tape measure around largest portion of the shank
Leg Length	Anterior superior iliac spine to medial malleolus
Tibia Length	Lateral epicondyle to medial malleolus

The MRI-aligned *OpenSim* markers and the articular contact sphere centroids were expanded, such that each unique *x, y* or *z* coordinate was its own unique feature when conducting PCA. For sets (1) and (2), the radii of the lateral and medial components were represented as vectors connecting the two centres, since the imposed constraints are equivalent in musculoskeletal modelling. Each set would produce a unique number of features, *m,* used in the analysis.

Regardless of set performed, a total number of n = 11 participants were used as the training sample for each set, with one participant excluded to validate the prediction. These participants can be organized into a matrix, **P**, where the rows map the coordinates of each marker, sphere centroid and combined femoral/tibial radii in the static position.

$$\boldsymbol{P} = \begin{bmatrix} | & | & & | \\ \mathbf{p}_1 & \mathbf{p}_2 & \cdots & \mathbf{p}_n \\ | & | & & | \end{bmatrix} \tag{2}$$

To calculate the principal components, the eigenvectors of the covariance matrix of the mean-subtracted data were calculated. First, the mean, **u**, is calculated from the rows of **P** and subtracted from each column. A matrix of ones, **h**, allows the mean of each row to be subtracted from **P** such that:

$$\overline{\mathbf{P}} = \mathbf{P} - \mathbf{u}\mathbf{h}^T \tag{3}$$

Once $\overline{\mathbf{P}}$ was obtained, we solved for the covariance matrix of $\overline{\mathbf{P}}$ using Equation 4

$$\mathbf{C} = \frac{1}{n-1}\overline{\mathbf{P}}\overline{\mathbf{P}}^T \tag{4}$$

The eigenvalues of our covariance matrix, **C**, correspond to the variance of each component, while the eigenvectors are the principal components in the data set. The eigenvectors are ordered by decreasing eigenvalue, meaning v1 is the eigenvector corresponding to the largest eigenvalue. To solve for these eigenvectors and eigenvalues, the independent solutions to Equation 5 are identified:

$$\mathbf{C}\mathbf{v}_i = \lambda_i \mathbf{v}_i \tag{5}$$

Now, each participant $\boldsymbol{p}_i$ can be represented as a linear combination of principal components. We can solve for our coefficient matrix, **A**, of the static position by reformatting using the following equation.

$$\mathbf{A} = \mathbf{V}^{-1}(\mathbf{P} - \mathbf{u}\mathbf{h}^T) \tag{6}$$

From here, we can eliminate principal components that have little variance, thus reducing the total order of the system. To identify the ideal number of principal components associated with this system, the variance of each component was summed to determine the cumulative variance of the principal components, with the goal of using the fewest number of components to predict variance (Jollife & Cadima, 2016; Moore et al., 2011). The matrix A can be reduced to a smaller matrix, *k x n*, to explain your desired amount variation in the data set.

In total, we attempted to predict 14 variables from the dataset for sets (1) and (2), and eight variables from sets (3) and (4). All variables correspond to the dimensions of the sphere, leaving either *m-14* or *m-8* variables that could be used to predict the final radius and sphere centroid. Given that there are only 11 participants that are being used as the training sample, there were more features than participants, resulting in an overdetermined set of linear equations. To accommodate this, the Moore-Penrose inverse was used to compute the least-squared solution to the system of linear equations from **P** (Barata & Hussein, 2011). Since **P** is a matrix where $m > n$, and the columns of the matrix are linearly independent, $\boldsymbol{P}^T\boldsymbol{P}$ is invertible, and the pseudoinverse is defined as follows:

$$\mathbf{P}^{+} = (\mathbf{P}^{T}\mathbf{P})^{-1}\mathbf{P}^{T} \tag{7}$$

The pseudoinverse of the modes of variation, $\boldsymbol{Z}^{+}$, multiplied by the mean-subtracted coordinates of marker positions each knee produced a unique reconstruction coefficient, $\boldsymbol{a}$, for each knee. To fully reconstruct each knee, each $\boldsymbol{a}$ must be multiplied by the original modes of variation matrix, $\mathbf{Z}$, before adding the mean. The solutions derived by computing the pseudoinverse of the training sample were then used to predict the expected coordinates and radii of the femur and tibial spheres by multiplying the resultant vector by the known 3D positions of the *OpenSim* marker coordinates and/or anatomical measurements.

4.9 Verification and Validation

For this thesis, the goal of the verification and validation stage is to identify if partially patient specific models are a suitable substitution to total patient specific models, as opposed to traditional scaling techniques discussed in Section 3.5.2. Before complex kinematic motion, specifically from functional movement tasks can be verified, the anatomical similarity of the models generated in Section 10.2.6 must be validated against an independent training sample that has been segmented using traditional patient-specific modelling methods.

For study one, morphological and kinematic differences in the adolescent knee abduction/adduction angles (AAA), internal/external rotation angles (IEA) and translations in *x, y* and *z* will be described, and compared to existing published passive kinematic data. As an additional validation step, ligament lengths during natural knee motion will also be validated against those generated during the two studies defined above. The process of validating output kinematics generated through musculoskeletal modelling is defined by Hicks et. Al (2015). To meet those requirements, kinematic outputs must fall within two standard deviations of existing data to be deemed successful.

For study two, a leave-one-out cross validation (LOOCV) was performed to reduce bias caused by different knees being used to build the model. The PCA and pseudoinverse process in Section 10.2.7 was conducted 12 times, each time with a different knee being used as the independent training sample. Figure 10-7 highlights the workflow for verification and validation for this thesis.

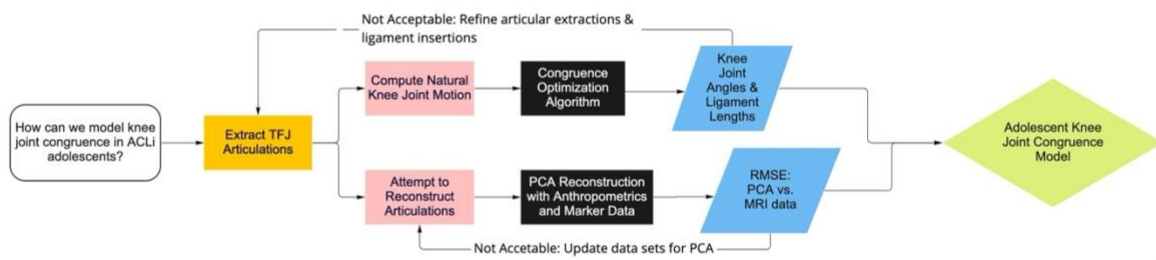

Figure 4-7 Verification & Validation (V&V) flowchart for this thesis

4.10 Statistics

The mean, standard deviation, and mean absolute error for each knee model was recorded for AA, IE and (anterior/posterior, medial/lateral and compression/distraction translations. Additionally, the same parameters were also collected for the changes in length and strain of the ACL, PCL, MCL and LCL. While all patients suffered an ACL tear, the origins could still be identified in the MRIs, and was therefore included for analysis in length. Lastly, a comparison of the original segmented to the optimized sphere radius for each of the four tibiofemoral condyles was computed using the root-mean squared error (RMSE).

CHAPTER 5: MANUSCRIPT 1

DEVELOPMENT OF A CONGRUENCE-BASED MUSCULOSKELETAL MODEL OF THE KNEE IN ANTERIOR CRUCIATE LIGAMENT INJURED ADOLESCENTS

Claire E. Warren[1], Michele Conconi[2], Nicola Sancisi[2], Sasha Carsen[3] and Daniel L. Benoit[4]

1: School of Human Kinetics, University of Ottawa, Canada

2: Department of Industrial Engineering – DIN, University of Bologna, Italy

3: Division of Orthopaedic Surgery, CHEO (the Children's Hospital of Eastern Ontario), Ottawa, Canada

4: School of Rehabilitation Sciences, University of Ottawa, 451 Smyth Rd, Ottawa, Canada

Abstract:

Background: To understand how an individual's joint morphology dictates their motion patterns, researchers have developed patient-specific musculoskeletal models using medical images of the tibiofemoral joint (TFJ). Congruence-based modelling optimizes the configuration of the tibiofemoral joint to reduce pressure during movement, mimicking functional adaptation. However, congruence-based models have not yet been applied to populations undergoing pubertal development. Therefore, the purpose of this research is to build a patient-specific knee model for modelling morphological and congruence-based knee joint kinematics of the adolescent knee. *Methods* Magnetic resonance images (MRI) of 12 adolescent knees with ACL injury (ACLi) were used to segment long bones of the tibiofemoral joint, including cartilage and menisci. Natural knee motion was determined using a previously developed and validated algorithm as the envelope of tibiofemoral configurations that maximize joint congruency during motion. Knee flexion was controlled through two-degree increments from 6 to 108°. Two rotational and three translational degrees of freedom (DOF) were optimized for maximized knee joint congruency, while simultaneously minimizing knee joint pressure. Anatomical reference systems (ARS) were computed by evaluating joint translations through the relative position of ARS origin and orientation through z-y-x cardanic sequence of rotation. Rotational kinematics were reported for all knees, in addition to average range of motion (ROM) across optimized degrees of freedom. Ligament strain was calculated as % elongation for the ACL, PCL, MCL and LCL respectively.

Results: Average ab-adduction and internal-external ROM were 1.05±0.38° and 6.22±1.8°, respectively. Optimized average AP, SI and ML ROM were 2.16±0.54mm 1.84±0.54mm and

1.84 ± 0.48mm. Average ligament strain for the ACL, PCL, MCL and LCL were 2.34± 2.1%, 8.65± 6.2%, 1.41± 0.5% and 1.75 ± 1.6% respectively.

Conclusion: Kinematics of natural knee motion in ACLi adolescents can be derived from patient-specific geometry. Femoral internal/external rotation and anterior/posterior translation varied the most between participants, although more participants are needed. Inter-subject variability in passive kinematic motion derived from patient-specific morphology suggests the need for personalized musculoskeletal models in growing populations.

Key Words: Adolescents, Musculoskeletal Modelling, Principal Component Analysis, Joint Congruence, Patient-Specific Modelling

INTRODUCTION

The anterior cruciate ligament (ACL) is the most frequently injured ligament in the knee (Sanders et al., 2016b), with increasing incidence rates are in paediatric and adolescent populations (Beck et al., 2017; Herzog et al., 2017; L. Shaw & Finch, 2017b). Numerous risk factors associated with increased ACL injury risk have been identified that are both neuromuscular (Flaxman et al., 2014; Romanchuk et al., 2020) and anatomic (Dare et al., 2015; O'Malley et al., 2015) among ACLi deficient children and adolescents. These risk factors can be classified as either modifiable or non-modifiable in nature (Price et al., 2017a). Modifiable concerns the act of execution with regards to mechanisms of ACL injury, such as landing mechanisms or muscular coactivations. These risk factors can be manipulated with movement retraining and/or strengthening surrounding musculature of the knee (Alentorn-Geli et al., 2009; Kristianslund et al., 2014). Non-modifiable risk factors, such as individual joint articulations and tibiofemoral joint (TFJ) morphology, are defined within the first trimester of pregnancy (Carsen et al., 2021) . Morphological differences at the TFJ, such as tibial slope and radius of curvature directly influence knee kinematics, particularly when establishing a baseline of natural knee motion (Conconi et al., 2018; D. A. Lansdown et al., 2017; Wahl et al., 2012a). Yet to the best of our knowledge, differences in natural knee motion in populations undergoing pubertal development have not been explored.

The impact of patient-specific joint articulations on natural knee motion can be studied through the development of personalized musculoskeletal models. These modelling techniques use medical images to build three-dimensional (3D) models of the tibiofemoral joint, and then simulate movement through either optimization and/or marker-based approaches (Conconi et al., 2018; Smale et al., 2019). The inclusion of magnetic resonance images (MRI) in musculoskeletal models has been successfully implemented in adult populations and mitigated kinematic error while maintaining physiological constraints (Brito da Luz et al., 2017; Jaremko et al., 2006; Nardini et al., 2020; Schmid et al., 2009; Smale et al., 2019). These images are particularly useful for this type of modelling, as soft tissue, like articular cartilage, and ligament insertions can be identified from the images in addition to bone from MRI (Gill et al., 2014). Moreover, radiation exposure is minimal when collecting MRIs, making it a suitable technology to collect data from adolescent populations (Lin, 2010). However, MRI-based modelling provides an instantaneous representation of the joint, and it is unclear whether it would produce physiologically representative kinematics in a growing population. Furthermore, the execution of MRI-based simulation is both labor and time intensive, and simplified approaches are needed that can encompass the effects of morphology on movement in an efficient manner.

One method of simplifying MRI-based modelling is through the optimization of joint congruence, an approach developed by Conconi et al (2014). Joint congruency describes how well two articulating surfaces mate together (Schneider et al., 2018). The larger the congruency of a joint, the larger the surface area shared between the two articulating structures (Conconi & Castelli, 2014). This increase in surface area leads to a decrease in overall joint pressure, mimicking the mechanotransduction properties of articular cartilage (Caravaggi et al., 2021; Conconi & Castelli, 2014). With respect to the knee joint, congruence algorithms have been validated using sensitivity analyses (Forlani et al., 2016), and can be applied to 3D tibiofemoral joint contact models to determine the path of unloaded natural knee motion that puts the least amount of pressure on the joint (Conconi et al., 2019, 2021). These models generate a baseline of movement, from which soft tissue deformation of cartilage and ligaments occur after load is applied (Conconi et al., 2021). Furthermore, congruence-based models have been applied to ACL deficient adult populations to decrease kinematic error and improve biofidelity (Smale et al., 2019). However, this modelling has not been conducted on adolescent populations, and it is unknown if natural knee motion can be derived from a congruency model in a growing population.

Therefore, the purpose of this research was to develop a congruence-based knee model that could describe morphological and kinematic differences in the adolescent knee. Knee models were constructed from the MRIs of 12 ACLi adolescents. Congruence was determined using an algorithm developed by Conconi et al. (2018), and ab/adduction, internal/external rotation, anteroposterior, mediolateral and proximodistal translations were optimized to minimize knee joint pressure. Resultant kinematics and changes in ligament length for the ACL, PCL, MCL and LCL were compared to reported literature values to determine physiological validity. It is hypothesized that the average resultant kinematics and ligament lengths will fall within two standard deviations of reported trajectories for passive knee motion (Hicks et al., 2015).

METHODS

Participants

The images of twelve ACL injured participants were recruited from the Children's Hospital of Eastern Ontario (CHEO). This study was approved by both the CHEO and University of Ottawa ethics committees. Inclusion criteria included primary ACL injury, no history of other major lower limb injury prior to study enrolment, and that their MR images were collected at CHEO. Participants were chosen using the Tanner stages of pubertal development (Marshall & Tanner, 1969, 1970) with one male and one female participant from each stage wherever possible, such that a wide range of adolescence was encompassed during model development. Mean values of participant age, height, weight and Tanner stage are summarized in Table 11-1.

Table 5-1 Summary of patient information for those used in the development of the adolescent knee congruency model

Participant Information			
Age (yrs)	Height (cm)	Weight (kg)	Tanner Stage
15.42 ± 1.4	165.8 ± 6.5	67.35 ± 15.6	3.92 ± 1.2

MRI Imaging and Segmentation

A multiplanar sequence of MR images was collected from each participant at 1.5 Tesla, repetition time/echo time 1400/17 ms, field of view: 160 mm and slice thickness 0.8mm (Siemens Magnetom Skyra, Siemens Healthineers AG, Germany) as part of their standard clinical visit following ACL injury. Sagittal, coronal and axial views of proton density cube weighted scans were used to segment the long bones of the lower limb (femur, tibia and fibula) and the medial and lateral menisci (Workbench 2018.04.2, MITK, Germany). The femur, tibia and fibula were segmented to include their respective cartilage, such that the joint could be represented as a single solid with an elastic surface. Femoral and tibial insertion sites of the anterior and posterior cruciate ligaments and medial and lateral collateral ligaments were designated as point clouds on their respective surfaces (Conconi et al., 2018; Smale et al., 2019). Segmented bones and menisci were then smoothed and decimated in *Geomagic Studio* (Geomagic Studio 2012, 3D Systems, USA) and articular surfaces were isolated using *Rhinoceros 3D* (Version 5.0, McNeel & Associates, Seattle, USA).

Anatomical Coordinate Systems

Anatomical coordinate systems (ACS) for the femur, tibia and fibula were defined on the MRI-based bone surfaces using virtual palpation. Axes were constructed using a custom-MATLAB script (2021a, MathWorks, Natick, MA) and were registered to each bone. Coordinate systems were based on the works of Gray et al (2019) and Benoit et al (2006) and summarized in Tables 11-2 and 11-3 respectively. Orientation of the femur (S_f) with respect to the tibia (S_t) was expressed using a ZYX cardanic sequence of rotation. Flexion (+)/extension (-), adduction (+)/abduction (-) and internal (+)/external (-) rotation angles occur about the z, x and y axes of S_f respectively. Translations of the S_f with respect to S_t were expressed in relation to the origin on S_f (O_f), where anterior (+)/posterior (-), proximal (+)/distal(-), and lateral (+)/medial (-) translations take place along the x, y and z axes of S_f.

Table 5-2 Femoral ACS axes and origin summary based on Gray et al (2019) and Benoit et al (2006)

Femur	
X_f	Cross product between Long axis and the Z_f
Y_f	Cross product between Z_f and X_f

Z_f	Vector directed to the right, passing through the centroid of the medial and lateral femoral condyles
O_f	Midpoint between the medial and lateral femoral condyles

Table 5-3 Tibial ACS axes and origin based on Gray et al (2019) and Benoit et al (2006)

Tibia & Fibula	
X_t	Cross product between Y_t and the vector between the tibial plateau vector
Y_t	Long axis vector starting from the midpoint of the tibial eminence
Z_t	Cross product between X_t and Y_t
O_t	Projection of onto Y_t

Joint Congruency and Optimization

Natural knee motion was determined using an algorithm developed by Conconi et al (2021) as the envelope of tibiofemoral configurations that maximize joint congruency. A measure of joint congruency for highly conforming surfaces (i.e., articular cartilage) was defined by Conconi and Parenti-Castelli (2014) based on Winkler's elastic foundation contact model (Johnson, 1985). The ratio between peak pressure and resultant contact force can be estimated based on the ability of a set of given articulating surfaces in any orientation to distribute applied load (Conconi & Castelli, 2014; Johnson, 1985). As a result, joint congruence is maximized when peak pressure is minimized (Conconi & Castelli, 2014). This approach has been validated using in-vitro testing (Forlani et al., 2016), sensitivity analysis (Conconi et al., 2015a) and has been successfully implemented for musculoskeletal modelling in an adult ACL injured population (Smale et al., 2019). It is summarized below for clarity:

Assume a rigid body is indenting a "mattress" of springs of constant stiffness k (N/m^3) resting on a rigid surface. There is no interaction between the adjacent springs of the model (Conconi et al., 2015b; Johnson, 1985).

As reported by Conconi et al. (2014) from Johnson et al. (1985), we can define the displacement of the spring at a position of *(x, y)* as δ (x, y), the contact pressure, p, at the same point can be written as

$$p(x,y) = k\,\delta(x,y) \quad (1)$$

Then we can also confirm that peak pressure, p_0, occurs at the point of maximum displacement, Δ, such that

$$p_0 = k\Delta \quad (2)$$

Allow A to represent the contact surface area projected onto a plane orthogonal to z, and dA to represent the surface area covered by a single spring, which is infinitesimally small. It follows that the resultant force generated by the pressure distribution becomes

$$F = \int_A p(x,y)dA = \int_A k\delta(x,y)dA = k\int_A \delta(x,y)dA = kV \quad (3)$$

Where V is the Boolean intersection between the two surfaces, represented by the dashed area in Figure 11-1 (Conconi et al., 2021).

The resulting equation allows for the ratio of resultant force and peak contact pressure to be expressed solely in geometric terms, giving us an empirical measure of joint congruence, i.e.:

$$\frac{F}{p0} = \frac{kV}{k\Delta} = \frac{V}{\Delta} \qquad (4)$$

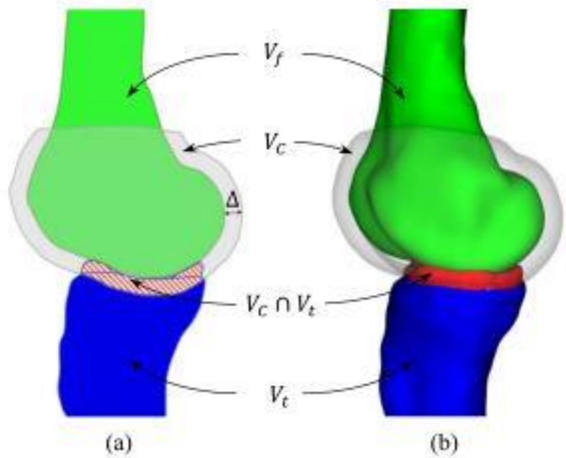

Figure 5-1 A simplified sketch of joint congruency of the femur (V_f) and tibia (V_t). The intersection volume (V_c) represents the volume of the femur with a fixed offset (Δ) applied. Congruence is the Boolean intersection of V_c and V_t

Image From: Conconi et al. (2021), IEEE Trans. Bio. Eng, 68(3),1084-1092

The ratio in Equation 4 provides us with the following information: as this ratio increases, so too does joint congruency, inherently minimizing joint contact pressure. Therefore, for any given configuration, it is possible to measure the congruency of the mating surfaces as the volume intersection between undeformed surfaces and maximum indentation. Equation 4 can also be used as a numerical model, by using a constant Δ and optimizing the configurations of the tibiofemoral envelope that will maximize *V*.

The coupled orientation and position of the femur with respect to the tibia was computed via optimization across individual flexion/extension range of motion originally defined as -10°-134°. Not all participants were able to generate data points over the full range of motion, but coupled positions were able to be identified between 6° and 108° across all participants. Under the condition of a constant value for the offset threshold Δ, the larger the intersection volume, the more congruent the joint will be. Building on the work of Conconi et al (2015), Δ was set at 6 mm to ensure other bone features did not affect the congruence measure, and to maximize the section of articular surface contained within the control volume (Conconi & Castelli, 2014). Following these steps, the most isometric fibre of the ACL, PCL, MCL and LCL were isolated from their respective point clouds, as ligament isometry is preserved during passive knee motion. Ligament length changes during passive knee motion were also recorded at each position of knee flexion, and used to calculate resulting ligament strain.

Statistics

Descriptive statistics of the MRI and optimized simplified articular spheres, optimized DOFs and ligament lengths were calculated over knee flexion angle using MATLAB (MATLAB R2021a. Natick, Massachusetts: The MathWorks Inc.). Individual rotational range of motion (ROM) of ab-adduction angles (AAA) and internal-external rotation angles IEA were computed for all participants. Means and standard deviations of resultant kinematic outputs were compared for physiological accuracy to literature describing the behavior of the knee during natural knee motion.

RESULTS

The lateral tibia (TL) sphere had the largest average radius approximation, both prior to and following optimization (Table 11-5). The average MRI-generated TL was 76.58 mm (± 13.6), while the average optimized TL radius was 75.61 mm (± 14.9). The average medial tibia sphere was larger than both femoral sphere articulations (Table 11-5), with an MRI-generated radius of 38.34 mm (± 6.8) and an optimized radius of 39.91 mm (± 6.31). Both the lateral and medial femur spheres had the smallest radii and less inter-subject variability. The MRI lateral and medial spheres had radii of 23.38 mm (± 5.3) and 22.34 mm (±1.8) respectively (Table 11-

5). Following optimization, the average radii of the lateral and medial femoral condyle spheres decreased to 23.15 mm (± 4.0) and 20.88 mm (± 3.6) respectively (Table 11-5).

Optimized passive knee joint kinematics of the femur relative to the tibia for all 12 knees were plotted against knee flexion and extension angle for each knee including adduction/abduction angle (AAA; Figure 11-2) and interna/external rotation angle (IEA, Figure 11-3), average knee AAA and IEA (Figure 11-4) and translations. The mean AAA total ROM was 1.60º abduction ± 0.7 while mean IEA total ROM was 7.64 º ± 2.3 external rotation. Average translations were the largest in the x direction, calculated as 2.16 mm anteriorly ± 3.4, followed by the z direction at -2.05 mm superiorly ± 1.7 then y, at 0.114 mm laterally ± 0.47 (Figure 11-5). Changes in ligament strain (% elongation) over knee flexion angle were defined for the ACL, PCL, MCL and LCL as 2.34± 2.1%, 8.65± 6.2%, 1.41± 0.5% and 1.75 ± 1.6% respectively (Figure 11-6).

Table 5-4 Coordinates of the four spherical approximation centroids derived from MRI

MRI-Measured Sphere Centroid Coordinates												
	Lateral Femur			**Medial Femur**			**Lateral Tibia**			**Medial Tibia**		
	Cx [mm]	*Cy [mm]*	*Cz [mm]*	*Cx [mm]*	*Cy [mm]*	*Cz [mm]*	*Cx [mm]*	*Cy [mm]*	*Cz [mm]*	*Cx [mm]*	*Cy [mm]*	*Cz [mm]*
Knee01	81.66	-20.98	-4.27	30.45	-23.97	-4.22	85.82	-23.14	34.36	30.76	-30.32	20.00
Knee02	-90.82	-10.97	1.98	-38.92	-30.64	-6.44	-87.01	-12.09	48.69	-36.45	-37.73	-0.80
Knee03	-91.40	-19.20	-4.62	-44.03	-12.27	-6.85	-93.83	-21.23	-95.22	-37.81	-14.29	18.38
Knee04	-89.60	-6.31	30.06	-41.34	-8.05	24.62	-89.61	-17.41	-70.87	-38.13	-12.90	40.35
Knee05	-85.40	-19.75	34.13	-39.89	-33.07	36.36	-85.59	-32.63	-77.06	-39.77	-39.37	45.94
Knee06	-97.97	-4.01	-0.32	-47.42	-15.75	-4.50	-109.87	-8.57	-115.66	-45.33	-22.11	10.15
Knee07	100.61	-16.19	-11.49	51.40	-22.85	-11.63	101.69	-3.31	-97.84	47.79	-24.95	8.55
Knee08	-92.09	-2.67	32.50	-46.02	-9.12	30.63	-97.54	-17.50	-85.68	-46.05	-14.66	38.85
Knee09	-94.26	-5.92	51.82	-38.76	-16.73	43.64	-96.58	-8.41	-38.49	-35.99	-25.46	59.91
Knee10	-93.62	-14.08	15.29	-45.95	-25.58	14.95	-98.19	-11.43	-92.76	-42.62	-31.92	31.92
Knee11	-96.19	21.69	19.72	-46.83	2.61	14.46	-109.01	-2.67	-75.46	-48.55	-4.80	29.88
Knee12	-86.55	-26.44	18.90	-41.43	-31.25	14.26	-88.37	-24.23	-54.59	-38.31	-36.23	18.49

Table 5-5 Radii of the four spherical approximations derived from MRI

MRI Measured Sphere Radii				
	Lateral Femur Radius [mm]	**Medial Femur Radius [mm]**	**Lateral Tibia Radius [mm]**	**Medial Tibia Radius [mm]**
Knee01	22.35	21.30	60.76	47.21
Knee02	25.04	24.65	72.02	32.75
Knee03	21.73	22.78	69.50	48.95
Knee04	21.78	21.93	79.60	39.31
Knee05	21.84	23.36	90.10	34.80
Knee06	21.65	23.02	94.33	38.91
Knee07	39.82	23.86	67.82	43.66
Knee08	20.25	23.07	98.64	32.59
Knee09	21.72	19.43	69.52	37.52
Knee10	22.94	24.62	85.91	42.85
Knee11	21.96	19.93	76.42	36.99
Knee12	19.46	20.12	54.41	24.50

Table 5-6 Coordinates of the four spherical approximation centroids derived via congruence optimization

Optimized Sphere Centroid Coordinates												
	Lateral Femur			**Medial Femur**			**Lateral Tibia**			**Medial Tibia**		
	Cx [mm]	*Cy [mm]*	*Cz [mm]*	*Cx [mm]*	*Cy [mm]*	*Cz [mm]*	*Cx [mm]*	*Cy [mm]*	*Cz [mm]*	*Cx [mm]*	*Cy [mm]*	*Cz [mm]*
Knee01	-0.71	-0.09	-20.65	-3.24	-0.39	26.04	11.52	39.09	-17.20	12.52	15.79	26.74
Knee02	0.98	0.40	23.07	-4.15	-1.91	-26.24	8.17	46.70	22.41	-3.88	7.92	-33.53
Knee03	-0.58	-0.37	25.85	-4.90	-1.51	-28.97	12.92	-86.16	20.74	-11.41	17.34	-37.31
Knee04	-0.21	-0.94	29.59	-0.15	0.11	-27.05	10.33	-94.95	21.38	-3.85	13.54	-32.42
Knee05	-0.45	-0.28	19.09	-2.45	-0.32	-22.60	6.79	-112.53	29.00	5.22	9.88	-29.07
Knee06	0.44	-0.12	21.03	-5.00	-0.35	-21.05	-12.69	-107.42	43.29	9.25	11.85	-28.01
Knee07	3.08	1.78	-19.83	-5.00	-0.87	29.83	14.19	-87.04	-38.22	-5.20	10.57	30.98
Knee08	-2.06	-1.33	20.77	-0.55	-0.59	-20.49	26.03	-119.82	18.22	2.05	10.89	-24.99
Knee09	-0.60	-0.37	23.63	-1.34	1.10	-30.59	-1.64	-87.77	31.97	9.41	13.87	-30.16
Knee10	-0.49	-0.30	19.52	-3.12	-0.61	-23.13	4.87	-104.53	41.95	1.98	15.02	-27.90
Knee11	-3.07	-2.94	30.74	-3.42	-0.89	-21.88	16.25	-92.80	22.85	2.64	15.07	-25.53
Knee12	0.26	0.34	22.28	-0.98	0.16	-17.81	7.29	-70.92	21.45	2.40	5.39	-27.22

Table 5.7 Optimized spherical approximation radii derived via optimization

Optimized Sphere Radii				
	Lateral Femur Radius [mm]	**Medial Femur Radius [mm]**	**Lateral Tibia Radius [mm]**	**Medial Tibia Radius [mm]**
Knee01	21.16	20.77	60.63	46.58
Knee02	21.58	20.44	67.03	34.30
Knee03	22.92	21.10	68.76	46.99
Knee04	22.31	22.20	78.65	39.16
Knee05	21.57	18.36	94.59	35.50
Knee06	24.46	21.06	89.33	43.07
Knee07	34.82	25.54	62.82	44.23
Knee08	21.57	21.79	102.23	36.03
Knee09	24.97	21.72	66.65	42.52
Knee10	21.58	27.47	87.64	47.83
Knee11	21.88	14.95	74.74	35.42
Knee12	19.00	15.12	54.29	27.31

*Table 5.**8** Average sphere radii for MRI-based and optimized spheres*

Sphere Radius (mm)	MRI Measured	Optimized
Lateral Femoral	23.82 ± 5.3	23.15 ± 4.0
Medial Femoral	22.34 ± 1.8	20.88 ± 3.6
Lateral Tibia	76.58 ± 13.6	75.61 ± 14.9
Medial Tibia	38.34 ± 6.8	39.91 ± 6.3

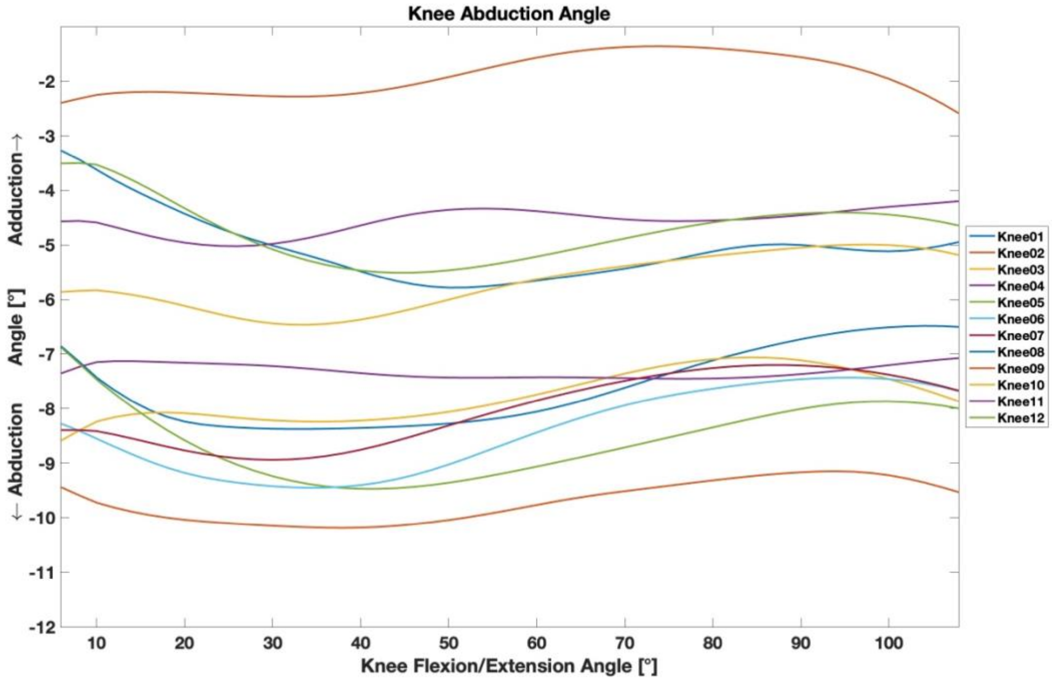

Figure 5-2 Knee ab/adduction angles for all participants during natural knee motion

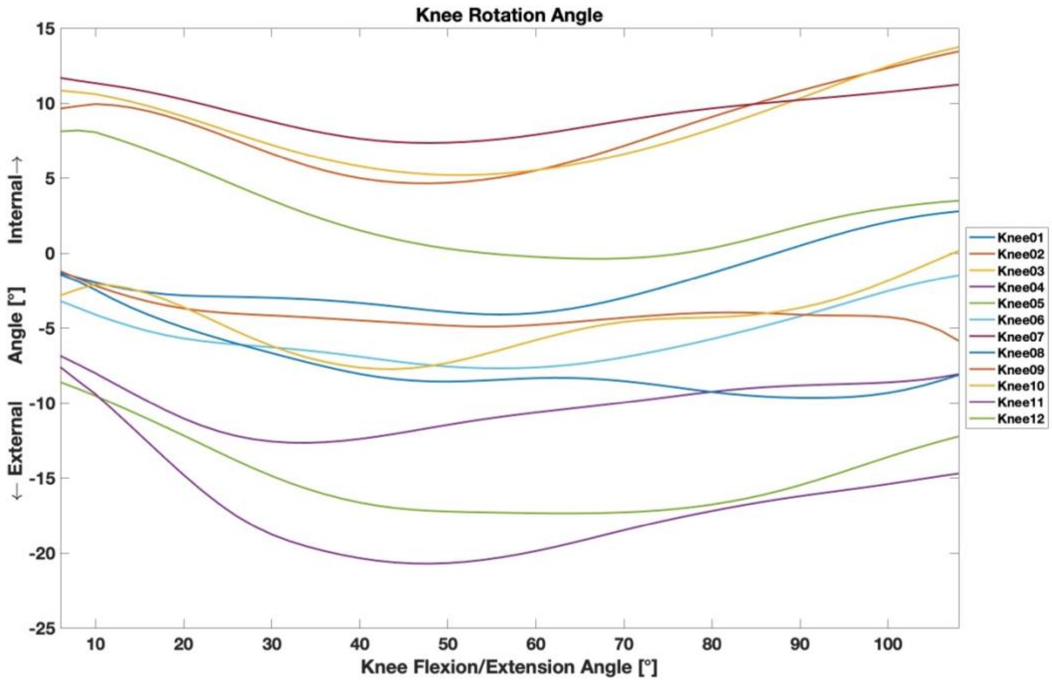

Figure 5-3 Knee internal/external rotation angles for all participants during natural knee motion

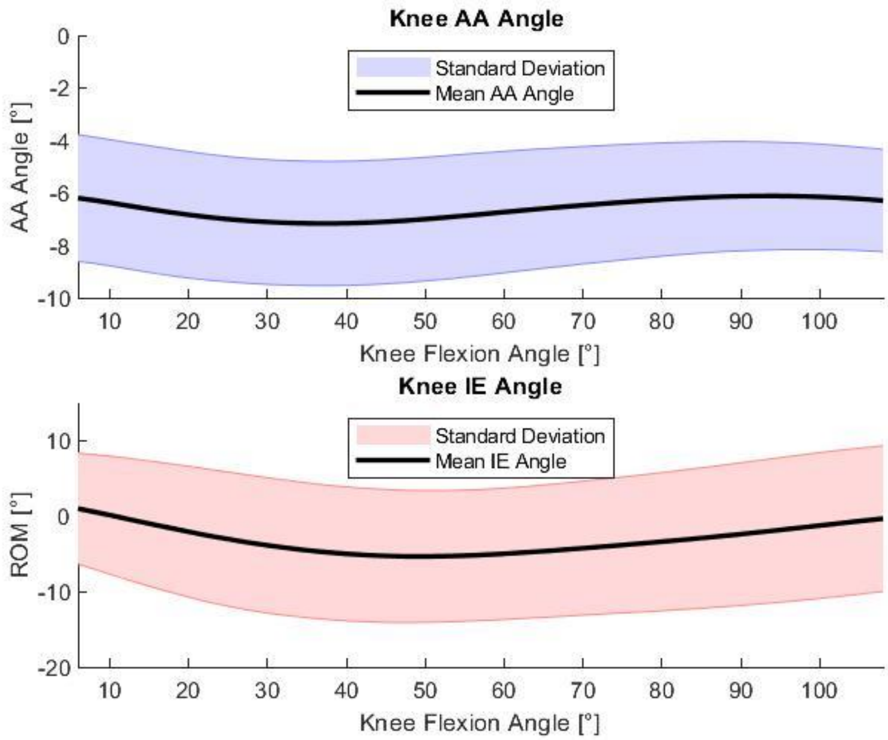

Figure 5-4 Average knee ab/adduction and internal/external rotation angles

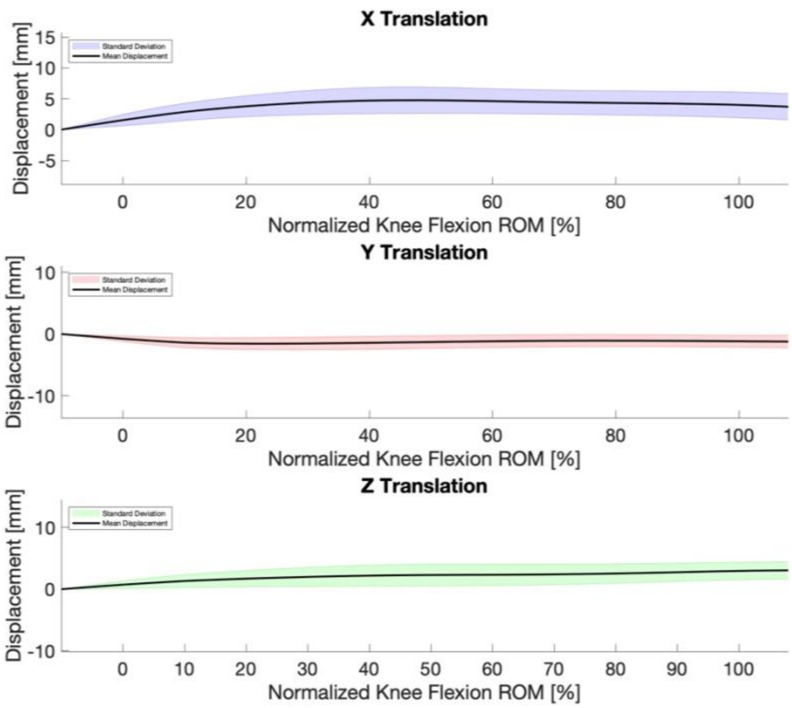

Figure 5-5 Displacement of femur relative to tibia through controlled flexion angle

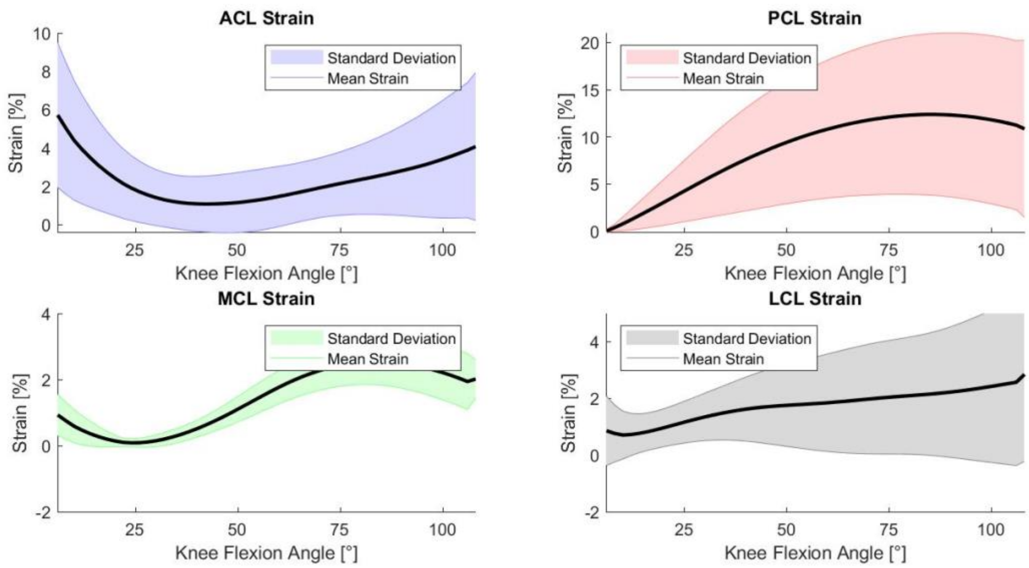

Figure 5-6 Ligament strains of four knee ligaments during controlled knee flexion

DISCUSSION

The purpose of this study was to develop congruence-based knee modelling techniques and build a congruence-based knee model to describe morphological and passive knee kinematic differences in ACLi adolescents. To achieve this MRIs were used to identify and simplify TFJ articulations and ligament insertions, such that TFJ configurations that minimized joint contact pressure could be identified. The resulting tibiofemoral orientations were then used to compute passive knee and ligament kinematics. Of the simplified articular contacts, the TL sphere radius varied the most between participants. Additionally, most participants presented more externally rotated kinematics with a large inter-subject variability, with an average ROM of 7.64 º ± 2.3.

Of the four simplified articular contacts, there was more inter-subject variability between medial and lateral tibial spheres than femoral spheres. The sphere representing the lateral tibial plateau was the largest in radius and exhibited the most variation between participants (76.58 mm ± 13.6). There is significant evidence in adult populations to support that lateral tibial plateau morphology varies substantially between individuals, particularly those who have suffered an ACL injury (Hashemi et al., 2008; D. Lansdown & Ma, 2018; Matsuda et al., 1999). Hashemi et al. (2008) described variations in concavity and convexity of the medial and lateral tibial slopes through magnetic resonance imaging, noting that while the lateral tibial plateau maintains an overall convex shape, the actual region of articulation can at times be quite flat. Fitting a sphere to a flatter articulation would then require a larger sphere to fit the curvature of the plateau, as is supported by Table 11-8. The variation in the condylar contacts is similar to literature on lateral tibial plateau morphology in ACLi adult knees by Wahl et al. (2012). They found that lateral tibial plateau curvature of 33.9 ± 8.89 mm between participants, and a shorter, more convex lateral tibial plateau is conducive with ACL injury risk (Wahl et al., 2012a). It should be noted however that the lower magnitudes of condyle radii could be caused by the method of measurement, as their measurements were made on the magnetic resonance image directly while excluding cartilaginous surfaces. In contrast, our measurements were defined on a segmented bone derived from MRIs, and with the inclusion of articular cartilage. However, the higher variation in lateral tibial plateau curvature when compared to other condylar contacts follows similar trends in adults, suggesting that simplified curvatures of articular contacts may be feasible for defining abnormal knee geometry (Wahl et al., 2012a).

The offset in initial AAA and IEA angles varies across all participants. This offset is due to the ACS alignment between the femur and the tibia prior to optimization. The angle of knee flexion at which the original MRI was collected, the amount of visible diaphysis length in the segmentation and the surface morphological features of the femur and the tibia influence the initial pose prior to optimization. This initial aligned position of femur relative to tibia is therefore unique for each participant. Future studies can mitigate this error by collecting MRIs at a fixed flexion angle (Barzan et al., 2019). Despite this, the trends of each curve for AAA and IEA are similar amongst participants, with the femur transitioning from an abducted and externally rotated position to an adducted and internally rotated position.

The variation in knee ROM between participants was smaller in AAA rather than IEA, as evidenced in Figure 11-2 and 11-3 respectively. Similarly, Benoit et al. (2007) found that similar profiles in AAA/IEA exist during gait analysis. Using *in*-vivo bone pin data, they also found more variance in knee rotation angles, having computed mean joint excursions of 6.0 ± 2.5° for AAA, and 11.0 ± 5.9° for IEA.

Studies have shown how tibiofemoral surface geometry influences knee joint kinematics in ACL injured patients. Mahfouz et al. (2004) demonstrated that lower IEA ROM is present in ACL-deficient knees at higher values of knee flexion when compared to normal knees. Additionally, tibiofemoral surface morphology, such as the tibial slope, influences knee kinematics by increasing femoral rollback. Furthermore, Shelburne et al. (2011) used musculoskeletal modelling to explore how anterior tibial translation is related to tibial slope and found that increasing slopes lead to increases in anterior tibial translation

(Zelle et al., 2010). Since the simplifications of articular contact are defined from the radii of curvature for all four compartments of the TFJ, and since those simplifications are fit to the point of articulation directly, it follows that the tibial slope would be encompassed in the optimization. Those variations in surface structure would elicit differences in kinematics. The convexity of the lateral tibial plateau can increase lateral translational motion in ACL injured knees (Tat et al., 2021), which is in agreement with the z-axis plot of Figure 11-5. Furthermore, the variations in kinematics amongst adolescents could be attributed to the onset of pubertal development. During pubertal development, rapid changes in stature, such as height, mass, skeletal alignment (Hewett et al., 2007) coupled with changes in hormone levels attribute to greater levels in joint laxity (Alentorn-Geli et al., 2009; Price et al., 2017b; Wild et al., 2012). Sample participants range from the peripubertal stage (Tanner stage 2-3) to late-stage pubertal development (Tanner stage 5), which could contribute to the variability in joint angle ROM across participants as well.

The average knee AAA amongst all participants was slightly abducted, with an average of 1.60 º abduction ± 0.6. It was also more externally rotated with a total IEA ROM of 7.64 º ± 2.3. These findings are in agreement with numerous studies, both on knee kinematics of the ACL injured and the "screw-home" mechanism of the knee. Firstly, a more abducted knee has been associated with increased ACL injury and re-injury risks by various researchers (Hewett et al., 2007; Larwa et al., 2021; Paterno et al., 2017). Physiologically, the average rotation of the femur is consistent with behaviours from published literature, where the femur rotates externally during early to mid-flexion, then internally rotates back to its original position as full flexion is reached (Kothari et al., 2012). The asymmetry between the femoral and tibial condyles causes the lateral femoral condyle to roll posteriorly, while the medial condyle remains fixed (Pinskerova et al., 2004).

Variability of the PCL strain was the largest amongst the four ligaments, with a % elongation of 8.65± 6.2%. Additionally, variation in PCL strain values across participants increased towards the end of knee flexion. During passive knee motion, the femur continues to follow the path of femoral rollback, which can increase the strain on the PCL (M. R. Mahfouz et al., 2004; Zelle et al., 2010). These strain rates for passive knee flexion were also in agreement with existing models of passive knee flexion ligament strain in adults. Marieswaran et al. (2018) found that an adult musculoskeletal knee model constructed with articular cartilage, menisci and additional soft tissue capsules would produce ligament strains greater than 10% during knee flexion. Additionally, the average ACL percent elongation was 2.34 ± 2.1%, with similar trends in ACL strain data to Beynnon et al. (1992) through passive range of motion. There are differences in magnitude, with Beynnon et al. (1992) reporting negative values for ACL strain. However, these differences can be attributed to differences in starting point, with Beynnon et al. (1992) starting from 0 º of knee flexion, and our model using the initial orientation of each knee model as the starting position (Beynnon et al., 1992). Figure 11-6 also shows the ACL strain decreases through flexion before increasing at roughly 50 degrees, which is in agreement with the aforementioned findings. This falls within the limits of validity defined by Hicks et al. (2015) and suggests that modelling ligaments as rigid links using properties of isometry during passive knee flexion is an accurate representation of knee joint constraints.

Furthermore, it indicates that segmenting origins and insertions from MRIs of torn ligaments allows researchers to make estimates of ligament lengths during motion, and that fully constrained motion (four ligaments and simplified articular contacts) can be simulated for those missing elements of structural stability (Xu et al., 2015).

Several assumptions were made during the construction of this model. Firstly, the kinematics were computed based on joint congruence, while relying on the traced surfaces of the MRI. While the spheres were determined as those that optimally maintain contacts, it is possible that co-penetration and/or separation determined by the model may take place when applying *in-vivo* captured motion. Too much co-penetration in not physiologically possible, as it indicates non-negligible deformation work is consistently taking place (Conconi & Castelli, 2012). However, simplifying articular contacts in this manner has been shown to successfully replicate kinematic constraints due to condylar contacts, and has been validated in adult populations for both simulating passive motion and functional movement tasks (Conconi et al., 2021; Ottoboni et al., 2010) in ACLi (Smale et al., 2019) and cadaveric knees (Conconi et al., 2021). It was also assumed that both medial and lateral contacts were rigid, to allow for rigid body mechanics modelling through the congruence optimization algorithm(Wilson & O'Connor, 1997).

There are certain limitations regarding the construction of the model as well. Firstly, the registration at the anatomical coordinate system required the virtual palpation of anatomical coordinates and extraction of patient-specific geometry unique to each patient, and the length of the diaphysis available to fit the long axis varied between participants. To accommodate this, a unique function was created to make slices of a defined width of the diaphysis and calculate the centroid of each slice. A line of best-fit was then fit through the centroids to define the long axis. Additionally, although following a standardized procedure, alignment of the participant within the coil during MRI acquisition varied between patients, as differences in anatomy would dictate the required flexion of the knee within the coil. This meant that each knee would be expressed in slightly different reference systems, which could attribute to differences in alignment, and/or in abduction-adduction and rotation angles. Furthermore, the model is dependent on the quality of the articular surface segmentation, which was conducted manually following a training procedure. Despite this, manual segmentation is still commonplace for segmenting MRIs of the knee (Barzan et al., 2019;

Brito da Luz et al., 2017; Clouthier et al., 2019; Conconi et al., 2021; Smale et al., 2019), particularly where knowledge regarding more complex details of the image is unknown (Aprovitola & Gallo, 2016). Additionally, this method is particularly suitable when the bone cartilage interface does not need to be isolated (Aprovitola & Gallo, 2016; Dalvi et al., 2007). Modelling the bone as a single solid allows for less robust segmentation methods to be applied rather than more complex automatic and semi-automatic algorithms (Aprovitola & Gallo, 2016). As such, manual segmentation of bone and soft tissue was appropriate for this study.

The successful construction of patient-specific knee models built using a congruence-based approach has several implications for future research of ACL injuries in adolescents. Firstly, using patient-specific geometry to optimize motion is six DOF provides a more biofidelic representation of the joint as opposed to using a standard hinge, and can be used as a unique baseline of kinematics when calculating joint angles during dynamic tasks. Secondly morphological changes to the joint are finalized during the onset of puberty (Carsen et al., 2021). Simplifying articular contacts to a spherical representation would allow passive knee motion to be modelled as puberty progresses by altering the dimensions of the sphere. This would allow researchers to obtain patient-specific models through the onset of growth or rehabilitation periods without requiring future images.

CONCLUSIONS

Congruence-based modelling produces a unique baseline motion for each participant dictated by their TFJ articulations. Inter-subject variability in passive kinematic motion derived from patient-specific morphology highlights the need for personalized musculoskeletal models in growing populations. Resulting motion follows expected movement patterns while highlighting that individual differences in geometry impact kinematics, and can be used to study pathological deviations in kinematics while considering the effects of TFJ articulation on movement patterns. This leads to more comprehensive research on ACL injury and re-injury mechanisms, particularly throughout adolescence

ACKNOWLEDGEMENTS

The authors would like to thank the Natural Sciences and Engineering Research Council (NSERC) and the University of Ottawa for their financial support during the completion of this research.

CONFLICT OF INTEREST

The authors have no professional relationships that stand to gain from the current study. All results of the present study are presented clearly, honestly and without any falsification or fabrication of the data.

REFERENCES

Alentorn-Geli, E., Myer, G. D., Silvers, H. J., Samitier, G., Romero, D., Lázaro-Haro, C., & Cugat, R. (2009). Prevention of non-contact anterior cruciate ligament injuries in soccer players. Part 1: Mechanisms of injury and underlying risk factors. *Knee Surgery, Sports Traumatology, Arthroscopy*, *17*(7), 705–729.

Aprovitola, A., & Gallo, L. (2016). Knee bone segmentation from MRI: A classification and literature review. In *Biocybernetics and Biomedical Engineering* (Vol. 36, Issue 2, pp. 437–449). PWN-Polish Scientific Publishers.

Bahl, J. S., Zhang, J., Killen, B. A., Taylor, M., Solomon, L. B., Arnold, J. B., Lloyd, D. G., Besier, T. F., & Thewlis, D. (2019). Statistical shape modelling versus linear scaling: Effects on predictions of hip joint centre location and muscle moment arms in people with hip osteoarthritis. *Journal of Biomechanics*, *85*, 164–172. https://doi.org/10.1016/j.jbiomech.2019.01.031

Barata, J. C. A., & Hussein, M. S. (2011). *The Moore-Penrose Pseudoinverse. A Tutorial Review of the Theory*.

Barzan, M., Modenese, L., Carty, C. P., Maine, S., Stockton, C. A., Sancisi, N., Lewis, A., Grant, J., Lloyd, D. G., & Brito da Luz, S. (2019). Development and validation of subject-specific pediatric multibody knee kinematic models with ligamentous constraints. *Journal of Biomechanics*, *93*, 194–203.

Beck, N. A., Lawrence, J. T. R., Nordin, J. D., DeFor, T. A., & Tompkins, M. (2017). ACL tears in school-aged children and adolescents over 20 years. *Pediatrics*, *139*(3).

Brito da Luz, S., Modenese, L., Sancisi, N., Mills, P. M., Kennedy, B., Beck, B. R., & Lloyd, D. G. (2017). Feasibility of using MRIs to create subject-specific parallel-mechanism joint models. *Journal of Biomechanics*.

Caravaggi, P., Assirelli, E., Ensini, A., Ortolani, M., Mariani, E., Leardini, A., Neri, S., & Belvedere, C. (2021). Biomechanical-Based Protocol for in vitro Study of Cartilage Response to Cyclic Loading: A Proof-of-Concept in Knee Osteoarthritis. *Frontiers in Bioengineering and Biotechnology*, *9*.

Carsen, S., Grammatopoulos, G., Zaltz, I., Ward, L., Smit, K., & Beaulé, P. E. (2021). The Effects of Physical Activity on Physeal and Skeletal Development. *JBJS Reviews*, *9*(10), 1–11.

Cheng, H., Garrick, D. J., & Fernando, R. L. (2017). Efficient strategies for leave-one-out cross validation for genomic best linear unbiased prediction. *Journal of Animal Science and Biotechnology*, *8*(1).

Clouthier, A. L., Smith, C. R., Vignos, M. F., Thelen, D. G., Deluzio, K. J., & Rainbow, M. J. (2019). The effect of articular geometry features identified using statistical shape modelling on knee biomechanics. *Medical Engineering and Physics*.

Conconi, M., & Castelli, V. P. (2012). Joint kinematics from functional adaptation: An application to the human ankle. *Applied Mechanics and Materials*, *162*, 266–275.

Conconi, M., & Castelli, V. P. (2014). A sound and efficient measure of joint congruence. *Proceedings of the Institution of Mechanical Engineers, Part H: Journal of Engineering in Medicine*, *228*(9), 935–941.

Conconi, M., Leardini, A., & Parenti-Castelli, V. (2015a). Joint kinematics from functional adaptation: A validation on the tibio-talar articulation. *Journal of Biomechanics*, *48*(12), 2960–2967.

Conconi, M., Leardini, A., & Parenti-Castelli, V. (2015b). Joint kinematics from functional adaptation: A validation on the tibio-talar articulation. *Journal of Biomechanics*, *48*(12), 2960–2967.

Conconi, M., Sancisi, N., & Parenti-Castelli, V. (2018). *Subject-Specific Model of Knee Natural Motion: A Non-invasive Approach*. 255–264.

Conconi, M., Sancisi, N., & Parenti-Castelli, V. (2019). The Geometrical Arrangement of Knee Constraints That Makes Natural Motion Possible: Theoretical and Experimental Analysis. *Journal of Biomechanical Engineering*, *141*(5), 1–6.

Conconi, M., Sancisi, N., & Parenti-Castelli, V. (2021). Prediction of Individual Knee Kinematics from an MRI Representation of the Articular Surfaces. *IEEE Transactions on Biomedical Engineering*, *68*(3), 1084–1092.

Dalvi, R., Abugharbieh, R., Wilson, D. C., & Wilson, D. R. (2007). Multi-contrast MR for enhanced bone imaging and segmentation. *Annual International Conference of the IEEE Engineering in Medicine and Biology - Proceedings*, 5620–5623.

Dare, D. M., Fabricant, P. D., McCarthy, M. M., Rebolledo, B. J., Green, D. W., Cordasco, F. A., & Jones, K. J. (2015). Increased lateral tibial slope is a risk factor for pediatric anterior cruciate ligament injury: An MRI-based case-control study of 152 patients. *American Journal of Sports Medicine*, *43*(7), 1632–1639.

Flaxman, T. E., Smith, A. J. J., & Benoit, D. L. (2014). Sex-related differences in neuromuscular control: Implications for injury mechanisms or healthy stabilisation strategies? *Journal of Orthopaedic Research*, *32*(2), 310–317.

Forlani, M., Sancisi, N., Conconi, M., & Parenti-Castelli, V. (2016). A new test rig for static and dynamic evaluation of knee motion based on a cable-driven parallel manipulator loading system. *Meccanica*, *51*(7), 1571–1581.

Gill, K. G., Nemeth, B. A., & Davis, K. W. (2014). Magnetic Resonance Imaging of the Pediatric Knee. *Magnetic Resonance Imaging Clinics of North America*, *22*(4), 743–763.

Hashemi, J., Chandrashekar, N., Gill, B., Beynnon, B. D., Slauterbeck, J. R., Schutt, R. C., Mansouri, H., & Dabezies, E. (2008). The geometry of the tibial plateau and its influence on the biomechanics of the tibiofemoral joint. *Journal of Bone and Joint Surgery - Series A*, *90*(12), 2724–2734.

Herzog, M. M., Marshall, S. W., Lund, J. L., Pate, V., Mack, C. D., & Spang, J. T. (2017). Incidence of anterior cruciate ligament reconstruction among adolescent females in the United States, 2002 through 2014. *JAMA Pediatrics*, *171*(8), 808–810.

Hewett, T. E., Shultz, S. J., Griffin, L. Y., & American Orthopaedic Society for Sports Medicine. (2007). *Understanding and preventing noncontact ACL injuries*. Human Kinetics.

Hicks, J. L., Uchida, T. K., Seth, A., Rajagopal, A., & Delp, S. L. (2015). Is My Model Good Enough? Best Practices for Verification and Validation of Musculoskeletal Models and Simulations of Movement. *Journal of Biomechanical Engineering*, *137*(2).

Jensen, R. K. (1986). The Growth of Children's Moment of Inertia. *Medicine & Science in Sports & Exercise*, *8*, 440–445.

Johnson, K. L. (1985). *Contact Mechanics*. Cambridge University Press.

Jollife, I. T., & Cadima, J. (2016). Principal component analysis: A review and recent developments. *Philosophical Transactions of the Royal Society A: Mathematical, Physical and Engineering Sciences*, *374*(2065).

Kothari, A., Haughom, B., Subburaj, K., Feeley, B., Li, X., & Ma, C. B. (2012). Evaluating rotational kinematics of the knee in ACL reconstructed patients using 3.0Tesla magnetic resonance imaging. *Knee*, *19*(5), 648–651.

Kristianslund, E., Faul, O., Bahr, R., Myklebust, G., & Krosshaug, T. (2014). Sidestep cutting technique and knee abduction loading: Implications for ACL prevention exercises. *British Journal of Sports Medicine*, *48*(9), 779–783.

Lansdown, D. A., Pedoia, V., Zaid, M., Amano, K., Souza, R. B., Li, X., & Ma, C. B. (2017). Variations in Knee Kinematics After ACL Injury and After Reconstruction Are Correlated With Bone Shape Differences. *Clinical Orthopaedics and Related Research*, *475*(10), 2427–2435.

Lansdown, D., & Ma, C. B. (2018). The Influence of Tibial and Femoral Bone Morphology on Knee Kinematics in the Anterior Cruciate Ligament Injured Knee. In *Clinics in Sports Medicine* (Vol. 37, Issue 1, pp. 127–136). W.B. Saunders.

Larwa, J., Stoy, C., Chafetz, R. S., Boniello, M., & Franklin, C. (2021). Stiff landings, core stability, and dynamic knee valgus: A systematic review on documented anterior cruciate ligament ruptures in male and female athletes. *International Journal of Environmental Research and Public Health*, *18*(7).

Lin, E. C. (2010). Radiation risk from medical imaging. *Mayo Clinic Proceedings*, *85*(12), 1142–1146.

Mahfouz, M. R., Komistek, R. D., Dennis, D. A., & Hoff, W. A. (2004). In vivo assessment of the kinematics in normal and anterior cruciate ligament-deficient knees. *Journal of Bone and Joint Surgery - Series A*, *86*(SUPPL. 2), 56–61.

Marra, M. A., Strzelczak, M., Heesterbeek, P. J. C., van de Groes, S. A. W., Janssen, D. W., Koopman, B. F. J. M., Wymenga, A. B., & Verdonschot, N. J. J. (2018). Anterior referencing of tibial slope in total knee arthroplasty considerably influences knee kinematics: a musculoskeletal simulation study. *Knee Surgery, Sports Traumatology, Arthroscopy*, *26*(5), 1540–1548.

Marshall, W. A., & Tanner, J. M. (1969). Variations in pattern of pubertal changes in girls. *Archives of Disease in Childhood*, *44*(235), 291–303.

Marshall, W. A., & Tanner, J. M. (1970). Variations in the Pattern of Pubertal Changes in Boys. In *Archives of Disease in Childhood* (Vol. 45).

Matsuda, S., Miura, H., Nagamine, R., Urabe, K., Ikenoue, T., Okazaki, K., & Iwamoto, Y. (1999). Posterior tibial slope in the normal and varus knee. *American Journal of Knee Surgery*, *12*((3)), 165–168.

Moore, J. K., Kooijman, J. D. G., Schwab, A. L., & Hubbard, M. (2011). Rider motion identification during normal bicycling by means of principal component analysis. *Multibody System Dynamics*, *25*(2), 225–244.

O'Malley, M. P., Milewski, M. D., Solomito, M. J., Erwteman, A. S., & Nissen, C. W. (2015). The association of tibial slope and anterior cruciate ligament rupture in skeletally immature patients. *Arthroscopy - Journal of Arthroscopic and Related Surgery*, *31*(1), 77–82.

Ottoboni, A., Parenti-Castelli, V., Sancisi, N., Belvedere, C., & Leardini, A. (2010). Articular surface approximation in equivalent spatial parallel mechanism models of the human knee joint: An experiment-based assessment. *Proceedings of the Institution of Mechanical Engineers, Part H: Journal of Engineering in Medicine*, *224*(9), 1121–1132.

Paterno, M. V., Huang, B., Thomas, S., Hewett, T. E., & Schmitt, L. C. (2017). Clinical Factors That Predict a Second ACL Injury After ACL Reconstruction and Return to Sport:

Preliminary Development of a Clinical Decision Algorithm. *Orthopaedic Journal of Sports Medicine*, *5*(12), 1–7.

Pinskerova, V., Johal, P., Nakagawa, S., Sosna, A., Williams, A., Gedroyc, W., & Freeman, M. A. R. (2004). Does the femur roll-back with flexion? *Journal of Bone and Joint Surgery - Series B*, *86*(6), 925–931.

Price, M. J., Tuca, M., Cordasco, F. A., & Green, D. W. (2017a). Nonmodifiable risk factors for anterior cruciate ligament injury. *Current Opinion in Pediatrics*, *29*(1), 55–64.

Price, M. J., Tuca, M., Cordasco, F. A., & Green, D. W. (2017b). Nonmodifiable risk factors for anterior cruciate ligament injury. *Current Opinion in Pediatrics*, *29*(1), 55–64.

Rajagopal, A., Dembia, C. L., DeMers, M. S., Delp, D. D., Hicks, J. L., & Delp, S. L. (2016). Full-Body Musculoskeletal Model for Muscle-Driven Simulation of Human Gait. *IEEE Transactions on Biomedical Engineering*, *63*(10), 2068–2079.

Romanchuk, N. J., Del Bel, M. J., & Benoit, D. L. (2020). Sex-specific landing biomechanics and energy absorption during unanticipated single-leg drop-jumps in adolescents: implications for knee injury mechanics. *Journal of Biomechanics*, *113*, 110064.

Sanders, T. L., Maradit Kremers, H., Bryan, A. J., Larson, D. R., Dahm, D. L., Levy, B. A., Stuart, M. J., & Krych, A. J. (2016). Incidence of anterior cruciate ligament tears and reconstruction: A 21-year population-based study. *American Journal of Sports Medicine*, *44*(6), 1502–1507.

Schneider, A., Si-Mohamed, S., Magnussen, R. A., Lustig, S., Neyret, P., & Servien, E. (2018). Tibiofemoral joint congruence is lower in females with ACL injuries than males with ACL injuries. *Knee Surgery, Sports Traumatology, Arthroscopy*, *26*(5), 1375–1383.

Shaw, L., & Finch, C. F. (2017). Trends in pediatric and adolescent anterior cruciate ligament injuries in Victoria, Australia 2005-2015. *International Journal of Environmental Research and Public Health*, *14*(6).

Smale, K. B., Conconi, M., Sancisi, N., Krogsgaard, M., Alkjaer, T., Parenti-Castelli, V., & Benoit, D. L. (2019). Effect of implementing magnetic resonance imaging for patient-specific OpenSim models on lower-body kinematics and knee ligament lengths. *Journal of Biomechanics*, *83*(November), 9–15.

Suwarganda, E. K., Diamond, L. E., Lloyd, D. G., Besier, T. F., Zhang, J., Killen, B. A., Savage, T. N., & Saxby, D. J. (2019). Minimal medical imaging can accurately reconstruct geometric bone models for musculoskeletal models. *PLoS ONE*, *14*(2), 1–16.

Tat, J., Crapser, D., Alaqeel, M., Schupbach, J., Lee-Howes, J., Tamimi, I., Burman, M., & Martineau, P. A. (2021). A Quantifiable Risk Factor for ACL Injury: Applied Mathematics to Model the Posterolateral Tibial Plateau Surface Geometry. *Orthopaedic Journal of Sports Medicine*, *9*(4), 1–7.

Wahl, C. J., Westermann, R. W., Blaisdell, G. Y., & Cizik, A. M. (2012). An association of lateral knee sagittal anatomic factors with non-contact ACL injury: Sex or geometry? *Journal of Bone and Joint Surgery - Series A*, *94*(3), 217–226.

Wild, C. Y., Steele, J. R., & Munro, B. J. (2012). Why Do Girls Sustain More Anterior Cruciate Ligament Injuries Than Boys? *Sports Medicine*, *42*(9), 733–749.

Wilson, D. R., & O'Connor, J. J. (1997). A three-dimensional geometric model of the knee for the study of joint forces in gait. *Gait and Posture*, *5*(2), 108–115

Wu, J. L., Hosseini, A., Kozanek, M., Gadikota, H. R., Gill IV, T. J., & Li, G. (2010). Kinematics of the anterior cruciate ligament during gait. *American Journal of Sports Medicine*, *38*(7), 1475–1482.

Xu, H., Bloswick, D., & Merryweather, A. (2015). An improved OpenSim gait model with multiple degrees of freedom knee joint and knee ligaments. *Computer Methods in Biomechanics and Biomedical Engineering*, *18*(11), 1217–1224.

Zelle, J., Heesterbeek, P. J. C., De Waal Malefijt, M., & Verdonschot, N. (2010). Numerical analysis of variations in posterior cruciate ligament properties and balancing techniques on total knee arthroplasty loading. *Medical Engineering and Physics*, *32*(7), 700–707.

CHAPTER 6: MANUSCRIPT 2

RECONSTRUCTION OF PATIENT-SPECIFIC TIBIOFEMORAL JOINT ARTICULATIONS FROM MARKER TRAJECTORIES AND ANTHROPOMETRICS

Claire E. Warren[1], Michele Conconi[2], Nicola Sancisi[2], Allison L. Clouthier[1], Sasha Carsen[3] and Daniel L. Benoit[1,4]

1: School of Human Kinetics, University of Ottawa, Canada

2: Department of Industrial Engineering – DIN, University of Bologna, Italy

3: Division of Orthopaedic Surgery, CHEO (the Children's Hospital of Eastern Ontario), Ottawa, Canada

4: School of Rehabilitation Sciences, University of Ottawa, 451 Smyth Rd, Ottawa, Canada

ABSTRACT:

Background: Patient-specific modelling through incorporating magnetic resonance imaging (MRI) improves biofidelity with respect to articulations, particularly at the knee. However, these models can be both labour and time intensive, and access to MRI is not possible for all researchers. The purpose of this research was to determine if patient-specific articulations of the tibiofemoral joint (TFJ) could be approximated from skin surface-based marker positions and anthropometrics in paediatric knees.

Methods: Magnetic resonance images (MRI) of 12 ACL-injured (ACLi) knees were segmented using *MITK Workbench*. Articular surfaces of the femur and tibia were simplified as best-fitting spheres. Six *OpenSim* markers of the lower limb were scaled to patient anthropometrics and extracted. *OpenSim* marker positions were aligned to the MRI reference frame in *Rhinoceros* using *Orient3pt* and visual inspection. Principal component analysis (PCA) was performed to enable reconstruction of the positions and radii of the best fitting spheres from marker trajectories and anthropometric measurements of the leg. Four sets of observations were tested: (1) MRI-Aligned markers of the femur and tibia; (2) MRI-aligned markers of the femur and tibia and anthropometric measurements; (3) MRI-Aligned femur markers only (reconstruct femur only); and (4) MRI-aligned femur markers and anthropometric measurements related to the femur. Average root mean squared error (RMSE) was calculated for all sets.

Results: Of the four sets of features used to run PCA, the combination of markers and anthropometrics related to the femur only (set 4) performed the best. RMSE were under 1mm for reconstructed lateral femoral radii and 5 mm for all reconstructed medial femoral radii. Reconstructed sphere centroids had a RMSE of 9.86 ± 8.8 mm or lower.

Conclusion: This research shows that simplifications of articular contacts can be reconstructed without the requiring use of medical images; however, tibial reconstruction remains a challenge. Eliminating the need for medical images to generate simplifications of articular contacts would make patient-specific modelling accessible to all researchers, regardless of equipment; however, more work is needed to achieve this goal.

Key Words: Adolescents, Musculoskeletal Modelling, Principal Component Analysis, Joint Congruence, Patient-Specific Modelling

INTRODUCTION

Musculoskeletal modelling (MM) techniques have emerged as a method of investigating the complexities of movement through computer simulation (Reinbolt, Seth, & Delp, 2011; Seth et al., 2018). The contribution of individual variables (e.g., kinematics, muscle parameters, etc.) can be modified non-invasively to explore cause-and-effect relationships, define pathological movement patterns, and determine muscle force contributions (De Groote & Falisse, 2021; Sylvester, Lautzenheiser, & Kramer, 2021). With regards to the knee, these models can range in complexity, with the simplest models employing a hinge knee joint to characterize motion (Rajagopal et al., 2016). However, hinge-based knee models can not accurately estimate ab/adduction and rotation angles. Moreover, these models are primarily based on cadaveric studies, and lead to generalities in muscle architecture, joint articulations and surface morphology (Walker, Rovick, & Robertson, 1988).

The inclusion of magnetic resonance images (MRI) in MM at the knee has allowed researchers to study the contributions of individual joint articulations to movement patterns (Barzan et al., 2019; Brito da Luz et al., 2017; Smale et al., 2019). For example, Smale et al. (2019) compared the effects of MRI-based models on knee kinematics during functional movement tasks to models with varying degrees of freedom (DOF) but generic articulations. They found that MRI-generated models produced more physiological solutions to inverse kinematics and ligament strain calculations than generic modelling. MRI-based models also reduced kinematic error from anatomically inaccurate articulations and soft tissue artifact (Smale et al., 2019). In addition to improving biofidelity, MRIs are also a safe method to obtain patient-specific joint articulations in comparison to imaging techniques that require radiation exposure or more invasive techniques (Lin, 2010). However, MRI-based modelling is both labour and time-intensive, and its advantages in physiological accuracy are limited by its issues in accessibility on a global scale. As such, a method that could leverage the use of a smaller number of MRI-based images as the basis for a scalable, yet anatomically customizable and accessible, model would be ideal.

Principal component analysis (PCA) has been used predict outcomes from sparse datasets (Clouthier et al., 2019; Lynch et al., 2019; Saliba, Clouthier, Brandon, Rainbow, & Deluzio, 2018). Clouthier et al. (2019) used PCA to reconstruct articular cartilage morphology and identify variations in particular surface geometry at the knee for the patellofemoral joint (PFJ) and tibiofemoral joint (TFJ). Saliba et al. (2018) used PCA to predict knee joint contact forces from external methods during gait retraining. However, to the best of our knowledge, PCA has not been used to reconstruct joint articulations solely from external measurements. Moreover, it is unclear whether PCA reconstruction of joint articulations is possible in a population undergoing changes in morphology due to pubertal development.

Therefore, the purpose of this research was to determine if patient-specific joint articulations could be reconstructed from external measurements in an adolescent population. To realise this, four simplified spherical representations of articular contact were generated from adolescent MRIs for the medial/lateral components of the femur and tibia. Following extraction, four combinations of marker trajectories and/or anthropometric measurements were used as features to reconstruct centroid and radii measurements of these simplified spheres. It was hypothesized that the root mean square error (RMSE) between the MRI-extracted and predicted articular contacts would be below 5mm for sets including both anthropometric and marker-based data, similar to existing morphological reconstruction studies (Bahl et al., 2019; Suwarganda et al., 2019).

METHODS

Participants

The images of twelve ACL injured participants were selected from a larger database of participants involved in a collaborative study between the Children's Hospital of Eastern Ontario (CHEO) and the University of Ottawa. Inclusion criteria were primary ACL injury, no other history of major lower limb injury prior to enrolment, and MRI collection at the CHEO institute. Participants were chosen to ensure the five Tanner stages of pubertal development (Marshall and Tanner, 1970, 1969) were represented in model development. Anthropometric measures of the lower limb used in the analysis can be found in Table 1-A of the Appendix. Mean values of participant age, height, weight and Tanner stage are summarized in Table 12-1. This study was approved by both the CHEO and University of Ottawa ethics committees (H09-17-10).

Table 6-1 Patient demographics of the 12 ACLi subjects

Participant Information			
Age (yrs)	Height (cm)	Weight (kg)	Tanner Stage
15.42 ± 1.4	165.8 ± 6.5	67.35 ± 15.6	3.92 ± 1.2

MRI Imaging and Segmentation

A multiplanar sequence of MR images was collected at 1.5 Tesla, repetition time/echo time of 1400/17 ms, field of view of 160 mm and slice thickness of 0.8mm (Siemens Magnetom Skyra, Siemens Healthineers AG, Germany). Sagittal, coronal and axial views of proton density (PD) cube weighted scans were used to segment the distal third of the femur, the proximal third of the tibia and fibula and the medial and lateral menisci (Workbench 2018.04.2, MITK, Germany). The femur, tibia and fibula were segmented to include their respective cartilage, such that the joint could be represented as a single solid with an elastic, highly deformable surface (Conconi et al., 2021; Johnson, 1985). Femoral and tibial insertion sites of the anterior and posterior cruciate ligaments and medial and lateral collateral ligaments were designated as point clouds on their respective surfaces (Conconi et al., 2018;

Smale et al., 2019). Segmented bones and menisci were then smoothed using *Geomagic Studio* (Geomagic Studio 2012, 3D Systems, USA) and articular surfaces were isolated and clipped using *Rhinoceros 3D* (Version 5.0, McNeel & Associates, Seattle, USA). The anatomical coordinate system (ACS) of the MRI frame was based on the work of Gray et al (2019) and Benoit et al (2006) and is defined in Tables 12-2 and 12-3 respectively.

Table 6-2 Femoral anatomical coordinate system (ACS) axes and origin summary based on Gray et al (2019) and Benoit et al (2006)

Femur	
$\mathbf{X_f}$	Cross product between Long axis and the Z_f
$\mathbf{Y_f}$	Cross product between Z_f and X_f
$\mathbf{Z_f}$	Vector directed to the right, passing through the centroid of the medial and lateral femoral condyles
$\mathbf{O_f}$	Midpoint between the medial and lateral femoral condyles

Table 6-3 Tibial anatomical coordinate system (ACS) axes and origin based on Gray et al (2019) and Benoit et al (2006)

Tibia & Fibula	
$\mathbf{X_t}$	Cross product between Y_t and the vector between the tibial plateau vector
$\mathbf{Y_t}$	Long axis vector starting from the midpoint of the tibial eminence
$\mathbf{Z_t}$	Cross product between X_t and Y_t
$\mathbf{O_t}$	Projection of O_f onto Y_t

MRI Frame Alignment

Segmented long bones were imported into *Rhinoceros 3D*, along with full-length generic femur and tibia model taken from the Rajagopal lower limb model (Rajagopal et al., 2016) developed for *OpenSim* (Smale et al., 2019). The full-length generic bones were then aligned to the MRI bones using knee joint centre, medial epicondyle and hip joint centre markers, with the goal of expressing anatomical landmarks from the *OpenSim* reference frame in a common MRI reference frame. For each set of MRI bones, the medial and lateral epicondyles of the knee were obtained through virtual palpation. The knee joint centre was defined as the midpoint between the two epicondyles in the frontal plane, and a planar approximation of the hip joint centre was defined for the deprecated MRI femur (Smale, 2018; Smale et al., 2019). From *OpenSim*, markers of the anterior superior iliac spine, hip joint centre, medial and lateral epicondyles and medial and lateral malleoli were exported in both the femur and the tibia reference frames respectively. The markers in the femoral reference frame were matched to a generic femur (Rajagopal et al., 2016) and then scaled using anthropometric measurements of leg length, tibia length and knee width that had been measured at the University of Ottawa. Leg length was measured with a measuring tape from the anterior superior iliac spine (ASIS) to the medial malleolus, while tibia length was measured from the lateral epicondyle to the lateral malleolus. Knee width was measured with calipers between the medial and lateral epicondyles.

This process was repeated for markers in the tibial reference frame using the generic tibia and was scaled using the same scale factors from anthropometric measures used in the femoral reference frame (Smale et al., 2019). The set of markers used in alignment, in addition to the set of scaling factors used, were defined in Tables 12-4 and 12-5 respectively. The generic bones and their corresponding marker set then underwent a two-part alignment: firstly, using the built-in *Rhino* function *Orient3pt* (Figure 12-1), markers for the medial epicondyles of the knee, the knee joint centre and an approximation of the hip joint centre were used to align the orientation of the generic bones to the MRI bones. Then, using visual inspection, the generic bone was manually adjusted if needed to maximize the volume shared between the MRI bones and the generic bones.

Table 6-4 Lower limb reflective surface markers used in alignment

Lower Leg Body	Anatomical Landmark
Hip Markers	Hip Joint Centre (HJC), Anterior Superior Iliac Spine (ASIS)
Knee Markers	Medial Epicondyle (MKNL), Lateral Epicondyle (LKNL)
Ankle Markers	Medial Malleolus (MANL), Lateral Malleolus (LANL)

Table 6-5 Scaling factors applied to generic bones using marker pairs

Scaled Component (direction)	Marker Pairs
Total Leg Length (y)	ASIS to MANL
Leg Width (z)	MKNL to LKNL
Tibia Length (y)	LKNL to LANL

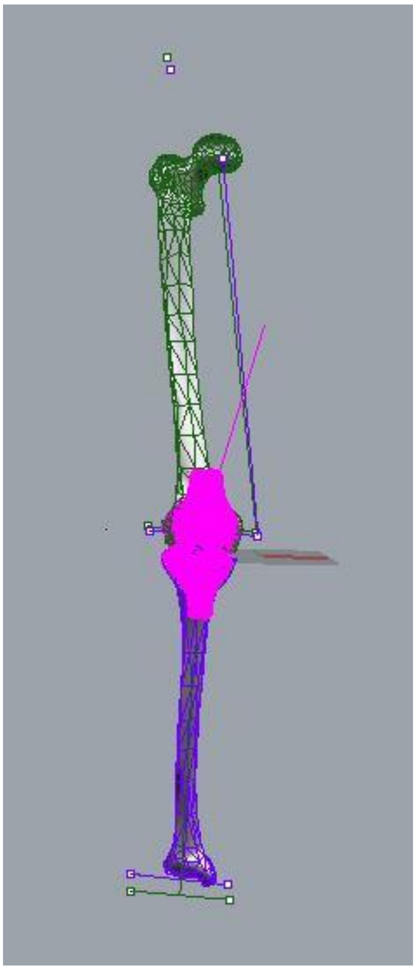

Figure 6-1 Alignment of MRI bones (pink) and generic OpenSim femur (green) and tibia (purple). White squares at the end of each solid line represent scaled OpenSim marker trajectories.

Patient Specific Sphere Definition

An approximation of both the femoral and tibial condyles was created from the contours of the segmented bones using *Geomagics* (Geomagic Studio 2012, 3D Systems, USA). These spheres are simplified representations of the articulating surfaces of the femur and tibia and were used to define patient specific natural knee motion, as defined by Conconi et al (2014). The centre of each medial and lateral sphere and its radius were extracted and optimized (maximum allowable variation: ±2 mm), to ensure medial and lateral contact over the entire range of motion. Additionally, the concave and convex natures of the medial and lateral tibial plateaus produced proximal medial and distal lateral contact spheres respectively.

Principal Component Analysis

Principal component analysis (PCA) was performed to identify features to be used in reconstructing patient-specific spheres from aligned marker trajectories and anthropometric measurements (see Table 12-6 for the measurements evaluated as PCA features). In total, four sets of features were used to build the PCA matrix, **P**, as described by Moore et al. (2011) to reconstruct articular contacts. The sets were: (1) the *OpenSim* coordinates of six lower-limb markers on both the femur and tibia aligned in the MRI reference frame (Table 12-4); (2) the *OpenSim* coordinates of six *OpenSim* lower-limb markers on both the femur and tibia, with the inclusion of subject anthropometrics (Table 12-6); (3) the *OpenSim* coordinates of four femoral markers aligned in the reference frame; (4) the *OpenSim* coordinates of four femoral markers aligned in the reference frame, with the inclusion of anthropometrics. For sets (3) and (4), only the feasibility of recreating the femoral articulating contact spheres was examined.

Table 6-6 Anthropometric measurements used in PCA sets (2) and (4)

Anthropometric Measurement	Definition
Height	Against wall, standing straight, measure from top of head to ground
Knee Width	Caliper measure between medial and lateral epicondyles
Thigh Circumference	Tape measure around largest portion of the thigh
Shank Circumference	Tape measure around largest portion of the shank
Leg Length	Anterior superior iliac spine to medial malleolus
Tibia Length	Lateral epicondyle to medial malleolus

The MRI-aligned *OpenSim* markers and the articular contact sphere centroids were expanded, such that each unique *x, y* or *z* coordinate was its own unique feature when conducting PCA. For sets (1) and (2), the radii of the lateral and medial components were represented as a rigid link connecting the two centres, since the imposed constraints are equivalent in musculoskeletal modelling. Since the number of markers and the inclusion of anthropometric measures varied between sets, the number of features, *m,* was also unique to each set. It total, there were 31 features in set (1), 38 in set (2), 19 in set (3) and 23 in set (4).

Regardless of data set used, a total number of 11 *(n)* participants were included as the training sample for each set, with one participant excluded to validate the prediction. Features corresponding to the marker trajectories and anthropometrics (when applicable) were used to predict the centroid *x, y* and *z* coordinates and radii of the patient-specific spheres. The pseudoinverse of the modes of variation multiplied by the mean-subtracted coordinates of marker positions each knee produced a unique reconstruction coefficient for each knee. To fully reconstruct each knee, each coefficient must be multiplied by the original modes of variation matrix before adding the mean. A leave-one-out cross-validation (LOOCV) was performed to ensure each knee was equally considered as part of the training sample or the validation sample (Cheng et al., 2017). The root mean squared error (RMSE) between the predicted marker and sphere location to the original patient-specific location was calculated at each iteration of the cross-validation. Resulting RMSEs were averaged to determine the effectiveness of the predictive model.

RESULTS

Ten principal components were identified from the PCA analysis and used to reconstruct the centroid positions and radii of each of the articular contact spheres in each of the four sets. A LOOCV was performed to ensure each knee was equally considered as part of the sample used to build the PCA matrix and to conduct the predictions. The original centroid positions and radii of all four articulation simplifications are presented in Table 12-7, while the average root means squared error (RMSE) after LOOCV between the predicted sphere geometry is presented in Table 12-8.

The lateral tibia (TL) sphere had the largest mean radius and inter-subject variation, measuring 76.58 ± 13.6 mm across all knees. The medial tibia, TM, followed in size and variation, with an average radius of 38.38 ± 6.8 mm. Both average tibial spheres were larger than average lateral femur (FL) and medial femur (FM) articulations, which measured 23.15 ± 4.0 mm and 20.88 ± 3.6 mm respectively.

For set one, using all marker positions to predict both tibial and femoral condyle positions and radii, there were large errors between the expected and predicted results across all metrics. The largest centroid position error occurred when predicting the z-coordinate of the TL condyle (RMSE = 173.92 ± 135.30 mm), and the predicted lateral and medial combined radii had errors of 39.07 ± 35.11 and 20.38 ± 26.98 mm respectively. These errors decreased in set two, with the addition of anthropometric measurements of the lower limb and total height. The largest centroid position error occurred once again at z-coordinate of the TL, with RMSE of 51.87 ± 31.35 mm. Combined radii of the lateral and medial contacts decreased to 22.76 ± 20.20 mm and 21.20 ± 17.84 mm respectively.

Sets three and four focused on recreating solely the femoral articular contact spheres. Set three used only marker positions related to the hip and knee to predict FL and FM respectively. The largest centroid position error occurred this time at the z-coordinate of FM, measuring 31.80 ± 47.24 mm. Predicted FL radii error were much lower than predicted FM radii errors. Average RMSE of the FL radii was calculated as 1.77 ± 2.66 mm, while average FM RMSE measured 17.28 ± 26.11 mm in comparison.

Set four used the combination of hip and knee markers in combination with anthropometric measurements related to the femur to predict FL and FM centroids and radii. It also showed the best results with cross-validation, with all RMSEs following prediction measuring less than 10mm. The x-coordinate of the lateral femur produced the largest errors, with average RMSE calculated as 9.68 ± 8.83mm. Reconstructed radii of FL and FM produced errors of 0.44 ± 0.31 mm and 4.89 ± 4.94 mm respectively.

Table 6-7 MRI measured centroid position and sphere radii date for simplified articular contacts

	MRI Measured																
	Lateral Femur				Medial Femur					Lateral Tibia				Medial Tibia			
	C_x *[mm]*	C_y *[mm]*	C_z *[mm]*	r [mm]	C_x *[mm]*	C_y *[mm]*	C_z *[mm]*	r [mm]		C_x *[mm]*	C_y *[mm]*	C_z *[mm]*	r [mm]	C_x *[mm]*	C_y *[mm]*	C_z *[mm]*	r [mm]
Knee01	81.66	-20.98	-4.27	22.35	30.45	-23.97	-4.22	21.30	**Knee01**	85.82	-23.14	34.36	60.76	30.76	-30.32	20.00	47.21
Knee02	-90.82	-10.97	1.98	25.04	-38.92	-30.64	-6.44	24.65	**Knee02**	-87.01	-12.09	48.69	72.02	-36.45	-37.73	-0.80	32.75
Knee03	-91.40	-19.20	-4.62	21.73	-44.03	-12.27	-6.85	22.78	**Knee03**	-93.83	-21.23	-95.22	69.50	-37.81	-14.29	18.38	48.95
Knee04	-89.60	-6.31	30.06	21.78	-41.34	-8.05	24.62	21.93	**Knee04**	-89.61	-17.41	-70.87	79.60	-38.13	-12.90	40.35	39.31
Knee05	-85.40	-19.75	34.13	21.84	-39.89	-33.07	36.36	23.36	**Knee05**	-85.59	-32.63	-77.06	90.10	-39.77	-39.37	45.94	34.80
Knee06	-97.97	-4.01	-0.32	21.65	-47.42	-15.75	-4.50	23.02	**Knee06**	-109.87	-8.57	-115.66	94.33	-45.33	-22.11	10.15	38.91
Knee07	100.61	-16.19	-11.49	39.82	51.40	-22.85	-11.63	23.86	**Knee07**	101.69	-3.31	-97.84	67.82	47.79	-24.95	8.55	43.66
Knee08	-92.09	-2.67	32.50	20.25	-46.02	-9.12	30.63	23.07	**Knee08**	-97.54	-17.50	-85.68	98.64	-46.05	-14.66	38.85	32.59
Knee09	-94.26	-5.92	51.82	21.72	-38.76	-16.73	43.64	19.43	**Knee09**	-96.58	-8.41	-38.49	69.52	-35.99	-25.46	59.91	37.52
Knee10	-93.62	-14.08	15.29	22.94	-45.95	-25.58	14.95	24.62	**Knee10**	-98.19	-11.43	-92.76	85.91	-42.62	-31.92	31.92	42.85
Knee11	-96.19	21.69	19.72	21.96	-46.83	2.61	14.46	19.93	**Knee11**	-109.01	-2.67	-75.46	76.42	-48.55	-4.80	29.88	36.99
Knee12	-86.55	-26.44	18.90	19.46	-41.43	-31.25	14.26	20.12	**Knee12**	-88.37	-24.23	-54.59	54.41	-38.31	-36.23	18.49	24.50

Table 6-8 RMSE between MRI predicted sphere parameters and PCA generated sphere parameters

RMSE of Articular Contact Sphere Reconstruction								
	All Markers		**All Markers, All Anthropometrics**		**Femur Markers Only**		**Femur Markers & Anthropometrics Only**	
Feature [mm]	RMSE [mm]	SD [mm]	RMSE [mm]	SD [mm]	RMSE [mm]	SD [mm]	RMSE [mm]	SD [mm]
TLx	40.18	34.23	18.03	13.23	----	----	----	----
TLy	63.61	42.65	20.31	17.31	----	----	----	----
TLz	173.92	135.30	51.87	31.35	----	----	----	----
TMx	20.13	13.12	8.67	8.20	----	----	----	----
TMy	21.76	14.75	11.68	10.49	----	----	----	----
TMz	6.65	7.49	5.57	4.03	----	----	----	----
FLx	10.33	15.65	12.16	10.78	25.15	37.82	9.68	8.83
FLy	4.54	4.77	12.98	12.80	4.54	6.76	5.07	4.66
FLz	7.66	8.31	6.82	5.28	9.15	14.29	5.52	4.14
FMx	17.77	15.66	10.68	8.01	25.83	38.56	7.20	8.98
FMy	12.72	11.95	13.45	14.49	25.72	38.19	6.64	8.88
FMz	15.11	13.38	12.13	10.43	31.80	47.24	4.37	4.25
Radius TL+FL	39.07	35.11	22.76	20.20	----	----	----	----
Radius TM-FM	20.38	26.98	21.20	17.84	----	----	----	----
Radius FL	----	----	----	----	1.77	2.66	0.44	0.31
Radius FM	----	----	----	----	17.28	26.11	4.89	4.94

DISCUSSION

The purpose of this research was to determine if patient-specific joint articulations could be reconstructed from external measurements in an adolescent population. To achieve this we used PCA to predict the centroid positions and radii for simplified articular contacts obtained from external marker locations and anthropometric measurements. Four combinations of different features were used to build the prediction matrices and the RMSE between the MRI-extracted (Warren et al., 2022) and predicted articular contacts were compared. It was hypothesized that the root mean square error (RMSE) between the MRI-extracted and predicted articular contacts would be below 5 mm for data sets including both anthropometric and marker-based data. This hypothesis was rejected since all approaches produced errors above 5 mm. Set 4 performed the best, with a largest mean RMSE of 9.86 ± 8.8 mm and predicted radii of 0.44 ± 0.31 mm and 4.89 ± 4.9 mm for the FL and FM respectively.

Average radii size varied for each of the four approximations of medial and lateral tibiofemoral articulations. The lateral tibial condyle, TL was the largest in size and varied the most between participants, with a condyle radius of 76.58 ± 13.6 mm. The asymmetry of the tibial plateau, specifically the individual variation of the lateral tibial plateau, has been studied extensively by others. Quintens et al. (2019) used PCA to study tibia asymmetry in adults, finding that five principal components contributed to 98.8% of the total variation between subjects with tibia fractures. While total tibia length and width was the largest principal component, the second largest contributor to variation was identified as medial tibial plateau size. More valgus tibias were linked to smaller medial tibial plateaus, and also exhibited steeper posterior tibial slopes. Wahl et al. (2012) and Tat et al. (2021) also determined that increases in convexity and lateral tibial slope correlated with ACL injury. Furthermore, Wahl et al. (2012)

added that the anterior-posterior length of the lateral tibial plateau is shorter in ACLI patients, measuring 33.9 mm in ACLi adolescents compared to 37.5 in healthy ones. Hashemi et al. (2008) described the lateral tibial plateau as convex overall in nature, but relatively flat at the point of articulation, which would explain the variations in size of the simplified contacts. Fitting a sphere to a flat articulation point would increase the size of the radius that would best-fit TL, as the spheres were created based on said region and not the radius of curvature of the entire plateau. These variations in TL and TM centroid positions and radii also translated into poor results when attempting to reconstruct the tibial spheres for sets one and two, with RMSE measuring above 17mm when attempting to reconstruct certain position trajectories. However, the aforementioned variation caused by tibial plateau asymmetry is likely the cause of these errors. With high variability across the TL (SD = 13.6 mm) and a small sample size, recreating specific morphology would require more information when conducting PCA. Additionally, significant differences in tibial plateau slope (Dare et al., 2015; Todd, Lalliss, Garcia, DeBerardino, & Cameron, 2010), radius of curvature (Hashemi et al., 2008) and overall shape (Clouthier et al., 2019; Lansdown & Ma, 2018) have been reported between sexes (Wahl, Westermann, Blaisdell, & Cizik, 2012) and across various ethnicities (Mahfouz, Fatah, Bowers, & Scuderi, 2012). It is possible that there is too much variation in the tibia to classify from external markers alone. Future studies should consider reconstructing these articulations with the addition of morphological measurements taken from medical images directly, or from a larger data of ACLi adolescents.

By comparison, PCA performed better when attempting to reconstruct FL and FM only in sets three and four. Specifically, RMSE was the lowest when including only femoral marker trajectories and anthropometrics. It follows that PCA performance improved with the addition of anthropometrics, as they provided additional dimensions to the size and shape of the spheres. The success of set four in particular is the most interesting, as all reported RMSE were below values of 10 mm (1cm) and all reconstructed radii had errors below 5mm. This can be attributed to both the simplicity of the distal femur morphology, but also its evolutionary progression since the discovery of a protoknee in tetrapods (Dye, 1987). Simple geometry, specifically 2-dimensional circles, have been successfully used to define variations in distal femur geometry from MRIs for modelling purposes (Monk, Choji, O'Connor, Goodfellow, & Murray, 2014). Furthermore, while there is morphological variation between the lateral and medial femoral condyles, the shape of the distal femur has remained relatively static since the Devonian period (Dye, 2003). It therefore falls within reason that the model would have success predicting simplified femoral geometry.

There are some limitations that should be considered. Firstly, alignment angle of the MRI was dictated by the anatomy of the participant to ensure that they fit into the coil, and not collected at a controlled angle. This does not impact the ability to extract simplified articular contacts; however, it would produce differences in alignment of the tibiofemoral joint. As a result, the alignment of the marker positions to the MRI segmented bones would reflect these differences in alignment. This was addressed by using *OpenSim* markers fit with patient-specific anthropometrics for the alignment in lieu of Vicon markers. This ensured all markers were scaled to the same location and would all fall along the same axes during alignment in *Rhino*. Furthermore, there were few participants selected for this study, but this was addressed through the LOOCV, assuring that the variation between participants was responsible for errors produced, not the selection of participants for each group. Increasing the number of participants would likely lead to improved results. Nevertheless, the sample encompassed a wide range of knee sizes at several different pubertal stages, showing that this model is able to predict patient-specific contacts from external measurements in a developing population.

The successful development of this model has several benefits for clinical practice. Firstly, it shows that it is possible to predict patient-specific articulations from external measurements alone, provided the population used in development is diverse enough to capture variation in bone morphology due to sex and puberty level. An improved model would eliminate the need for medical images to generate biofidelic models of tibiofemoral contact, which could be used to derive natural knee motion. This would make patient-specific imaging more accessible on a global scale. Furthermore, using only external measurements allows the model to be easily scaled to accommodate rapid changes in growth, like when pubertal development and ACL injury rehabilitation occur simultaneously. Future directions should explore adding additional measures to the model that could better quantify the variation in tibial plateau morphology. For example, rather than trying to predict both femoral and tibial geometry from external skin measurements, a robust range of shapes of the femur and tibia through adolescence could be used to build a shape model to improve predictions. This model could be used in conjunction with weighting existing scale factors to improve PCA predictions. Additionally, future model users could use this approach to estimate patient-specific articular geometry, as variations in tibial plateau radius of curvature are difficult to account for using solely external measurements. Knee motion derived from predicted articular contacts should be compared against motion generated by its true geometry, to validate generation of patient-specific kinematic data without patient-specific articulations.

CONCLUSION

This proof of concept study predicted patient-specific approximations of articular contact from various combinations of marker trajectories and anthropometrics. When compared to MRI-extracted articular contacts, set (4) performed the best (i.e., RMSE between MRI and predicted articular contacts were the lowest) and yielded similar results, however above our hypothesised 5mm error. Additionally, we discovered that femoral simplifications of articular contacts were easier to predict from skin-surface markers and anthropometrics than tibial simplifications. This work contributes to a future where the construction of patient-specific models does not require access to medical imaging that can considers various differences in personalized tibiofemoral morphology while accommodating periods of growth.

ACKNOWLEDGEMENTS

The authors would like to thank the Natural Sciences and Engineering Research Council (NSERC) and the University of Ottawa for their financial support during the completion of this research.

CONFLICT OF INTEREST

The authors have no professional relationships that stand to gain from the current study. All results of the present study are presented clearly, honestly and without any falsification or fabrication of the data.

REFERENCES

Barzan, M., Modenese, L., Carty, C. P., Maine, S., Stockton, C. A., Sancisi, N., … Brito da Luz, S. (2019). Development and validation of subject-specific pediatric multibody knee kinematic models with ligamentous constraints. *Journal of Biomechanics*, *93*, 194–203.

Brito da Luz, S., Modenese, L., Sancisi, N., Mills, P. M., Kennedy, B., Beck, B. R., & Lloyd, D. G. (2017). Feasibility of using MRIs to create subject-specific parallel-mechanism joint models. *Journal of Biomechanics*.

Clouthier, A. L., Smith, C. R., Vignos, M. F., Thelen, D. G., Deluzio, K. J., & Rainbow, M. J. (2019). The effect of articular geometry features identified using statistical shape modelling on knee biomechanics. *Medical Engineering and Physics*.

Conconi, M., Sancisi, N., & Parenti-Castelli, V. (2021). Prediction of Individual Knee Kinematics from an MRI Representation of the Articular Surfaces. *IEEE Transactions on Biomedical Engineering*, *68*(3), 1084–1092.

Dare, D. M., Fabricant, P. D., McCarthy, M. M., Rebolledo, B. J., Green, D. W., Cordasco, F. A., & Jones, K. J. (2015). Increased lateral tibial slope is a risk factor for pediatric anterior cruciate ligament injury: An MRI-based case-control study of 152 patients. *American Journal of Sports Medicine*, *43*(7), 1632–1639.

De Groote, F., & Falisse, A. (2021). Perspective on musculoskeletal modelling and predictive simulations of human movement to assess the neuromechanics of gait. *Proceedings of the Royal Society B: Biological Sciences*, *288*(1946).

Dye, S. F. (1987). An evolutionary perspective of the knee. *Journal of Bone and Joint Surgery – American Volume*, *69*(7), 976–983.

Dye, S. F. (2003). Functional morphologic features of the human knee: An evolutionary perspective. *Clinical Orthopaedics and Related Research*, *410*(410), 19–24.

Hashemi, J., Chandrashekar, N., Gill, B., Beynnon, B. D., Slauterbeck, J. R., Schutt, R. C., … Dabezies, E. (2008). The geometry of the tibial plateau and its influence on the biomechanics of the tibiofemoral joint. *Journal of Bone and Joint Surgery – Series A*, *90*(12), 2724–2734.

Johnson, K. L. (1985). *Contact Mechanics*. Cambridge University Press.

Lansdown, D., & Ma, C. B. (2018, January 1). The Influence of Tibial and Femoral Bone Morphology on Knee Kinematics in the Anterior Cruciate Ligament Injured Knee. *Clinics in Sports Medicine*. W.B. Saunders.

Lin, E. C. (2010). Radiation risk from medical imaging. *Mayo Clinic Proceedings*, *85*(12), 1142–1146.

Lynch, J. T., Schneider, M. T. Y., Perriman, D. M., Scarvell, J. M., Pickering, M. R., Asikuzzaman, M., … Smith, P. N. (2019). Statistical shape modelling reveals large and distinct subchondral bony differences in osteoarthritic knees. *Journal of Biomechanics*, *93*, 177–184.

Mahfouz, M., Fatah, E. E. H. A., Bowers, L. S., & Scuderi, G. (2012). Three-dimensional morphology of the knee reveals ethnic differences. *Clinical Orthopaedics and Related Research*, *470*(1), 172–185.

Monk, A. P., Choji, K., O'Connor, J. J., Goodfellow, J. W., & Murray, D. W. (2014). The shape of the distal femur: A geometrical study using MRI. *Bone and Joint Journal*, *96B* (12), 1623–1630.

Rajagopal, A., Dembia, C. L., DeMers, M. S., Delp, D. D., Hicks, J. L., & Delp, S. L. (2016). Full-Body Musculoskeletal Model for Muscle-Driven Simulation of Human Gait. *IEEE Transactions on Biomedical Engineering*, *63*(10), 2068–2079.

Reinbolt, J. A., Seth, A., & Delp, S. L. (2011). Simulation of human movement: Applications using *OpenSim*. In *Procedia IUTAM*.

Saliba, C. ., Clouthier, A. L., Brandon, S. C. ., Rainbow, M. . ., & Deluzio, K. J. (2018). Prediction of knee joint contact forces from external measures using principal component prediction and reconstruction. *Journal of Applied Biomechanics*, *34*(5), 419–423.

Seth, A., Hicks, J. L., Uchida, T. K., Habib, A., Dembia, C. L., Dunne, J. J., … Delp, S. L. (2018). *OpenSim*: Simulating musculoskeletal dynamics and neuromuscular control to study human and animal movement. *PloS Computational Biology*, *14*(7), 1–20.

Smale, K. B., Conconi, M., Sancisi, N., Krogsgaard, M., Alkjaer, T., Parenti-Castelli, V., & Benoit, D. L. (2019). Effect of implementing magnetic resonance imaging for patient-specific *OpenSim* models on lower-body kinematics and knee ligament lengths. *Journal*

Sylvester, A. D., Lautzenheiser, S. G., & Kramer, P. A. (2021). A review of musculoskeletal modelling of human locomotion. *Interface Focus*, *11*(5).

Todd, M. S., Lalliss, S., Garcia, E., DeBerardino, T. M., & Cameron, K. L. (2010). The relationship between posterior tibial slope and anterior cruciate ligament injuries. *American Journal of Sports Medicine*, *38*(1), 63–67.

Wahl, C. J., Westermann, R. W., Blaisdell, G. Y., & Cizik, A. M. (2012). An association of lateral knee sagittal anatomic factors with non-contact ACL injury: Sex or geometry? *Journal of Bone and Joint Surgery – Series A*, *94*(3), 217–226.

Walker, P. S., Rovick, J. S., & Robertson, D. D. (1988). The effects of knee brace hinge design and placement on joint mechanics. *Journal of Biomechanics*, *21*(11).

APPENDIX A: Anthropometrics

Table 1-A Anthropometrics measurements used for PCA

Height	Against wall, standing straight, measure from top of head to ground
Knee Width	Caliper measure between medial and lateral epicondyles
Thigh Circumference	Tape measure around largest portion of the thigh
Shank Circumference	Tape measure around largest portion of the shank
Leg Length	Anterior superior iliac spine to medial malleolus
Tibia Length	Lateral epicondyle to medial malleolus

CHAPTER 7: GENERAL DISCUSSION

The aim of my Master's thesis was two-fold: Firstly, we sought to determine if congruence-based modelling could be applied to an adolescent population of various Tanner stages and produce kinematic outputs (Q1). Secondly, we attempted to simplify representations of articular contact to determine if tibio-femoral joint morphology could be predicted from external measurements using principal component analysis (Q2).

Q1) Can a congruence-based model be applied to an adolescent population of various Tanner stages and produce physiological kinematic outputs?

We hypothesized that congruence-based modelling can be applied to developing populations, and that kinematic outputs would mimic physiological mechanisms of the knee. We determined that congruence-based modelling techniques are able to be applied to a population of varying levels of pubertal development, producing passive rotational kinematics of AA and IE that are consistent with ACL injured knees (Hewett et al., 2007; Kothari et al., 2012; Larwa et al., 2021; Paterno et al., 2017; Pinskerova et al., 2004). Furthermore, our study found that the TL condyle varied the most between participants, suggesting variations in convexity (Hashemi et al., 2008; Wahl et al., 2012b) and/or tibial slope (Dare et al., 2015; O'Malley et al., 2015) amongst participants. Future studies should investigate the impacts of these morphological features on natural knee motion.

Q2) Can simplified representations of articular contact be reconstructed from external measurements using principal component analysis?

We hypothesized that we would be able to predict articular surface approximations from marker locations and/or anthropometrics measurements within 5mm of error from the MRI-generated articular contacts. Four sets were used for the analysis: 1) femur and tibia marker positions only to predict the femoral/tibial condyle approximations; 2) femur and tibia marker positions and anthropometrics to predict femoral/tibial condyle approximations; 3) femur marker positions to predict femoral approximations and 4) femur marker positions and anthropometrics to predict femoral approximations. Set 4) performed the best and was able to get radii of both condyle spheres to within 5mm of error for all subjects. This was likely due to the simplicity of modelling the distal femoral condyles as spheres that is possible given its relatively little change in its development over 300 million years (Dye, 1987, 2003; Monk et al., 2014)

7.1 Variations in Articular Contact Sphere Radii

Of the average radii pertaining to the four simplified articular contact spheres, the lateral tibial plateau, TL, had the largest radius and variability amongst participants. There was a 44.23mm difference between the largest and smallest approximation of articular contact for TL, yet even the smallest TL radius was greater than any TM, FL or FM radius across all subjects. Both subjects at either ends of the extreme were female, yet the subject with the largest TL was less skeletally mature and had a smaller knee width (Tanner stage 4, 99 mm) than the participant with the smallest TL sphere (Tanner stage 4, 106 mm). There are multiple possibilities that could explain these phenomena. Firstly, concave vs. convex nature of the regions of articulation for the medial and the tibial plateaus influenced the size of the articular contact spheres. This is confirmed by Hashemi et al. (2008), who reported differences in tibial plateau geometry using the MRIs of 33 female and 22 male subjects. They found that with respect to the tibial plateau, the subchondral bone on the lateral aspect is mostly flat, while the medial tibial plateau has a more pronounced depth, measuring 2.7 ± 0.76 mm amongst females and 3.1 ± 0.99 mm amongst males (Hashemi et al., 2008). The radius of the sphere pertaining to the flatter surface must be larger to accommodate a smaller arc, rather than a sphere fit to condyle with a more rounded curvature. Furthermore, the anterior-posterior width of the tibial plateau would also influence the size of the TL sphere, as a shorter tibial plateau would reduce the arc of the convex surface, inherently needing a smaller sphere. These differences in curvature in addition to the large variability between subjects explain why the RMSE between the PCA-predicted and MRI-extracted articular contacts was large (study 2). In order to dictate the size of the spheres to represent the tibial plateau, measurements taken directly from the medical images are needed, namely radius of curvature, anteroposterior tibial length and tibial slope. Future studies are needed to investigate the addition of such parameters on the ability to reconstruct patient-specific contacts.

7.2 Kinematics & Ligament Strain

Kinematics and changes in ligament length were successfully obtained via optimization of orientation through passive knee flexion. Variations in knee ROM were apparent across all participants, and average AA and IE ROM were calculated as 1.60° ± 0.6 and 7.64 º ± 2.3 respectively. A more abducted knee has been identified as a risk factor for ACL injury by previous researchers and has been studied through a variety of functional movements (Hewett et al., 2007; Larwa et al., 2021; Paterno et al., 2017). Since all participants were ACLi, it is plausible that they would exhibit a more abducted movement pattern solely from surface geometry. With respect to rotation, the congruence optimizer calculates the rotation of the femur with respect to the tibia, and the resulting rotations follow the patterns of the “screw-home” mechanism, with the femur rotating externally in lower flexion angles, then internally to support the internal rotation of the tibia (Kothari et al., 2012; Pinskerova et al., 2004). When examining the IEA of all knees, the model agreed with published literature from an interventional MRI based study from Johal et al. (2005), finding that the femur externally rotates about 14°, with most of the rotation occurring after 45° flexion (Johal et al., 2005).

Of the four ligaments, the PCL varied the most amongst participants, and there was greater strain variation at higher values of knee flexion. This could be attributed to several possibilities relating to the increased laxity at the knee joint near pubertal development (Wild et al., 2012). Firstly, with regards to the ACL, changes in hormone levels coupled with rapid developmental changes in stature could all increase changes in knee ligament length (Woodhouse et al., 2007). The sample of participants used to construct the model consists of peri-pubertal (Tanner stage 2-3) and late pubertal (Tanner stage 5) adolescents, and it follows that hormone levels would vary across the sample.

7.3 Success of PCA Model

The PCA model used to predict femoral simplifications of contact from marker positions and anthropometric measurements of the femur only (set 4) performed the best. Root mean squared error between MRI-extracted articular contacts and predicted values had a maximum of 9.86 ± 8.83 mm, and predicted radii of FL and FM were 0.44 ± 0.31 mm and 4.89 ± 4.94 respectively. Across all participants, FL and FM spheres were similar in radii, and exhibited a smaller inter-subject variability than coincident tibial spheres. Variability in distal femur morphology has been studied previously, and differences in medial and lateral femoral condyles between sexes and different ethnicities (M. Mahfouz et al., 2012; Yang et al., 2014). Gillespie et al. (2011) reported that females exhibit a significantly smaller aspect ratio, defined as the mediolateral distance of the distal femur in relation to the anteroposterior distance, than males. Furthermore, Mahfouz et al. (2012) determined that females have a more curved distal femur, regardless of ethnicity. While these differences exist, the classification of these geometric features and their influence on total distal femur shape has successfully been simplified (Everhart et al., 2016; Monk et al., 2014). Monk et al. (2014) successfully used circular representations of the radii of curvature on multiplanar MRIs. This explains why the PCA model could only predict femoral geometry with good agreement, as the morphology of the distal femur can be generalized regardless of race, age or sex. This can be further explained when considering the evolution of the knee, as morphology and overall shape of tibiofemoral articulation has remained relatively static since the discovery of asymmetric knee geometry in tetrapods (Dye, 1987, 2003).

7.4 Limitations

There are certain limitations that must be considered with regards to the work of this thesis. Firstly, the sample size for both studies was rather small at only 12 participants. It should be noted that originally, there were 15 participants enrolled at this study, but three had to be omitted. Two omissions were due to data sharing issues between CHEO and the University of Ottawa, while the third was due to a build-up of edema that made soft-tissue contours impossible to distinguish in the MRI. However, we attempted to capture a large amount of variation within the data set to highlight the effectiveness of congruence-based modelling for diverse populations. Furthermore, few participants were needed to define a workflow, and the implemented model produced physiologically correct outputs despite the variations in size and shape across all knees. Future studies should aim to recruit a minimum of 25 participants, in order to adequately encompass each Tanner stage.

Another limitation is that the angle of knee flexion at the time of MRI collection was not consistent between participants. Given the differences in anthropometrics, the leg had to be adjusted to fit the coil, with larger participants requiring more knee flexion. This would alter the marker alignment of the *OpenSim* reference frame to the MRI frame and would influence the final position of the markers extracted. However, PCA was still able to predict simplified femoral articular contacts from the marker positions with RMSEs under 10mm, indicating results with good agreement are achievable despite these limitations. Individual anatomical differences also influenced the ACS used to define the congruence model for each subject. Coordinate systems were built using landmarks obtained through virtual palpation, and by fitting an axis through the diaphysis. However, the length of the diaphysis that could be used to build the coordinate system varied amongst participants. As a result, reference systems had to be individually tailored to each knee, which could have introduced differences in alignment and/or generated kinematics. This error was mitigated as best as possible by having an independent researcher visually inspect each subject's ACS.

7.5 Future Considrations:

The completion of this thesis brings forward new ideas for improving the workflow and the results of this research. Firstly, ensuring the MRIs of each participant were collected at the same angle would improve the creation of anatomical coordinate systems. This would have made joint alignment and extracting the range of natural knee motion available more consistent between participants. Additionally, with more participants encompassing a larger pubertal development range, we could determine a range of tibial plateau sizes generated through PCA. We could also use the simplified articulations we reconstructed using principal components to determine how much these variations in surface morphology influence kinematics in ACL injured groups. This research has the potential to improve ACL injury research from a clinical and modelling perspective. By eliminating the need for medical images to generate simplifications of articular contacts, we can make patient-specific modelling accessible to all researchers, regardless of equipment. Additionally, relying on external markers and anthropometrics for model construction allows them to be scaled to accommodate growth, for example during adolescence or through a knee rehabilitation protocol.

A thorough validation of this procedure, similar to Figure 5-A in Appendix A, is needed before future studies can take place. The lack of reference data, particularly for the adolescent population, was a limiting factor in this endeavour. This modelling was able to be validated for adult knees and ankles using data collected from bone pins in a custom-built cadaveric rig(Conconi et al., 2015a, 2018; Forlani et al., 2016). Using the same rig with paediatric and adolescent cadavers to compute passive knee joint motion would give a baseline of natural motion for a developing population. The methods outlined in Study 1 of this thesis could be re-applied to segment and extract articulations of the cadaveric knee, providing proof of validation for this demographic. It would be extremely beneficial to be able to collect *in-vitro* and *in-silico* data for future validation.

CHAPTER 8: CONCLUSION

The overall objective of this thesis was to develop a patient-specific model of the ACLi knee in adolescents across various levels of pubertal development, then to reconstruct said model solely from external measurements so that it can be used regardless of user access to research. Firstly, we were able to successfully apply congruence-based modelling techniques to ACLi adolescent populations. Using MRIs, TFJ articulations were segmented and approximated as spheres, and used to determine the envelope that put the least amount of pressure on the joint, or natural knee motion. The success of this application will allow for a baseline of natural movement to be applied to musculoskeletal models, that consider the impact of articulations, ligament insertions, and joint configurations. This will lead to more biofidelic representations of knee movement, particularly in future studies where more complex movements are performed.

Secondly, we were able to reconstruct the aforementioned articulations at the femur using anthropometric measures and marker position data through PCA.

This research has the potential to lead to more robust modelling of ACL injuries through adolescence. The ability to reconstruct patient-specific extracted data from external measurements means we are one step closer to building accessible, personalized musculoskeletal models for adolescents. Additionally, the fact this could be applied to a growing population indicates that personalized models have the potential to be scaled to accommodate changes in stature.

CHAPTER 9: GENERAL REFERENCES

Alentorn-Geli, E., Myer, G. D., Silvers, H. J., Samitier, G., Romero, D., Lázaro-Haro, C., & Cugat, R. (2009). Prevention of non-contact anterior cruciate ligament injuries in soccer players. Part 1: Mechanisms of injury and underlying risk factors. *Knee Surgery, Sports Traumatology, Arthroscopy*, *17*(7), 705–729. https://doi.org/10.1007/s00167-009-0813-1

Ali, N., Andersen, M. S., Rasmussen, J., Robertson, D. G. E., & Rouhi, G. (2014). The application of musculoskeletal modeling to investigate gender bias in non-contact ACL injury rate during single-leg landings. *Computer Methods in Biomechanics and Biomedical Engineering*, *17*(14), 1602–1616. https://doi.org/10.1080/10255842.2012.758718

Anderson, A. E., Ellis, B. J., & Weiss, J. A. (2012). *Verification, Validation and Sensitivity Studies in Computational Biomechanics*. 1–24. https://doi.org/10.1080/10255840601160484.Verification

Andrews, M., Noyes, F. R., & Barber-Westin, S. D. (1994). Anterior cruciate ligament reconstruction in the skeletally immature. *The American Journal of Sports Medicine*, *22*(1), 48–54. https://doi.org/10.1097/01.bco.0000192886.89391.be

Aprovitola, A., & Gallo, L. (2016). Knee bone segmentation from MRI: A classification and literature review. In *Biocybernetics and Biomedical Engineering* (Vol. 36, Issue 2, pp. 437–449). PWN-Polish Scientific Publishers. https://doi.org/10.1016/j.bbe.2015.12.007

Arbes, S., Resinger, C., Vécsei, V., & Nau, T. (2007). The functional outcome of total tears of the anterior cruciate ligament (ACL) in the skeletally immature patient. *International Orthopaedics*, *31*(4), 471–475. https://doi.org/10.1007/s00264-006-0225-5

Arnold, E. M., Ward, S. R., Lieber, R. L., & Delp, S. L. (2010). A model of the lower limb for analysis of human movement. *Annals of Biomedical Engineering*, *38*(2), 269–279. https://doi.org/10.1007/s10439-009-9852-5

Babuska, I., & Oden, J. T. (2004). Verification and validation in computational engineering and science: Basic concepts. *Computer Methods in Applied Mechanics and Engineering*, *193*(36–38), 4057–4066. https://doi.org/10.1016/j.cma.2004.03.002

Bahl, J. S., Zhang, J., Killen, B. A., Taylor, M., Solomon, L. B., Arnold, J. B., Lloyd, D. G., Besier, T. F., & Thewlis, D. (2019). Statistical shape modelling versus linear scaling: Effects on predictions of hip joint centre location and muscle moment arms in people with hip osteoarthritis. *Journal of Biomechanics*, *85*, 164–172. https://doi.org/10.1016/j.jbiomech.2019.01.031

Barata, J. C. A., & Hussein, M. S. (2011). *The Moore-Penrose Pseudoinverse. A Tutorial Review of the Theory*. https://doi.org/10.1007/s13538-011-0052-z

Barzan, M., Modenese, L., Carty, C. P., Maine, S., Stockton, C. A., Sancisi, N., Lewis, A., Grant, J., Lloyd, D. G., & Brito da Luz, S. (2019). Development and validation of subject-specific pediatric multibody knee kinematic models with ligamentous constraints. *Journal of Biomechanics*, *93*, 194–203. https://doi.org/10.1016/j.jbiomech.2019.07.001

Beck, N. A., Lawrence, J. T. R., Nordin, J. D., DeFor, T. A., & Tompkins, M. (2017). ACL tears in school-aged children and adolescents over 20 years. *Pediatrics*, *139*(3). https://doi.org/10.1542/peds.2016-1877

Benoit, D. L., Ramsey, D. K., Lamontagne, M., Xu, L., Wretenberg, P., & Renström, P. (2006). Effect of skin movement artifact on knee kinematics during gait and cutting motions measured in vivo. *Gait and Posture*, *24*(2), 152–164. https://doi.org/10.1016/j.gaitpost.2005.04.012

Beynnon, B., Howe, J. G., Pope, M. H., Johnson, R. J., & Fleming, B. C. (1992). The measurement of anterior cruciate ligament strain in vivo*. In *International Orthopaedics (SICOT* (Vol. 16).

Brito da Luz, S., Modenese, L., Sancisi, N., Mills, P. M., Kennedy, B., Beck, B. R., & Lloyd, D. G. (2017). Feasibility of using MRIs to create subject-specific parallel-mechanism joint models. *Journal of Biomechanics*. https://doi.org/10.1016/j.jbiomech.2016.12.018

Buchanan, T. S., & Lloyd, D. G. (1997). Muscle activation at the human knee during isometric flexion-extension and varus-valgus loads. *Journal of Orthopaedic Research*, *15*(1), 11–17. https://doi.org/10.1002/jor.1100150103

Cahuzac Ph., J., Vardon, D., & Sales De Gauzy, J. (1995). Development of the clinical tibiofemoral angle in normal adolescents: A study of 427 normal subjects from 10 to 16 years of age. *Journal of Bone and Joint Surgery - Series B*, *77*(5), 729–732. https://doi.org/10.1302/0301-620x.77b5.7559698

Caravaggi, P., Assirelli, E., Ensini, A., Ortolani, M., Mariani, E., Leardini, A., Neri, S., & Belvedere, C. (2021). Biomechanical-Based Protocol for in vitro Study of Cartilage Response to Cyclic Loading: A Proof-of-Concept in Knee Osteoarthritis. *Frontiers in Bioengineering and Biotechnology*, *9*. https://doi.org/10.3389/fbioe.2021.634327

Carbone, V., Fluit, R., Pellikaan, P., van der Krogt, M. M., Janssen, D., Damsgaard, M., Vigneron, L., Feilkas, T., Koopman, H. F. J. M., & Verdonschot, N. (2015). TLEM 2.0 - A comprehensive musculoskeletal geometry dataset for subject-specific modeling of lower extremity. *Journal of Biomechanics*, *48*(5), 734–741. https://doi.org/10.1016/j.jbiomech.2014.12.034

Carsen, S., Grammatopoulos, G., Zaltz, I., Ward, L., Smit, K., & Beaulé, P. E. (2021). The Effects of Physical Activity on Physeal and Skeletal Development. *JBJS Reviews*, *9*(10), 1–11. https://doi.org/10.2106/jbjs.rvw.21.00060

Chen, Z., Zhang, X., Ardestani, M. M., Wang, L., Liu, Y., Lian, Q., He, J., Li, D., & Jin, Z. (2014). Prediction of in vivo joint mechanics of an artificial knee implant using rigid multi-body dynamics with elastic contacts. *Proceedings of the Institution of Mechanical Engineers, Part H: Journal of Engineering in Medicine*, *228*(6), 564–575. https://doi.org/10.1177/0954411914537476

Cheng, H., Garrick, D. J., & Fernando, R. L. (2017). Efficient strategies for leave-one-out cross validation for genomic best linear unbiased prediction. *Journal of Animal Science and Biotechnology*, *8*(1). https://doi.org/10.1186/s40104-017-0164-6

Clouthier, A. L., Smith, C. R., Vignos, M. F., Thelen, D. G., Deluzio, K. J., & Rainbow, M. J. (2019). The effect of articular geometry features identified using statistical shape modelling on knee biomechanics. *Medical Engineering and Physics*. https://doi.org/10.1016/j.medengphy.2019.02.009

Conconi, M., & Castelli, V. P. (2012). Joint kinematics from functional adaptation: An application to the human ankle. *Applied Mechanics and Materials*, *162*, 266–275. https://doi.org/10.4028/www.scientific.net/AMM.162.266

Conconi, M., & Castelli, V. P. (2014). A sound and efficient measure of joint congruence. *Proceedings of the Institution of Mechanical Engineers, Part H: Journal of Engineering in Medicine*, *228*(9), 935–941. https://doi.org/10.1177/0954411914550848

Conconi, M., Halilaj, E., Parenti Castelli, V., & Crisco, J. J. (2014). Is early osteoarthritis associated with differences in joint congruence? *Journal of Biomechanics*, *47*(16), 3787–3793. https://doi.org/10.1016/j.jbiomech.2014.10.030

Conconi, M., Leardini, A., & Parenti-Castelli, V. (2015a). Joint kinematics from functional adaptation: A validation on the tibio-talar articulation. *Journal of Biomechanics*, *48*(12), 2960–2967. https://doi.org/10.1016/j.jbiomech.2015.07.042

Conconi, M., Leardini, A., & Parenti-Castelli, V. (2015b). Joint kinematics from functional adaptation: A validation on the tibio-talar articulation. *Journal of Biomechanics*, *48*(12), 2960–2967. https://doi.org/10.1016/j.jbiomech.2015.07.042

Conconi, M., Sancisi, N., & Parenti-Castelli, V. (2018). *Subject-Specific Model of Knee Natural Motion: A Non-invasive Approach*. 255–264. https://doi.org/10.1007/978-3-319-56802-7_27

Conconi, M., Sancisi, N., & Parenti-Castelli, V. (2019). The Geometrical Arrangement of Knee Constraints That Makes Natural Motion Possible: Theoretical and Experimental Analysis. *Journal of Biomechanical Engineering*, *141*(5), 1–6. https://doi.org/10.1115/1.4043028

Conconi, M., Sancisi, N., & Parenti-Castelli, V. (2021). Prediction of Individual Knee Kinematics from an MRI Representation of the Articular Surfaces. *IEEE Transactions on Biomedical Engineering*, *68*(3), 1084–1092. https://doi.org/10.1109/TBME.2020.3018113

Dalvi, R., Abugharbieh, R., Wilson, D. C., & Wilson, D. R. (2007). Multi-contrast MR for enhanced bone imaging and segmentation. *Annual International Conference of the IEEE Engineering in Medicine and Biology - Proceedings*, 5620–5623. https://doi.org/10.1109/IEMBS.2007.4353621

Damsgaard, M., Rasmussen, J., Christensen, S. T., Surma, E., & de Zee, M. (2006). Analysis of musculoskeletal systems in the AnyBody Modeling System. *Simulation Modelling Practice and Theory*, *14*(8), 1100–1111. https://doi.org/10.1016/j.simpat.2006.09.001

Dare, D. M., Fabricant, P. D., McCarthy, M. M., Rebolledo, B. J., Green, D. W., Cordasco, F. A., & Jones, K. J. (2015). Increased lateral tibial slope is a risk factor for pediatric anterior cruciate ligament injury: An MRI-based case-control study of 152 patients. *American Journal of Sports Medicine*, *43*(7), 1632–1639. https://doi.org/10.1177/0363546515579182

Davico, G., Pizzolato, C., Killen, B. A., Barzan, M., Suwarganda, E. K., Lloyd, D. G., & Carty, C. P. (2019). Best methods and data to reconstruct paediatric lower limb bones for musculoskeletal modelling. *Biomechanics and Modeling in Mechanobiology*. https://doi.org/10.1007/s10237-019-01245-y

Dekker, T. J., Godin, J. A., Dale, K. M., Garrett, W. E., Taylor, D. C., & Riboh, J. C. (2017). Return to sport after pediatric anterior cruciate ligament reconstruction and its effect on subsequent anterior cruciate ligament injury. *Journal of Bone and Joint Surgery - American Volume*, *99*(11), 897–904. https://doi.org/10.2106/JBJS.16.00758

Dekker, T. J., Rush, J. K., & Schmitz, M. R. (2018). What's New in Pediatric and Adolescent Anterior Cruciate Ligament Injuries? *Journal of Pediatric Orthopaedics*, *38*(3), 185–192. https://doi.org/10.1097/BPO.0000000000000792

Delp, S. L., Anderson, F. C., Arnold, A. S., Loan, P., Habib, A., John, C. T., Guendelman, E., & Thelen, D. G. (2007). OpenSim: Open-source software to create and analyze dynamic simulations of movement. *IEEE Transactions on Biomedical Engineering*, *54*(11), 1940–1950. https://doi.org/10.1109/TBME.2007.901024

Delp, S. L., Loan, J. P., Hoy, M. G., Zajac, F. E., Topp, E. L., & Rosen, J. M. (1990). An Interactive Graphics-Based Model of the Lower Extremity to Study Orthopaedic Surgical Procedures. *IEEE Transactions on Biomedical Engineering*, *37*(8), 757–767. https://doi.org/10.1109/10.102791

Ding, Z., Tsang, C. K., Nolte, D., Kedgley, A. E., & Bull, A. M. J. (2019). Improving musculoskeletal model scaling using an anatomical atlas: The importance of gender and anthropometric similarity to quantify joint reaction forces. *IEEE Transactions on Biomedical Engineering*, *66*(12), 3444–3456. https://doi.org/10.1109/TBME.2019.2905956

Dye, S. F. (1987). An evolutionary perspective of the knee. *Journal of Bone and Joint Surgery - American Volume*, *69*(7), 976–983.

Dye, S. F. (2003). Functional morphologic features of the human knee: An evolutionary perspective. *Clinical Orthopaedics and Related Research*, *410*(410), 19–24. https://doi.org/10.1097/01.blo.0000063563.90853.23

Edmonds, E. W., Bathen, M., & Bastrom, T. P. (2014). *Normal Parameters of the Skeletally Immature Knee: Developmental Changes on Magnetic Resonance Imaging*.

Englund, M., Roos, H., & Lohmander, L. S. (2004). *High Prevalence of Knee Osteoarthritis, Pain , and Functional Limitations in Female Soccer Players Twelve Years After Anterior Cruciate Ligament Injury*. *50*(10), 3145–3152. https://doi.org/10.1002/art.20589

Everhart, J. S., Chaudhari, A. M. W., & Flanigan, D. C. (2016). Creation of a simple distal femur morphology classification system. *Journal of Orthopaedic Research*, *34*(6), 924–931. https://doi.org/10.1002/jor.23102

Fabricant, P. D., Robles, A., Downey-Zayas, T., Do, H. T., Marx, R. G., Widmann, R. F., & Green, D. W. (2013). Development and validation of a pediatric sports activity rating scale:

The hospital for special surgery pediatric functional activity brief scale (HSS Pedi-FABS). *American Journal of Sports Medicine*, *41*(10), 2421–2429. https://doi.org/10.1177/0363546513496548

Fayad, L. M., Parellada, J. A., Parker, L., & Schweitzer, M. E. (2003). MR imaging of anterior cruciate ligament tears: Is there a gender gap? *Skeletal Radiology*, *32*(11), 639–646. https://doi.org/10.1007/s00256-003-0694-1

Fernandez, J. W., Akbarshahi, M., Kim, H. J., & Pandy, M. G. (2008). Integrating modelling, motion capture and x-ray fluoroscopy to investigate patellofemoral function during dynamic activity. *Computer Methods in Biomechanics and Biomedical Engineering*, *11*(1), 41–53. https://doi.org/10.1080/10255840701551046

Flanigan, C., Fields, S. K., & Comstock, R. D. (2014). Epidemiology of Knee Injuries among US high school. *American College of Sports Medicine*, *45*(3), 462–469. https://doi.org/10.1249/MSS.0b013e318277acca.EPIDEMIOLOGY

Flaxman, T. E., Smith, A. J. J., & Benoit, D. L. (2014). Sex-related differences in neuromuscular control: Implications for injury mechanisms or healthy stabilisation strategies? *Journal of Orthopaedic Research*, *32*(2), 310–317. https://doi.org/10.1002/jor.22510

Fleute, M., Lavallée, S., & Julliard, R. (1999). Incorporating a statistically based shape model into a system for computer-assisted anterior cruciate ligament surgery. *Medical Image Analysis*, *3*(3), 209–222. https://doi.org/10.1016/S1361-8415(99)80020-6

Forlani, M., Sancisi, N., Conconi, M., & Parenti-Castelli, V. (2016). A new test rig for static and dynamic evaluation of knee motion based on a cable-driven parallel manipulator loading system. *Meccanica*, *51*(7), 1571–1581. https://doi.org/10.1007/s11012-015-0124-1

Fregly, B. J., Besier, T. F., Lloyd, D. G., Delp, S. L., Banks, S. A., Pandy, M. G., & D'Lima, D. D. (2012). Grand challenge competition to predict in vivo knee loads. *Journal of Orthopaedic Research*, *30*(4), 503–513. https://doi.org/10.1002/jor.22023

Fripp, J., Crozier, S., Warfield, S. K., & Ourselin, S. (2010). Automatic segmentation and quantitative analysis of the articular cartilages from magnetic resonance images of the knee. *IEEE Transactions on Medical Imaging*, *29*(1), 55–64. https://doi.org/10.1109/TMI.2009.2024743

Gill, K. G., Nemeth, B. A., & Davis, K. W. (2014). Magnetic Resonance Imaging of the Pediatric Knee. *Magnetic Resonance Imaging Clinics of North America*, *22*(4), 743–763. https://doi.org/10.1016/j.mric.2014.07.010

Hamner, S. R., Seth, A., & Delp, S. L. (2010). Muscle contributions to propulsion and support during running. *Journal of Biomechanics*, *43*(14), 2709–2716. https://doi.org/10.1016/j.jbiomech.2010.06.025

Hashemi, J., Chandrashekar, N., Gill, B., Beynnon, B. D., Slauterbeck, J. R., Schutt, R. C., Mansouri, H., & Dabezies, E. (2008). The geometry of the tibial plateau and its influence on the biomechanics of the tibiofemoral joint. *Journal of Bone and Joint Surgery - Series A*, *90*(12), 2724–2734. https://doi.org/10.2106/JBJS.G.01358

Heitz, G., Rohlfing, T., & Maurer, C. R. (2005). Statistical Shape Model Generation Using Nonrigid Deformation of a Template Mesh. *Medical Imaging 2005: Image Processing*, *5747*, 1411–1421.

Henninger, H. B., Reese, S. P., Anderson, A. E., & Weiss, J. A. (2010). Validation of computational models in biomechanics. *Proceedings of the Institution of Mechanical*

Engineers, Part H: Journal of Engineering in Medicine, *224*(7), 801–812. https://doi.org/10.1243/09544119JEIM649

Herzog, M. M., Marshall, S. W., Lund, J. L., Pate, V., Mack, C. D., & Spang, J. T. (2017). Incidence of anterior cruciate ligament reconstruction among adolescent females in the United States, 2002 through 2014. *JAMA Pediatrics*, *171*(8), 808–810. https://doi.org/10.1001/jamapediatrics.2017.0740

Herzog, M. M., Marshall, S. W., Lund, J. L., Pate, V., Mack, C. D., & Spang, J. T. (2018a). Trends in Incidence of ACL Reconstruction and Concomitant Procedures Among Commercially Insured Individuals in the United States, 2002-2014. *Sports Health*, *10*(6), 523–531. https://doi.org/10.1177/1941738118803616

Herzog, M. M., Marshall, S. W., Lund, J. L., Pate, V., Mack, C. D., & Spang, J. T. (2018b). Trends in Incidence of ACL Reconstruction and Concomitant Procedures Among Commercially Insured Individuals in the United States, 2002-2014. *Sports Health*, *10*(6), 523–531. https://doi.org/10.1177/1941738118803616

Hewett, T. E., Shultz, S. J., Griffin, L. Y., & American Orthopaedic Society for Sports Medicine. (2007). *Understanding and preventing noncontact ACL injuries*. Human Kinetics.

Hicks, J. L., Uchida, T. K., Seth, A., Rajagopal, A., & Delp, S. L. (2015). Is My Model Good Enough? Best Practices for Verification and Validation of Musculoskeletal Models and Simulations of Movement. *Journal of Biomechanical Engineering*, *137*(2). https://doi.org/10.1115/1.4029304

Jaremko, J. L., Cheng, R. W. T., Lambert, R. G. W., Habib, A. F., & Ronsky, J. L. (2006). Reliability of an efficient MRI-based method for estimation of knee cartilage volume using surface registration. *Osteoarthritis and Cartilage*, *14*(9), 914–922. https://doi.org/10.1016/j.joca.2006.03.004

Jensen, R. K. (1986). The Growth of Children's Moment of Inertia. *Medicine & Science in Sports & Exercise*, *8*, 440–445.

Jensen, R. K., & Nassas, G. (1988). Growth of segment principal moments of inertia between four and twenty years. *Medicine and Science in Sports and Exercise*.

Johal, P., Williams, A., Wragg, P., Hunt, D., & Gedroyc, W. (2005). Tibio-femoral movement in the living knee. A study of weight bearing and non-weight bearing knee kinematics using "interventional" MRI. *Journal of Biomechanics*, *38*(2), 269–276. https://doi.org/10.1016/j.jbiomech.2004.02.008

Johnson, K. L. (1985). *Contact Mechanics*. Cambridge University Press.

Jollife, I. T., & Cadima, J. (2016). Principal component analysis: A review and recent developments. *Philosophical Transactions of the Royal Society A: Mathematical, Physical and Engineering Sciences*, *374*(2065). https://doi.org/10.1098/rsta.2015.0202

Joseph, A. M., Collins, C. L., Henke, N. M., Yard, E. E., Fields, S. K., & Comstock, R. D. (2013). A multisport epidemiologic comparison of anterior cruciate ligament injuries in high school athletics. *Journal of Athletic Training*, *48*(6), 810–817. https://doi.org/10.4085/1062-6050-48.6.03

Killen, B. A. (2019). *Muscular stabilisation of the knee and development of automated and tuned subject-specific musculoskeletal models for gait simulations* (Issue February) [Griffith University]. https://doi.org/https://doi.org/10.25904/1912/705

Kocher, M. S., Saxon, H. S., Hovis, W. D., & Hawkins, R. J. (2002). Management and Complications of Anterior Cruciate Ligament Injuries in Skeletally Immature Patients:

Survey of The Herodicus Society and The ACL Study Group. *Journal of Pediatric Orthopaedics*, *22*(4), 452–457. https://doi.org/10.1097/01241398-200207000-00008

Kocher, M. S., Smith, J. T., Iversen, M. D., Brustowicz, K., Ogunwole, O., Andersen, J., Yoo, W. J., McFeely, E. D., Anderson, A. F., & Zurakowski, D. (2011). Reliability, validity, and responsiveness of a modified international knee documentation committee subjective knee form (Pedi-IKDC) in children with knee disorders. *American Journal of Sports Medicine*, *39*(5), 933–939. https://doi.org/10.1177/0363546510383002

Kothari, A., Haughom, B., Subburaj, K., Feeley, B., Li, X., & Ma, C. B. (2012). Evaluating rotational kinematics of the knee in ACL reconstructed patients using 3.0Tesla magnetic resonance imaging. *Knee*, *19*(5), 648–651. https://doi.org/10.1016/j.knee.2011.12.001

Kristianslund, E., Faul, O., Bahr, R., Myklebust, G., & Krosshaug, T. (2014). Sidestep cutting technique and knee abduction loading: Implications for ACL prevention exercises. *British Journal of Sports Medicine*, *48*(9), 779–783. https://doi.org/10.1136/bjsports-2012-091370

Krosshaug, T., Nakamae, A., Boden, B. P., Engebretsen, L., Smith, G., Slauterbeck, J. R., Hewett, T. E., & Bahr, R. (2007). Mechanisms of anterior cruciate ligament injury in basketball: Video analysis of 39 cases. *American Journal of Sports Medicine*, *35*(3), 359–367. https://doi.org/10.1177/0363546506293899

Landry, S. C., McKean, K. A., Hubley-Kozey, C. L., Stanish, W. D., & Deluzio, K. J. (2007). Neuromuscular and lower limb biomechanical differences exist between male and female elite adolescent soccer players during an unanticipated run and crosscut maneuver. *American Journal of Sports Medicine*, *35*(11), 1901–1911. https://doi.org/10.1177/0363546507307400

Langholz, J. B., Westman, G., & Karlsteen, M. (2016). Musculoskeletal Modelling in Sports- Evaluation of Different Software Tools with Focus on Swimming. *Procedia Engineering*, *147*, 281–287. https://doi.org/10.1016/j.proeng.2016.06.278

Lansdown, D. A., Pedoia, V., Zaid, M., Amano, K., Souza, R. B., Li, X., & Ma, C. B. (2017). Variations in Knee Kinematics After ACL Injury and After Reconstruction Are Correlated With Bone Shape Differences. *Clinical Orthopaedics and Related Research*, *475*(10), 2427–2435. https://doi.org/10.1007/s11999-017-5368-8

Lansdown, D., & Ma, C. B. (2018). The Influence of Tibial and Femoral Bone Morphology on Knee Kinematics in the Anterior Cruciate Ligament Injured Knee. In *Clinics in Sports Medicine* (Vol. 37, Issue 1, pp. 127–136). W.B. Saunders. https://doi.org/10.1016/j.csm.2017.07.012

Larwa, J., Stoy, C., Chafetz, R. S., Boniello, M., & Franklin, C. (2021). Stiff landings, core stability, and dynamic knee valgus: A systematic review on documented anterior cruciate ligament ruptures in male and female athletes. *International Journal of Environmental Research and Public Health*, *18*(7). https://doi.org/10.3390/ijerph18073826

Leardini, A., Chiari, A., Della Croce, U., & Cappozzo, A. (2005). Human movement analysis using stereophotogrammetry Part 3. Soft tissue artifact assessment and compensation. *Gait and Posture*, *21*(2), 212–225. https://doi.org/10.1016/j.gaitpost.2004.05.002

Lerner, Z. F., DeMers, M. S., Delp, S. L., & Browning, R. C. (2015). How tibiofemoral alignment and contact locations affect predictions of medial and lateral tibiofemoral contact forces. *Journal of Biomechanics*, *48*(4), 644–650. https://doi.org/10.1016/j.jbiomech.2014.12.049

Lin, E. C. (2010). Radiation risk from medical imaging. *Mayo Clinic Proceedings*, *85*(12), 1142–1146. https://doi.org/10.4065/mcp.2010.0260

Lipps, D. B., Oh, Y. K., Ashton-Miller, J. A., & Wojtys, E. M. (2012). Morphologic characteristics help explain the gender difference in peak anterior cruciate ligament strain during a simulated pivot landing. *American Journal of Sports Medicine*, *40*(1), 32–40. https://doi.org/10.1177/0363546511422325

Liu, R. W., Farrow, L. D., Messerschmitt, P. J., Gilmore, A., Goodfellow, D. B., & Cooperman, D. R. (2008). An anatomical study of the pediatric intercondylar notch. *Journal of Pediatric Orthopaedics*, *28*(2), 177–183. https://doi.org/10.1097/BPO.0b013e318165219b

Liukkonen, M. K., Mononen, M. E., Tanska, P., Saarakkala, S., Nieminen, M. T., & Korhonen, R. K. (2017). Application of a semi-automatic cartilage segmentation method for biomechanical modeling of the knee joint. *Computer Methods in Biomechanics and Biomedical Engineering*, *20*(13), 1453–1463. https://doi.org/10.1080/10255842.2017.1375477

Lund, M. E., Andersen, M. S., de Zee, M., & Rasmussen, J. (2015). Scaling of musculoskeletal models from static and dynamic trials. *International Biomechanics*, *2*(1), 1–11. https://doi.org/10.1080/23335432.2014.993706

Lund, M. E., De Zee, M., Andersen, M. S., & Rasmussen, J. (2012). On validation of multibody musculoskeletal models. *Proceedings of the Institution of Mechanical Engineers, Part H: Journal of Engineering in Medicine*, *226*(2), 82–94. https://doi.org/10.1177/0954411911431516

Lynch, J. T., Schneider, M. T. Y., Perriman, D. M., Scarvell, J. M., Pickering, M. R., Asikuzzaman, M., Galvin, C. R., Besier, T. F., & Smith, P. N. (2019). Statistical shape modelling reveals large and distinct subchondral bony differences in osteoarthritic knees. *Journal of Biomechanics*, *93*, 177–184. https://doi.org/10.1016/j.jbiomech.2019.07.003

Mahfouz, M., Fatah, E. E. H. A., Bowers, L. S., & Scuderi, G. (2012). Three-dimensional morphology of the knee reveals ethnic differences. *Clinical Orthopaedics and Related Research*, *470*(1), 172–185. https://doi.org/10.1007/s11999-011-2089-2

Mahfouz, M. R., Komistek, R. D., Dennis, D. A., & Hoff, W. A. (2004). In vivo assessment of the kinematics in normal and anterior cruciate ligament-deficient knees. *Journal of Bone and Joint Surgery - Series A*, *86*(SUPPL. 2), 56–61. https://doi.org/10.2106/00004623-200412002-00009

Malina R, Bouchard C, & Bar-Or O. (2004). *Growth, maturation and physical activity* (2nd ed.). Human kinetics.

Manal, K., & Buchanan, T. S. (2013). An electromyogram-driven musculoskeletal model of the knee to predict in vivo joint contact forces during normal and novel gait patterns. *Journal of Biomechanical Engineering*, *135*(2), 1–7. https://doi.org/10.1115/1.4023457

Mantovani, G., & Lamontagne, M. (2017). How Different Marker Sets Affect Joint Angles in Inverse Kinematics Framework. *Journal of Biomechanical Engineering*, *139*(4), 1–7. https://doi.org/10.1115/1.4034708

Marouane, H., Shirazi-Adl, A., & Hashemi, J. (2015). Quantification of the role of tibial posterior slope in knee joint mechanics and ACL force in simulated gait. *Journal of Biomechanics*, *48*(10), 1899–1905. https://doi.org/10.1016/j.jbiomech.2015.04.017

Marra, M. A., Strzelczak, M., Heesterbeek, P. J. C., van de Groes, S. A. W., Janssen, D. W., Koopman, B. F. J. M., Wymenga, A. B., & Verdonschot, N. J. J. (2018). Anterior referencing of tibial slope in total knee arthroplasty considerably influences knee kinematics: a musculoskeletal simulation study. *Knee Surgery, Sports Traumatology, Arthroscopy*, *26*(5), 1540–1548. https://doi.org/10.1007/s00167-017-4561-3

Marshall, W. A., & Tanner, J. M. (1969). Variations in pattern of pubertal changes in girls. *Archives of Disease in Childhood*, *44*(235), 291–303. https://doi.org/10.1136/adc.44.235.291

Marshall, W. A., & Tanner, J. M. (1970). Variations in the Pattern of Pubertal Changes in Boys. In *Archives of Disease in Childhood* (Vol. 45).

Matsuda, S., Miura, H., Nagamine, R., Urabe, K., Ikenoue, T., Okazaki, K., & Iwamoto, Y. (1999). Posterior tibial slope in the normal and varus knee. *American Journal of Knee Surgery*, *12*((3)), 165–168.

Moissenet, F., Chèze, L., & Dumas, R. (2014). A 3D lower limb musculoskeletal model for simultaneous estimation of musculo-tendon, joint contact, ligament and bone forces during gait. *Journal of Biomechanics*, *47*(1), 50–58. https://doi.org/10.1016/j.jbiomech.2013.10.015

Moissenet, F., Modenese, L., & Dumas, R. (2017). Alterations of musculoskeletal models for a more accurate estimation of lower limb joint contact forces during normal gait: A systematic review. *Journal of Biomechanics*, *63*, 8–20. https://doi.org/10.1016/j.jbiomech.2017.08.025

Monk, A. P., Choji, K., O'Connor, J. J., Goodfellow, J. W., & Murray, D. W. (2014). The shape of the distal femur: A geometrical study using MRI. *Bone and Joint Journal*, *96B* (12), 1623–1630. https://doi.org/10.1302/0301-620X.96B12.33964

Moore, J. K., Kooijman, J. D. G., Schwab, A. L., & Hubbard, M. (2011). Rider motion identification during normal bicycling by means of principal component analysis. *Multibody System Dynamics*, *25*(2), 225–244. https://doi.org/10.1007/s11044-010-9225-8

Murshed, K. A., Çiçekcibaşi, A. E., Karabacakoglu, A., Şeker, M., & Ziylan, T. (2005). Distal femur morphometry: A gender and bilateral comparative study using magnetic resonance imaging. *Surgical and Radiologic Anatomy*, *27*(2), 108–112. https://doi.org/10.1007/s00276-004-0295-2

Myer, G. D., Ford, K. R., & Hewett, T. E. (2005). The effects of gender on quadriceps muscle activation strategies during a maneuver that mimics a high ACL injury risk position. *Journal of Electromyography and Kinesiology*, *15*(2), 181–189. https://doi.org/10.1016/j.jelekin.2004.08.006

Myer, G., Faigenbaum, A., Foss, K., Xu, Y., Khoury, J., Dolan, L., McCambridge, T., & Hewett, T. (2014). Injury initiates unfavourable weight gain and obesity markers in youth. *British Journal of Sports Medicine*, *48*(20), 1477–1481. https://doi.org/10.1136/bjsports-2012-091988.Injury

Nardini, F., Belvedere, C., Sancisi, N., Conconi, M., Leardini, A., Durante, S., & Parenti-Castelli, V. (2020). An Anatomical-Based Subject-Specific Model of In-Vivo Knee Joint 3D Kinematics From Medical Imaging. *Applied Sciences*, *10*(6), 2100. https://doi.org/10.3390/app10062100

Olsen, O. E., Myklebust, G., Engebretsen, L., & Bahr, R. (2004). Injury mechanisms for anterior cruciate ligament injuries in team handball: A systematic video analysis. *American Journal of Sports Medicine*, *32*(4), 1002–1012. https://doi.org/10.1177/0363546503261724

O'Malley, M. P., Milewski, M. D., Solomito, M. J., Erwteman, A. S., & Nissen, C. W. (2015). The association of tibial slope and anterior cruciate ligament rupture in skeletally immature patients. *Arthroscopy - Journal of Arthroscopic and Related Surgery*, *31*(1), 77–82. https://doi.org/10.1016/j.arthro.2014.07.019

Ottoboni, A., Parenti-Castelli, V., Sancisi, N., Belvedere, C., & Leardini, A. (2010). Articular surface approximation in equivalent spatial parallel mechanism models of the human knee joint: An experiment-based assessment. *Proceedings of the Institution of Mechanical Engineers, Part H: Journal of Engineering in Medicine*, *224*(9), 1121–1132. https://doi.org/10.1243/09544119JEIM684

Paterno, M. V., Huang, B., Thomas, S., Hewett, T. E., & Schmitt, L. C. (2017). Clinical Factors That Predict a Second ACL Injury After ACL Reconstruction and Return to Sport: Preliminary Development of a Clinical Decision Algorithm. *Orthopaedic Journal of Sports Medicine*, *5*(12), 1–7. https://doi.org/10.1177/2325967117745279

Pinskerova, V., Johal, P., Nakagawa, S., Sosna, A., Williams, A., Gedroyc, W., & Freeman, M. A. R. (2004). Does the femur roll-back with flexion? *Journal of Bone and Joint Surgery - Series B*, *86*(6), 925–931. https://doi.org/10.1302/0301-620X.86B6.14589

Price, M. J., Tuca, M., Cordasco, F. A., & Green, D. W. (2017a). Nonmodifiable risk factors for anterior cruciate ligament injury. *Current Opinion in Pediatrics*, *29*(1), 55–64. https://doi.org/10.1097/MOP.0000000000000444

Price, M. J., Tuca, M., Cordasco, F. A., & Green, D. W. (2017b). Nonmodifiable risk factors for anterior cruciate ligament injury. *Current Opinion in Pediatrics*, *29*(1), 55–64. https://doi.org/10.1097/MOP.0000000000000444

Prince, J. S., Laor, T., & Bean, J. A. (2005). MRI of anterior cruciate ligament injuries and associated findings in the pediatric knee: Changes with skeletal maturation. *American Journal of Roentgenology*, *185*(3), 756–762. https://doi.org/10.2214/ajr.185.3.01850756

Rajagopal, A., Dembia, C. L., DeMers, M. S., Delp, D. D., Hicks, J. L., & Delp, S. L. (2016). Full-Body Musculoskeletal Model for Muscle-Driven Simulation of Human Gait. *IEEE Transactions on Biomedical Engineering*, *63*(10), 2068–2079. https://doi.org/10.1109/TBME.2016.2586891

Rasmussen, J. (2003). *AnyBody-a software system for ergonomic optimization*.

Rasmussen, J.;, Zee, M. D., Damsgaard, M. ;, Christensen, S. T., Marek, C. ;, & Siebertz, K. (2005). A General Method for Scaling Musculo-Skeletal Models. In *International Symposium on Computer Simulation*.

Reinbolt, J. A., Schutte, J. F., Fregly, B. J., Koh, B. Il, Haftka, R. T., George, A. D., & Mitchell, K. H. (2005). Determination of patient-specific multi-joint kinematic models through two-level optimization. *Journal of Biomechanics*, *38*(3), 621–626. https://doi.org/10.1016/j.jbiomech.2004.03.031

Reinbolt, J. A., Seth, A., & Delp, S. L. (2011). Simulation of human movement: Applications using OpenSim. *Procedia IUTAM*. https://doi.org/10.1016/j.piutam.2011.04.019

Reinschmidt, C., Van Den Bogert, A. J., Nigg, B. M., Lundberg, A., & Murphy, N. (1997). Effect of skin movement on the analysis of skeletal knee joint motion during running. *Journal of Biomechanics*, *30*(7), 729–732. https://doi.org/10.1016/S0021-9290(97)00001-8

Romanchuk, N. J., Del Bel, M. J., & Benoit, D. L. (2020). Sex-specific landing biomechanics and energy absorption during unanticipated single-leg drop-jumps in adolescents:

implications for knee injury mechanics. *Journal of Biomechanics*, *113*, 110064. https://doi.org/10.1016/j.jbiomech.2020.110064

Sanders, T. L., Maradit Kremers, H., Bryan, A. J., Larson, D. R., Dahm, D. L., Levy, B. A., Stuart, M. J., & Krych, A. J. (2016a). Incidence of anterior cruciate ligament tears and reconstruction: A 21-year population-based study. *American Journal of Sports Medicine*, *44*(6), 1502–1507. https://doi.org/10.1177/0363546516629944

Sanders, T. L., Maradit Kremers, H., Bryan, A. J., Larson, D. R., Dahm, D. L., Levy, B. A., Stuart, M. J., & Krych, A. J. (2016b). Incidence of anterior cruciate ligament tears and reconstruction: A 21-year population-based study. *American Journal of Sports Medicine*, *44*(6), 1502–1507. https://doi.org/10.1177/0363546516629944

Schellenberg, F., Taylor, W. R., Jonkers, I., & Lorenzetti, S. (2017). Robustness of kinematic weighting and scaling concepts for musculoskeletal simulation. *Computer Methods in Biomechanics and Biomedical Engineering*, *20*(7), 720–729. https://doi.org/10.1080/10255842.2017.1295305

Scheys, L., Desloovere, K., Suetens, P., & Jonkers, I. (2011). Level of subject-specific detail in musculoskeletal models affects hip moment arm length calculation during gait in pediatric subjects with increased femoral anteversion. *Journal of Biomechanics*, *44*(7), 1346–1353. https://doi.org/10.1016/j.jbiomech.2011.01.001

Schmid, J., Sandholm, A., Chung, F., Thalmann, D., Delingette, H., & Magnenat-Thalmann, N. (2009). Musculoskeletal Simulation Model Generation from MRI Data Sets and Motion Capture Data. In N. Magnenat-Thalmann, J. J. Zhang, & D. D. Feng (Eds.), *Recent Advances in the 3D Physiological Human* (pp. 3–19). Springer London. https://doi.org/10.1007/978-1-84882-565-9_1

Schneider, A., Si-Mohamed, S., Magnussen, R. A., Lustig, S., Neyret, P., & Servien, E. (2018). Tibiofemoral joint congruence is lower in females with ACL injuries than males with ACL injuries. *Knee Surgery, Sports Traumatology, Arthroscopy*, *26*(5), 1375–1383. https://doi.org/10.1007/s00167-017-4756-7

Seth, A., Hicks, J. L., Uchida, T. K., Habib, A., Dembia, C. L., Dunne, J. J., Ong, C. F., DeMers, M. S., Rajagopal, A., Millard, M., Hamner, S. R., Arnold, E. M., Yong, J. R., Lakshmikanth, S. K., Sherman, M. A., Ku, J. P., & Delp, S. L. (2018). OpenSim: Simulating musculoskeletal dynamics and neuromuscular control to study human and animal movement. *PLoS Computational Biology*, *14*(7), 1–20. https://doi.org/10.1371/journal.pcbi.1006223

Shaw, K. A., Dunoski, B., Mardis, N., & Pacicca, D. (2015). Knee morphometric risk factors for acute anterior cruciate ligament injury in skeletally immature patients. *Journal of Children's Orthopaedics*, *9*(2), 161–168. https://doi.org/10.1007/s11832-015-0652-1

Shaw, L., & Finch, C. F. (2017a). Trends in pediatric and adolescent anterior cruciate ligament injuries in Victoria, Australia 2005-2015. *International Journal of Environmental Research and Public Health*, *14*(6). https://doi.org/10.3390/ijerph14060599

Shaw, L., & Finch, C. F. (2017b). Trends in pediatric and adolescent anterior cruciate ligament injuries in Victoria, Australia 2005-2015. *International Journal of Environmental Research and Public Health*, *14*(6). https://doi.org/10.3390/ijerph14060599

Shelburne, K. B., Kim, H. J., Sterett, W. I., & Pandy, M. G. (2011). Effect of posterior tibial slope on knee biomechanics during functional activity. *Journal of Orthopaedic Research*, *29*(2), 223–231. https://doi.org/10.1002/jor.21242

Siegel, L., Vandenakker-Albanese, C., & Siegel, D. (2012). Anterior cruciate ligament injuries: Anatomy, physiology, biomechanics, and management. *Clinical Journal of Sport Medicine*, *22*(4), 349–355. https://doi.org/10.1097/JSM.0b013e3182580cd0

Smale, K. B. (2018). *Relating subjective and objective knee function after anterior cruciate ligament injury through biomechanical and neuromusculoskeletal modelling approaches*. University of Ottawa.

Smale, K. B., Conconi, M., Sancisi, N., Krogsgaard, M., Alkjaer, T., Parenti-Castelli, V., & Benoit, D. L. (2019). Effect of implementing magnetic resonance imaging for patient-specific OpenSim models on lower-body kinematics and knee ligament lengths. *Journal of Biomechanics*, *83*(November), 9–15. https://doi.org/10.1016/j.jbiomech.2018.11.016

Stein, C. J., & Micheli, L. J. (2010). Overuse injuries in youth sports. *Physician and Sportsmedicine*, *38*(2), 102–108. https://doi.org/10.3810/psm.2010.06.1787

Suwarganda, E. K., Diamond, L. E., Lloyd, D. G., Besier, T. F., Zhang, J., Killen, B. A., Savage, T. N., & Saxby, D. J. (2019). Minimal medical imaging can accurately reconstruct geometric bone models for musculoskeletal models. *PLoS ONE*, *14*(2), 1–16. https://doi.org/10.1371/journal.pone.0205628

Tat, J., Crapser, D., Alaqeel, M., Schupbach, J., Lee-Howes, J., Tamimi, I., Burman, M., & Martineau, P. A. (2021). A Quantifiable Risk Factor for ACL Injury: Applied Mathematics to Model the Posterolateral Tibial Plateau Surface Geometry. *Orthopaedic Journal of Sports Medicine*, *9*(4), 1–7. https://doi.org/10.1177/2325967121998310

Tsai, L. C., Colletti, P. M., & Powers, C. M. (2012). Magnetic resonance imaging-measured muscle parameters improved knee moment prediction of an EMG-driven model. *Medicine* *and Science in Sports and Exercise*, *44*(2), 305–312. https://doi.org/10.1249/MSS.0b013e31822dfdb3

Valente, G., Crimi, G., Vanella, N., Schileo, E., & Taddei, F. (2017). NMSBUILDER: Freeware to create subject-specific musculoskeletal models for OpenSim. *Computer Methods and Programs in Biomedicine*, *152*, 85–92. https://doi.org/10.1016/j.cmpb.2017.09.012

van Diek, F. M., Wolf, M. R., Murawski, C. D., van Eck, C. F., & Fu, F. H. (2014). Knee morphology and risk factors for developing an anterior cruciate ligament rupture: An MRI comparison between ACL-ruptured and non-injured knees. *Knee Surgery, Sports Traumatology, Arthroscopy*, *22*(5), 987–994. https://doi.org/10.1007/s00167-013-2588-7

Wahl, C. J., Westermann, R. W., Blaisdell, G. Y., & Cizik, A. M. (2012a). An association of lateral knee sagittal anatomic factors with non-contact ACL injury: Sex or geometry? *Journal of Bone and Joint Surgery - Series A*, *94*(3), 217–226. https://doi.org/10.2106/JBJS.K.00099

Wahl, C. J., Westermann, R. W., Blaisdell, G. Y., & Cizik, A. M. (2012b). An association of lateral knee sagittal anatomic factors with non-contact ACL injury: Sex or geometry? *Journal of Bone and Joint Surgery - Series A*, *94*(3), 217–226. https://doi.org/10.2106/JBJS.K.00099

Werner, B. C., Yang, S., Looney, A. M., & Gwathmey, F. W. (2016). Trends in Pediatric and Adolescent Anterior Cruciate Ligament Injury and Reconstruction. *Journal of Pediatric Orthopaedics*, *36*(5), 447–452. https://doi.org/10.1097/BPO.0000000000000482

Wild, C. Y., Steele, J. R., & Munro, B. J. (2012). Why Do Girls Sustain More Anterior Cruciate Ligament Injuries Than Boys? *Sports Medicine*, *42*(9), 733–749. https://doi.org/10.1007/bf03262292

Wilson, D. R., & O'Connor, J. J. (1997). A three-dimensional geometric model of the knee for the study of joint forces in gait. *Gait and Posture*, *5*(2), 108–115. https://doi.org/10.1016/S0966-6362(96)01080-6

Winter, D. A. (2009). Biomechanics and Motor Control of Human Movement: Fourth Edition. In *Biomechanics and Motor Control of Human Movement: Fourth Edition*. https://doi.org/10.1002/9780470549148

Woodhouse, E., Schmale, G. A., Simonian, P., Tencer, A., Huber, P., & Seidel, K. (2007). Reproductive hormone effects on strength of the rat anterior cruciate ligament. *Knee Surgery, Sports Traumatology, Arthroscopy*, *15*(4), 453–460. https://doi.org/10.1007/s00167-006-0237-0

Wu, J. L., Hosseini, A., Kozanek, M., Gadikota, H. R., Gill IV, T. J., & Li, G. (2010). Kinematics of the anterior cruciate ligament during gait. *American Journal of Sports Medicine*, *38*(7), 1475–1482. https://doi.org/10.1177/0363546510364240

Xu, H., Bloswick, D., & Merryweather, A. (2015). An improved OpenSim gait model with multiple degrees of freedom knee joint and knee ligaments. *Computer Methods in Biomechanics and Biomedical Engineering*, *18*(11), 1217–1224. https://doi.org/10.1080/10255842.2014.889689

Yang, B., Yu, J. K., Zheng, Z. Z., Lu, Z. H., & Zhang, J. Y. (2014). Comparative study of sex differences in distal femur morphology in osteoarthritic knees in a Chinese population. *PLoS ONE*, *9*(2), 1–5. https://doi.org/10.1371/journal.pone.0089394

Yu, H. J., Chang, A., Fukuda, Y., Terada, Y., Nozaki, T., & Yoshioka, H. (2016). Comparison of semi-automated and manual segmentation of knee cartilage. *Osteoarthritis and Cartilage*, *24*(2016), S311. https://doi.org/10.1016/j.joca.2016.01.560

Zelle, J., Heesterbeek, P. J. C., De Waal Malefijt, M., & Verdonschot, N. (2010). Numerical analysis of variations in posterior cruciate ligament properties and balancing techniques on total knee arthroplasty loading. *Medical Engineering and Physics*, *32*(7), 700–707. https://doi.org/10.1016/j.medengphy.2010.04.013

Zeng, C., Gao, S. Guang, Wei, J., Yang, T. bao, Cheng, L., Luo, W., Tu, M., Xie, Q., Hu, Z., Liu, P. Fei, Li, H., Yang, T., Zhou, B., & Lei, G. Hua. (2013). The influence of the intercondylar notch dimensions on injury of the anterior cruciate ligament: A meta-analysis. *Knee Surgery, Sports Traumatology, Arthroscopy*, *21*(4), 804–815. https://doi.org/10.1007/s00167-012-2166-4

Zhang, J., Sorby, H., Clement, J., Thomas, C. D. L., Hunter, P., Nielsen, P., Lloyd, D., Taylor, M., & Besier, T. (2014). *The MAP Client: User-Friendly Musculoskeletal Modelling Workflows*. https://github.com/MusculoskeletalAtlasProject/mapclient.

Zheng, L., Li, K., Shetye, S., & Zhang, X. (2014). Integrating dynamic stereo-radiography and surface-based motion data for subject-specific musculoskeletal dynamic modeling. *Journal of Biomechanics*, *47*(12), 3217–3221. https://doi.org/10.1016/j.jbiomech.2014.08.009

CHAPTER 10: APPENDIX A (FIGURES)

TABLE 1: Anterior Cruciate Ligament (ACL) Injuries Detected on MRI

Patient Characteristics	Group 1	Group 2	Group 3	Total
No. of knees	31	27	24	82
Age (yr)				
Range	7–17	12–17	15–19	7–19
Mean	12.4	15.6	16.6	14.7
Sex				
Male	27	11	8	46
Female	4	16	16	36
ACL injury **(% of cases)**				
Complete tear	48	81	88	71
Partial tear	26	15	8	17
Tibial spine avulsion fracture	26	4	4	12

Figure 10-1 Results from a study by Prince et al (2005) comparing ACL injury types in skeletally immature (Group 1), partially mature (Group 2) and skeletally mature (Group 3) subjects

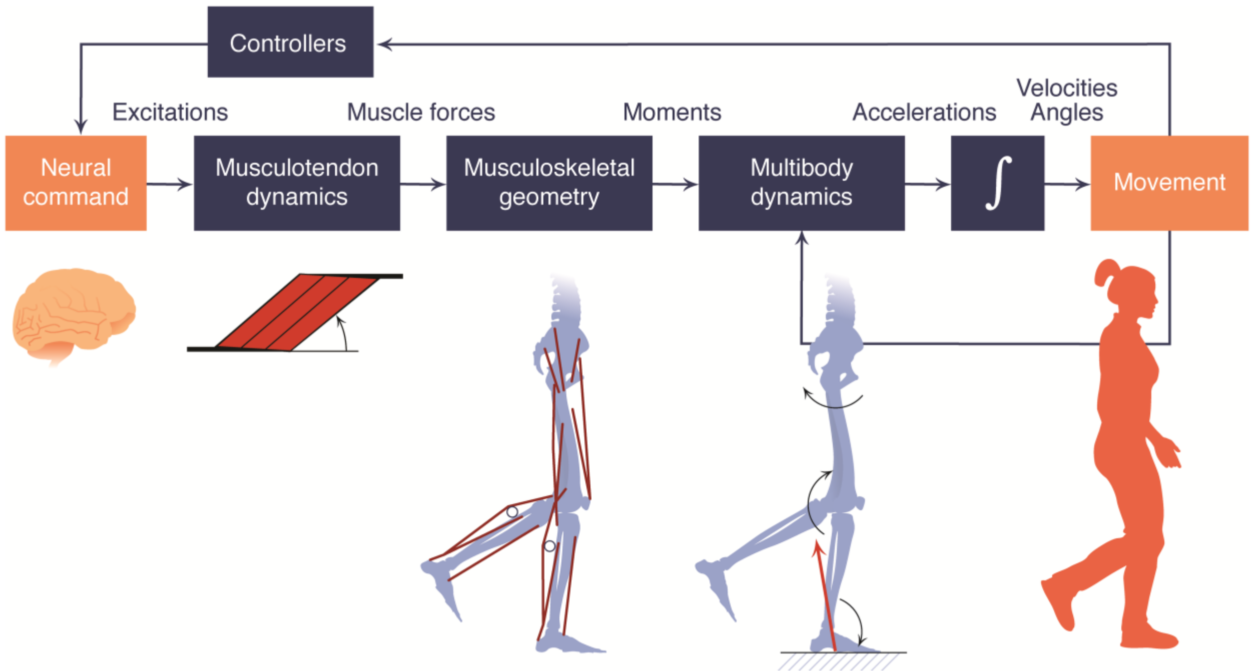

Figure 10-2 Functional capabilities of the musculoskeletal modelling software OpenSim (Seth et al, 2018

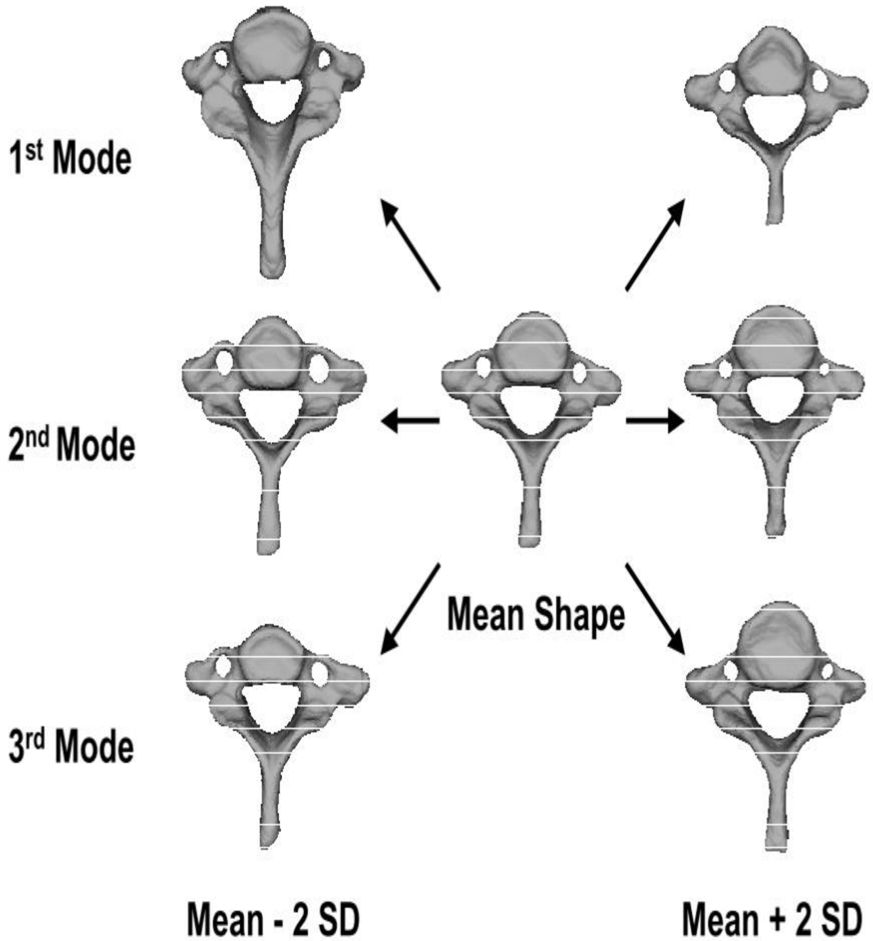

Figure 10-3 Shape model generated modes of variation for a cervical vertebra (Heitz et al., 2005)

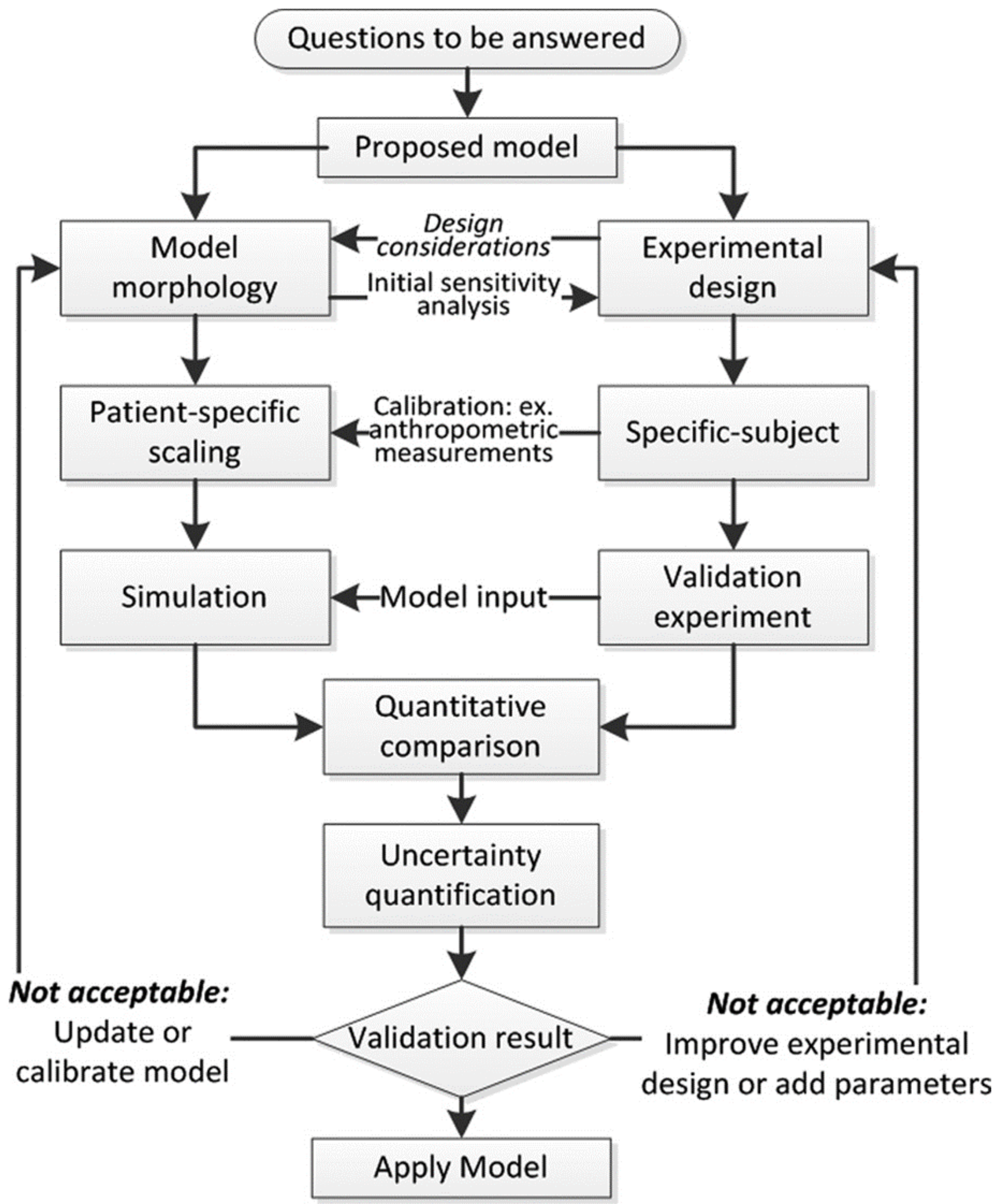

Figure 10-4 The Verification and Validation (V&V) Process defined by Lund et al (2015)

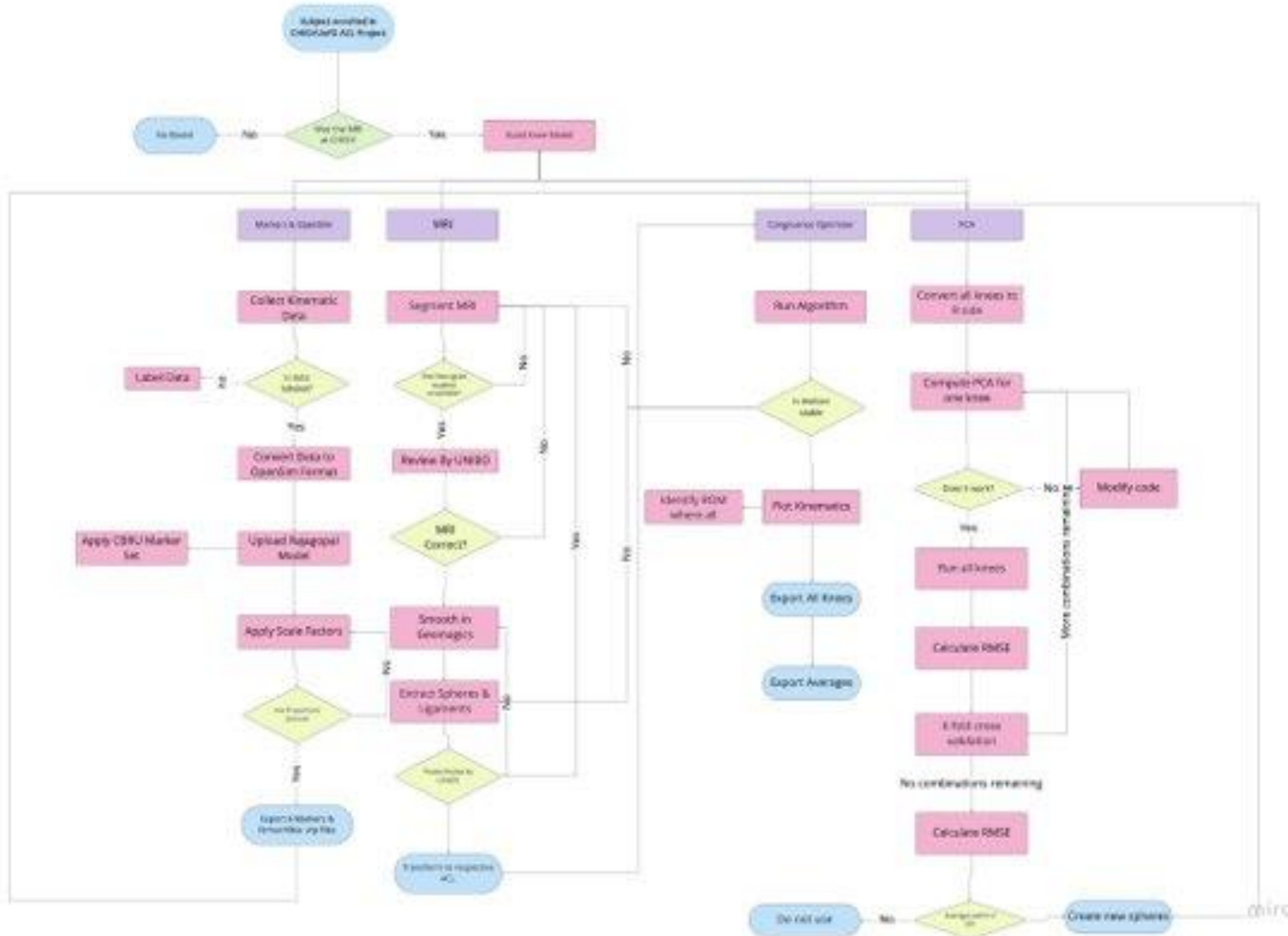

Figure 10-5 Workflow of this thesis and outline for reproducibility checks

CHAPTER 11: APPENDIX B (TABLES)

Task Name	Description
Maximum Voluntary Isometric Contraction – Knee Flexion	Participant seated in isokinetic dynamometer, with knee at 60 degrees, flexes knee as hard as possible for 5 seconds
Maximum Voluntary Isometric Contraction – Knee Extension	Participant seated in isokinetic dynamometer, with knee at 60 degrees, extends knee as hard as possible for 5 seconds
Maximum Voluntary Isometric Contraction – Plantar Flexion	Participant seated in isokinetic dynamometer, with knee at 0 degrees, plantarflexes as hard as possible for 5 seconds
Maximum Voluntary Isometric Contraction – Hip Abduction	Participant stood with leg rested against pad of isokinetic dynamometer, between 0-10 degrees, extends leg as hard as possible for 5 seconds
Max Anterior Hop	Participants are instructed to hop as far as they can on one foot facing forward
Max Lateral Hop	participants are instructed to hop as far as they can on one foot to the side, facing perpendicular to the direction of the marked line on the laboratory floor

Timed 6m Hop	Participants are instructed to hop on one foot as fast as they can to cover a distance of 6 meters
Triple Hops	participants are instructed to hop on one foot three times in a row for maximum distance
Cross Hop	participants are instructed to hop on one foot back and forth three times across two marked lines separated by 15cm on the laboratory floor, while attempting to cover maximum distance
Squat	Participants standing with feet shoulder width apart on separate force plates with hands on head to account for arm motion variability, and will be instructed to squat as low as comfortable and return to standing
Counter Movement Jump (CMJ)	participants standing with feet shoulder-width apart on separate force plates, with their hands on their head to account for arm motion variability, and will be instructed to squat down in order to help them jump as high as possible

Single Leg Lunge	Participants standing facing force plates with hands on head. Will be instructed to step onto a force plate and descend into a lunge and then return to standing, while keeping hands on head.
Side Cut	A side-cut trial will be deemed successful if the participant plants and cuts with the appropriate foot, plants their entire foot on the force platform, and accelerates out of the foot-plant at a 45o angle (pylons in the lab will provide a ±10o target area)
Drop Vertical Jump (DVJ)	Participants stand on a box positioned at knee height with their hands on their head. They're instructed to step off the box landing with both feet on the force platforms in front of them, then jump as high as they can.
Isokinetic Test – Flexion-Extension	At a fixed speed of 60 rad/s, participant must complete 40 knee flexions and extension at an ROM between 20-100 degrees of flexion. The participant must produce as large of a torque as possible and sustain it as best as possible